# The role of OTUD5-dependent deubiquitination on the maintenance of nuclear homeostasis

**Dissertation**

zur Erlangung des Grades

“Doktor der Naturwissenschaften”

(Dr. rer. nat.)

Am Fachbereich Biologie

der Johannes Gutenberg-Universität Mainz



Caio Almeida Batista de Oliveira

Geboren am 23.07.1993 in Valença, Brasilien

Mainz, 16 Januar 2026

**Dekan:** Prof. Dr. Eckhard Thines

**1. Berichterstatter:** Redacted

**2. Berichterstatter:** Redacted

**Tag der mündlichen Prüfung:** 09.03.2026

# DECLARATION OF AUTHORSHIP

I, Caio Almeida Batista de Oliveira, hereby declare that the work presented in this thesis is my own. All the literature and other sources that were used for retrieval of information are properly cited. I would like to kindly acknowledge the contribution received during the development of this work: first, redacted for the supervision and support on experimental design; redacted, who performed the analysis that resulted in the data presented in Figure 13; redacted, who generated samples that resulted in the data presented in Figure 8; IMB Protein Production core facility for producing the OtUBD probe, used to generate the data presented in Figure 8; IMB Genomics core facility, for generating the RNA-Sequencing data, and IMB Bioinformatics core facility (namely redacted), for the analysis of this data, which is presented in Figures 9D and 10; IMB Flow Cytometry core facility, for assistance in generation of the data presented in Figure 16A and 16C; lastly, the aforementioned and other group colleagues for assistance in routine tasks.

# ABSTRACT

Ubiquitin is a 76 residues polypeptide, which works as a post-translational modification that can be attached to proteinaceous substrates, either as monomers or as protein polymers by the sequential attachment of ubiquitin monomers on top of each other. Modification of substrates by ubiquitin leads to diverse outcomes, such as alterations in their stability, shuttling to specific cellular compartments or working as a molecular switch to control the substrate activity. The attachment of ubiquitin is mediated by a three-step process, which can be reversed by the employment of a dedicated set of enzymes to perform the removal of ubiquitin signal.

OTUD5 is a deubiquitinating enzyme that removes the modification from its substrates. Recently, OTUD5 has emerged as a prominent regulator of nuclear processes and linked to a severe developmental syndrome, based on the absence of its catalytic activity. Although its impact on some nuclear homeostasis events has been described, its full spectrum of *bona fide* substrates has not been systematically explored in order to explain by which means it controls the associated processes.

We employed unbiased mass spectrometry-based approaches to determine the endogenous proteins that have their ubiquitination status altered by OTUD5 knockout, showing novel high-confidence substrates of OTUD5 involved in chromosome spatial organization. By analysis of the proteome, we quantified elevated levels of OTUD5 new substrates and their elevated chromatin-bound status. Furthermore, we established a new nuclear interaction between OTUD5 and VCP, mediated by NPLOC4.

Altogether, we uncovered novel pathways by which cells control their nuclear homeostasis, using the deubiquitinase OTUD5 to regulate the abundance of the modification on specific factors. Ultimately, this leads to a tight modulation of substrate levels and chromatin binding that, in turn, modulates essential processes, such as cell cycle and cellular growth, demonstrating the central role OTUD5 has in these events.

# ZUSAMMENFASSUNG

Ubiquitin, ein Polypeptid bestehend aus 76 Aminosäuren, kann als post-translationale Modifikation in Form von Monomeren oder Polymeren an proteinerge Substrate angefügt werden. Diese Modifikation von Proteinen kann zu Veränderungen in deren Stabilität, dem Transport in spezifische zelluläre Subkompartimente oder als molekularer Schalter zur Regulierung der Aktivität des Substrates führen. Das Anfügen von Ubiquitin ist ein Prozess, der in drei Schritten verläuft und reversibel ist. Für das Entfernen des Ubiquitinsignals verwenden Zellen eine ausgewählte Gruppe von Proteinen – sogenannte desubiquitinierender Enzyme (DUBs).

Eines dieser DUBs ist das Enzym OTUD5, welches in den vergangenen Jahren als Regulator nukleärer Prozesse aufgetreten ist und mit schwerwiegenden Entwicklungsstörungen in Verbindung gebracht wurde, wenn dessen katalytische Aktivität beeinträchtigt ist. Obwohl die Rolle von OTUD5 in der Regulierung der nukleärer Homöostase bekannt ist, konnten bislang nicht alle Substrate identifiziert werden, die in diesen Prozessen involviert sind, weswegen der genaue Wirkungsmechanismus wenig verstanden ist.

Mit Hilfe von Massenspektrometrie versuchen wir herauszufinden welche endogenen Proteine ihren Ubiquitinierungsstatus verändern, wenn OTUD5 ausgeknockt wird. Hierdurch konnten wir neue Substrate identifizieren, welche in die räumliche Organisation von Chromosomen involviert sind. Durch Untersuchungen des Proteoms konnte festgestellt werden, dass diese Substrate in erhöhtem Maße an Chromatin binden. Des Weiteren konnten wir eine neuartige Wechselwirkung zwischen OTUD5 und VCP belegen, welche durch NPLOC4 vermittelt wird.

Zusammenfassend zeigen wir einen neuen Signaltransduktionsweg, durch welchen Zellen ihre nukleäre Homöostase regulieren, indem OTUD5 das Auftreten der Ubiquitinmodifikation spezifischer Faktoren verändert. Dies führt zu einer strikten Modulation der Substratlevel und deren Lokalisation, welche wiederum essenzielle Prozesse wie Zellzyklus und Zellwachstum reguliert. Dies demonstriert die essenzielle Rolle von OTUD5 in diesem Kontext.

# CONTENTS

# LIST OF TABLES

# LIST OF FIGURES

# 1. Introduction

## 1.1. The ubiquitin system

In 1975, a small polypeptide of circa 8.5 kDa, named as ubiquitous immunopoietic polypeptide (UBIP), was described in bovine thymus to be an inducer of differentiation of both T- and B-cells. Interestingly, UBIP was also seen to be highly conserved from different organisms, being identified in several tissues of varied animals, as well as plants and fungi[1]. Furthermore, another report determined the primary sequence of UBIP – now already called ubiquitin – to be, at this point, a 74 amino acid residues polypeptide[2].

Later on, histone 2A was observed to be conjugated to a non-histone peptide forming the chromatin associated protein so-called protein A24. In this situation, the non-histone part of A24 was seen to be linked to the histone 2A segment through an isopeptide bond, specifically through the side chain of lysine 119 in histone 2A sequence with a di-glycine from the non-histone portion[3] – although at this point no connection was made, comparison between ubiquitin and N-terminus of non-histone A24 shows a complete sequence alignment of first 37 residues of both polypeptides.

In parallel, a system that is ATP-dependent and responsible for protein degradation in reticulocytes was described, which later was seen to be composed of several factors, including a non-proteolytic and heat-stable component, of around 9 kDa, named APF-1[4–6]. APF-1 was observed, then, to form covalent bonds with lysozyme (including the attachment of more than one monomer of APF-1 to a single molecule of the enzyme), a known substrate of this proteolytic pathway[7].

It was only in 1980 that the integration between these seemingly separated topics was made. By comparing sequence and activity of ubiquitin and APF-1, it was seen that both are the same polypeptide, capable of activating the ATP-dependent proteolysis[8]. Shortly after, the three main components of this system were described and named E1, E2 and E3 enzymes[9], which in association are capable of modifying substrates with the attachment of ubiquitin, leading to degradation through an ATP-dependent protease[10] – later identified as the proteasome.

Today, we know ubiquitin is a polypeptide consisting of 76 amino acids – the two C-terminal glycine residues connecting the non-histone portion to histone 2A were the only region in the

primary structure of ubiquitin to be absent in the first sequencing of the protein[2,3]. In mammals, it is encoded by four different genes (Figure 1A), in which two of those generate tandem repeats of ubiquitin (*UBB*, *UBC*), while the other two (*RPS27A*, *UBA52*) express a fusion version of ubiquitin to ribosomal proteins. In both cases, the available pool of ubiquitin is maintained through proteolysis of these translated versions, generating free molecules to be later attached to substrates[11,12]. Furthermore, ubiquitin is one of the most highly expressed proteins in eukaryotic cells, counting up to 5% of total proteins, and ubiquitination is among the most common types of post-translation modifications (PTMs) encountered[11,13].

The process of attaching ubiquitin to a substrate is composed of three sequential steps (Figure 1B): first, an E1 enzyme, in mammals encoded by two genes (*UBA1* and *UBA6*), adenylates the C-terminal glycine residue of ubiquitin via the cost of ATP and then links it to its active cysteine residue, generating an E1-ubiquitin thioester[14–16]. Afterwards, the E1 enzymes transfer the activated ubiquitin to the E2 enzymes, which also possess an active cysteine residue to form a covalent bond through a thioester – in mammals, the estimation of E2 enzymes is in the range of 40 different proteins[15,17,18].

Lastly, the E3 ligases come into play – a group composed of at least 600 individual members – to be the factor that defines the substrates to be modified, either by bringing the substrate to a close proximity to E2 so the ubiquitin transfer can happen or by covalently binding to ubiquitin before its transfer to the substrate (later detailed in section 1.3)[15,17]. Given that ubiquitination is a reversible process, a group of around 100 members are responsible for the deubiquitination – hence, enzymes with this activity are called deubiquitinases (DUBs) – of modified substrates, removing the signal[19] (Figure 1B).

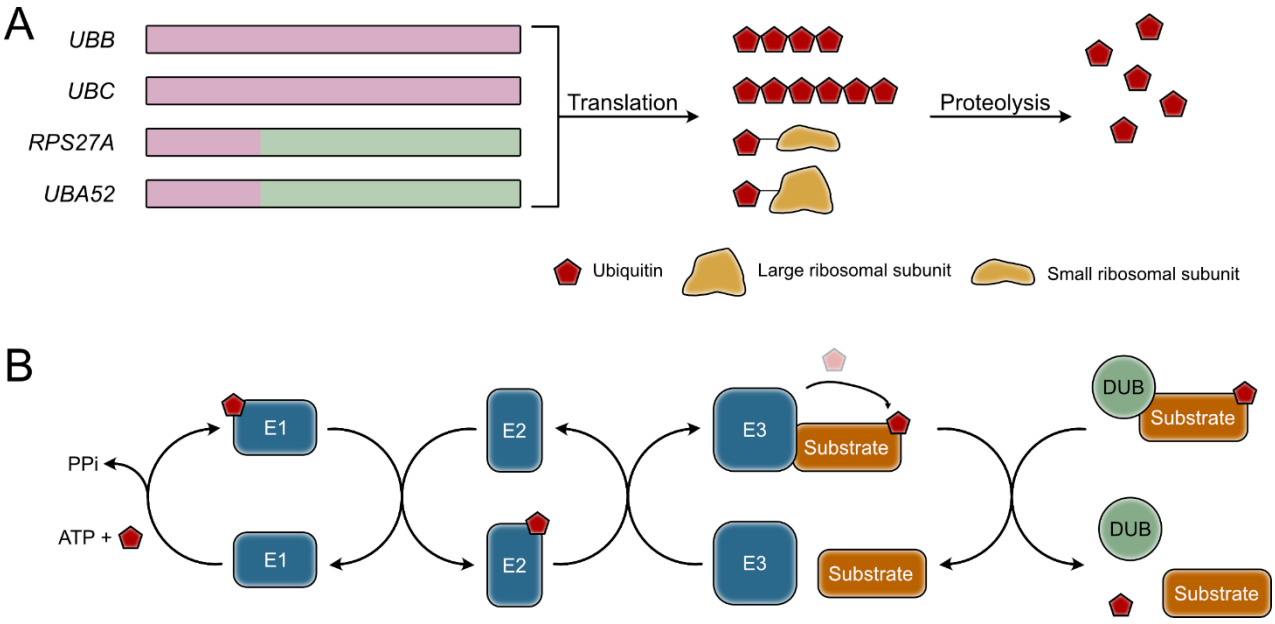


Figure 1: Ubiquitin expression and the ubiquitination cascade.
A) Schematics of the genes that encode for ubiquitin and the respective translation outcomes. B) Schematics of the ubiquitination cascade, indicating the transfer of ubiquitin through sequential reactions until the modification of a substrate, which can have its modification removed by the action of DUBs.

## 1.2. The ubiquitin code

As of described for histone 2A, the first substrate of ubiquitination identified[3], the formation of the isopeptide bond between the carboxy-terminal of Gly76 (G76) in ubiquitin and the substrate occurs, in its majority, in lysines, through the ε-amino group in its lateral chain[20].

The addition of only one ubiquitin molecule in a single residue results in monoubiquitination, the most common type of ubiquitin modification in human cells[21] and an important signaling event known to modulate different processes, such as transcription (histone H2B ubiquitination at Lys120)[22], DNA replication (PCNA ubiquitination at Lys164)[23] and DNA repair (FANCD2 ubiquitination at Lys561)[24] (Figure 2C). Substrates can also receive the attachment of single ubiquitin molecules at several different points in their structure, resulting in multi-monoubiquitination, seen to control, for example, cytoskeleton activity and cell morphology[25] (Figure 2C).

The formation of isopeptide bonds between G76 and an amino group can directly affect ubiquitin itself, as it contains in its sequence eight free amino groups that can be acceptors of

another ubiquitin moiety: the N-terminus and the seven lysine (K) residues – K6, K11, K27, K29, K33, K48 and K63 –, which were all observed in cells[26] (Figure 2A-B). Polymerization of ubiquitin molecules into chains was first described by the observation that K48-linked homotypic chains, up to 20 monomers, led a substrate to be degraded, while the mutation in this lysine residue would impair its recycling[27].

Different types of chains lead to different outcomes due to the spatial conformation that different linkages cause the polymers to have. K48-linked chains, for example, adopt a more compact conformation in contrast to K63- and M1-linked chains, which form more open, extended conformations[28]. A summary of the function of homotypic chains is shown in Figure 2D.

Homotypic chains are the simplest architecture ubiquitin chains can form. On top of that, when ubiquitin moieties are linked to each other via different lysine residues but in a single point of each molecule, a mixed ubiquitin chain is formed[29] (Figure 2C). Although any combination of linkages is theoretically possible, the synthesis efficiency of mixed chains seems to be dependent on the linkage of the proximal ubiquitin monomers (i. e., the first molecules to be seeded into a chain) and the linkage of the those that will be extending the chain[30]. *In vivo*, these types of chains have been observed to modulate different processes within cells. The activity of HOIP, an E3 ubiquitin ligase involved in activation of inflammatory response and NF-κB pathway that is able to form M1-linked chains, was seen to be dependent on previously seeded K63-linked chains, leading to the formation of hybrid K63/M1 polymers[31]. In addition, the E3 ligase TRIAD3A was reported to form K11/K63 mixed chains, regulating its association with autophagosomes and its association with tau protein, an important player in proteotoxic stress linked to neurodegeneration[32].

A further extension of the ubiquitin dictionary is the formation of branched chains. Although similar to mixed chains as they incorporate different linkages between monomers in its architecture, the difference is the attachment of more than one distal monomer to a proximal ubiquitin molecule[29] (Figure 2C). The increase in complexity of ubiquitin signaling is represented by the number of possible configurations when considering only two kinds of linkages in the same chain – in contrast to the eight types of homotypic chains, 28 possible combinations would be possible[33]. Similarly to mixed, there are suggestions that depending on the first linkage that is seeded, the extension of chains by branching may be biased to specific lysine residues in ubiquitin[30].

The two most abundant linkages, respectively K48 and K63[34–36], may be the best example to showcase the capacity of branched chains to expand ubiquitin signaling from the functions of homotypic ones. Usually seen as a non-proteasomal signal, K63 chains were observed to be added to the apoptosis modulator TXNIP, which was followed by the modification via K48[37], leading to degradation of this protein. This shows how the interplay of different linkages can transform the signal, adding another layer in ubiquitin regulation.

Atypical ubiquitin linkages (i. e., non-K48/K63) were also reported to form branched chains. A well described kind of branch comes from the APC/C E3 ligase, an essential enzyme in cell cycle control. Through association with different E2s, it can efficiently form K11/K48 to degrade its substrates during mitosis, leading to proteasomal degradation with a more potent signal than the respective homotypic chains of both linkages[38,39].

Combination between different E3 ligases can also lead to formation of branched chains. UBR4 and UBR5, for example, were seen to join forces to form K11/K48 polymers inducing degradation of misfolded proteins[38], while UBR5 was also seen in combination with TRIP12 forming K48/K29 chains, regulating stability of their target[40].

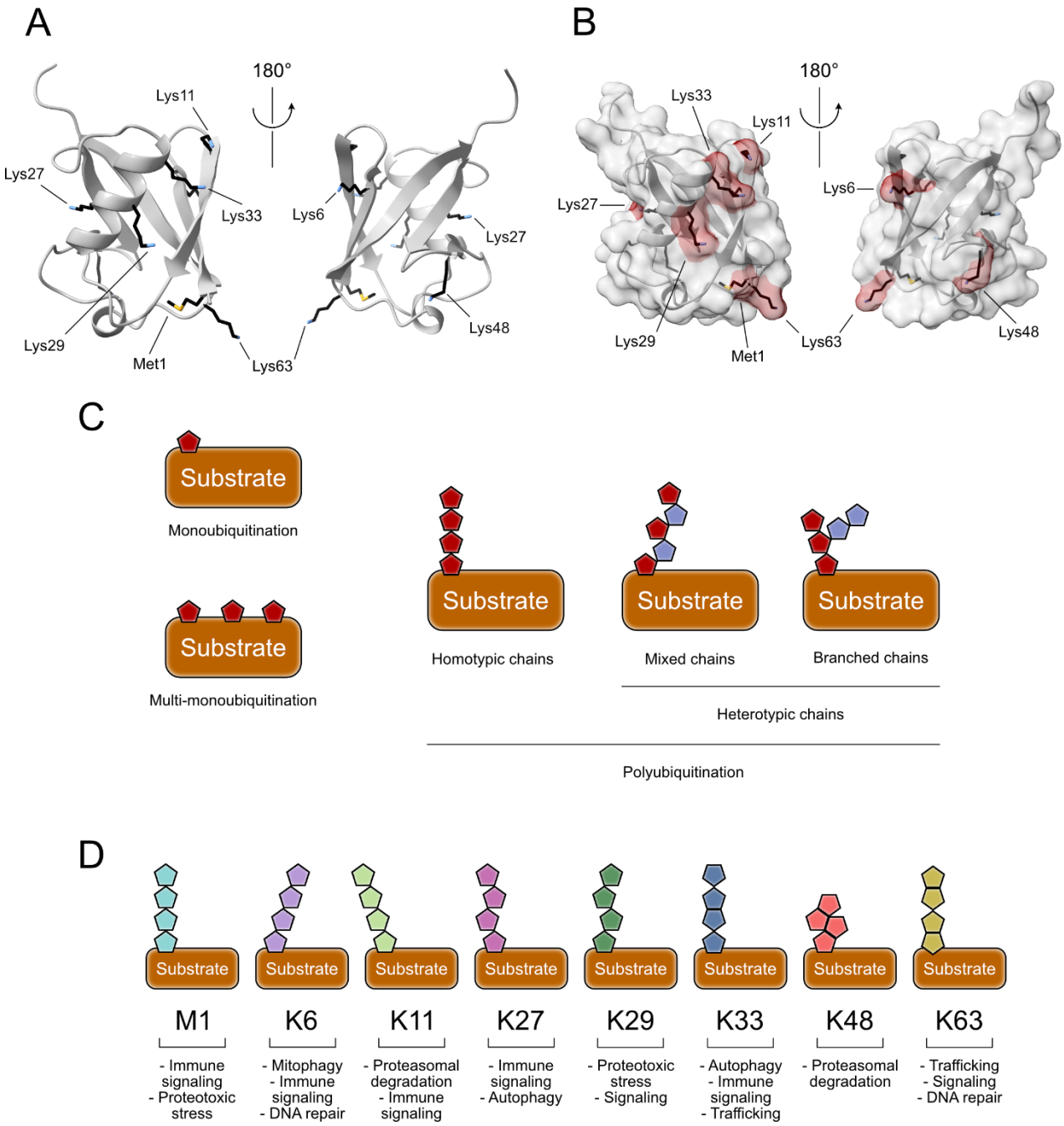


Figure 2: Ubiquitin structure and types of ubiquitin modification.
A-B) Ubiquitin structure (PDB accession number 1UBQ) depicted in ribbon diagrams (with surface overlayed in B) with indication of each lysine residue and N-terminal methionine (with surfaces in red for each of those residues in B). Lateral chains are indicated and color coded by atoms: carbon in black, nitrogen in blue and sulfur in yellow. C) Types of possible ubiquitin modification in substrates. Different colors of ubiquitin monomers are depicted to indicate different linkages in the chains, either mixed or branched. D) Example functions of homotypic chains of each linkage type[34,41–43].

## 1.2.1. Ubiquitin modifications

Ubiquitination is a vastly researched field, explored in several dimensions that already showed the broad range of its impact. Among the realm of PTMs, it is one of the most common type of modification[13] – according to the dbPTM database, the third most abundant in cells. The only counterparts of ubiquitination that are present more extensively are, respectively, phosphorylation and acetylation[13]. Therefore, by being a protein and able to be modified, ubiquitin is also target of different post-translational modifications.

Phosphorylation of ubiquitin was described by multiple groups as an initiating step during mitophagy process. Damage to mitochondria, commonly induced in cellular model by treatment of cells with CCCP, was previously observed to stabilize the kinase PINK1 on the outer mitochondrial membrane (OMM), which in turn works as a platform for the activation of the E3 ligase Parkin. Once Parkin is located at the OMM, it modifies the proteins in proximity, leading to their proteasomal degradation and signaling the cell to initiate the formation of autophagosomes containing the damaged mitochondria, eliminating the non-functional organelle[44].

Parkin activation by PINK1 occurs through the phosphorylation of its ubiquitin-like domain, which auto-inhibits the catalytic domain when not phosphorylated. This domain in Parkin is very close in structure to ubiquitin, to the point it possesses a serine residue in the exact same position as in ubiquitin, Ser65. Mutated Parkin, in which Ser65 is removed to a residue uncapable of being phosphorylated, was still active if ubiquitin was modified, but not active if the mutation occurred in ubiquitin structure – indicating the primary step in activation of this E3 ligase. This signaling is so strong that the amount of phospho-ubiquitin in mitochondria after depolarization of the organelle can reach up to 20% of the total number of ubiquitin molecules[44–47].

Ubiquitin phosphorylation seems to be a very restricted and powerful signal, as the modification was reported to induce structural changes in the conformation of the protein, leading to a decreased ability of the phospho-version to be conjugated into chains and to cause DUBs to have a lower activity in comparison to non-phosphorylated ubiquitin[48].

Ubiquitin molecules can also be modified through acetylation. Interestingly, due to the fact that addition of acetyl groups also occurs in lysine residues, this modification is a direct competitor of ubiquitin itself when it comes to substrates modification[44]. Expanding the view from only ubiquitin as a substrate, competition between acetylation and ubiquitination was seen to modulate

the stability of proteins, for example by impeding the ubiquitination of p53 by MDM2 under DNA damage stress[49].

On top of that, acetyl groups on basic residues (as in the case of lysine) tend to alter the lateral chain charge of such residues, altering their interaction with binders and, in case of ubiquitin, perturbing non-covalent interactions with E2 enzymes[50,51]. Furthermore, the impact of acetylation is not only due to modification of charges, but the kinetics of incorporation into the cascade are also altered. Activation by E1 and the loading of E2 with acetylated ubiquitin was shown to be slower when compared to the unmodified protein[52].

Out of the seven lysines in ubiquitin, six were seen to be acetylated – with the exception of K29[53]. The incorporation into chains is impaired, obviously in those formed by the linkage in which the lysine is acetylated but not necessarily only in these cases. Acetylation of K6 or K48 was suggested to impact formation of other chains, such as K11- and K63-linked[51]. In addition, acetylation of K11 was reported to modify ubiquitin structure, disturbing its conformation and the interaction with the ubiquitin-associated domain (UBA) of Ubiquilin-2, a high-affinity ubiquitin binder[54].

Overall, acetylation is suggested to strongly interfere with the regular functioning of the ubiquitination cascade, perturbing the formation of ubiquitin chains and altering its interactions with associated partners – showing its potential to modulate the events associated with protein ubiquitination.

### 1.2.2. Non-canonical ubiquitination

Since its first discovery as a modification of histones[3], ubiquitination has been extensively observed to form an isopeptide bond between the ε-amino group of a lysine residue and the carboxy-terminal of an ubiquitin molecule, making this residue the most common acceptor for this PTM[13].

However, within the cascade, ubiquitin can be attached to non-lysine residues, such as the active cysteines in E1 and E2 enzymes[16,18]. Cysteine residues being final acceptors of ubiquitin have also been observed, playing a role in diverse processes. The earliest observation was regarding modulation of the immune response by a viral E3 ligase responsible for the modification of cysteines in the major histocompatibility complex (MHC) sequence. As it happens with lysine

ubiquitination, this cysteine modification led to destabilization of its substrate, avoiding cytotoxic activity by host response and cell lysis[55]. Within the same pathway, ubiquitination of serine and threonine residues were observed to influence the activity of the endoplasmic reticulum-associated degradation (ERAD), ultimately influencing the stability of the modified protein[56]. Furthermore, cysteine modification was also associated with peroxisomal activity. The monoubiquitination of the receptor PEX5 was seen to be important for its recycling and to avoid its further modification by topologies that would lead to its degradation instead – so it can coordinate several cycles of peroxisomal loading[57].

As it occurs for lysine ubiquitination, DUBs can counteract the modification of alternative residues. In a non-lysine deubiquitinating profiling of active DUBs, the cleavage of isopeptide bonds from Lys was comparable to the activity against Cys/Ser/Thr. DUBs from several families (later detailed in section 1.5) showed no depletion of their activity when comparing lysine to non-lysine ubiquitination – with an exception of OTU DUBs, which are dedicated to target Lys-ubiquitin[58].

The expansion of the ubiquitin code also encompasses modification of non-protein substrates, as elucidate in recent years[59]. As example, a shared mechanism between yeast and mammalian involves the addition of ubiquitin to the terminal amino group of a phospholipid, phosphatidylethanolamine, using the same chemical strategy as in lysine residues. Of note, no specific enzymes within the ubiquitin cascade were observed to be necessary for this particular modification, since for all steps the enzymes involved were canonical E1, E2 and E3s[60]. In addition, the yeast DUB Doa4 – ortholog to mammalian USP2 – was noted to be able to remove the signal from this phospholipid[60].

Another facet of non-protein substrates is the modification of carbohydrates via an oxyester bond, similar to ubiquitin attachment to Ser/Thr residues[57,59]. Canonically related to formation of M1-linked/linear chains, HOIL-1 E3 ligase was reported to monoubiquitinate hydroxyl groups in glucose, which was phenotypically related to recycling of saccharides in cells to avoid damaging deposition of these molecules[61]. The association of the ubiquitin machinery to carbohydrates also led to the discovery of nucleic acids as substrates of the cascade *in vitro*. The E3 ligase DTX3L was characterized to add ubiquitin to hydroxyl group in both single-stranded RNA and DNA, although *in vivo* characterization is still needed to assess the functional outcomes of this modification[62,63].

In order to conclude, one very interesting example of the expansion of the ubiquitin code is the presence of ubiquitin cascade-like enzymes in bacteria, that are used in combination with mammalian host proteins during cellular infection. Some prokaryote enzymes are able to fully replace the eukaryotic machinery and attach ubiquitin independently of E1, E2 and E3s and without the cost of ATP. In addition, it does not use the terminal G76 residue, but instead uses R42 to conjugate the PTM to cysteine residues on the target protein[20,64], completely subverting the canonical activity of the ubiquitin machinery.

### 1.2.3. Ubiquitin-like proteins

The conjugation of a small protein as post-translation modification to control the substrate activity and the process it is involved in is not an exclusivity of ubiquitin. Several other ubiquitin-like proteins (UBLs) are present in eukaryotes, either being attached to a substrate or as part of proteins as a domain[65]. There are more than 10 different UBLs that are classified in 9 families: ATG8, ATG12, FAT10, FUBI, ISG15, NEDD8, SUMO, UFM1 and URM1 – some of them include more than one member, as SUMO, for example, which contains five members (SUMO1-5)[66].

In numbers, however, the abundance of UBLs and their substrates are far lower than the ubiquitin substrates. While SUMO is the best characterized family of UBLs, the number of identified substrates for this particular family is roughly ~10% of the identified for ubiquitin[65,66]. Furthermore, not all of them were reported to produce chains *in vivo* as for ubiquitin[65].

Their similarity with ubiquitin does not rely on the primary structure, as the amino acid sequence of UBLs is highly variable in comparison to ubiquitin. They, however, share a conserved 3D structure with ubiquitin, forming similar local secondary structures and in some cases the C-terminal GlyGly motif used for attachment to substrate[12,67].

The conjugation cascade for UBLs also relies on a three-step process that goes from activation to final attachment of the UBL to substrate. Although the usage of E2 and E3 enzymes tend to be shared between ubiquitin and UBLs, the set of E1 activating enzymes is particular to each type of small protein modification[16,65]. The only exceptions are UBA6 – serving as an E1 for both ubiquitin and FAT10 – and ATG7, shared between the two types of ATG UBLs, ATG8/12[16,65].

As ubiquitin, UBLs are also a reversible type of modification. The removal of the signal from the modified substrate can be performed either by a subset of DUBs able to recognize such

signals (UCHL3 and COPS5/CSN5 for NEDD8; USPL1 for SUMO; USP36 and USP16 for FUBI; USP5, USP14, USP16, USP18, USP21 and USP36 for ISG15) or by ubiquitin-like proteases (ULPs). Among ULPs, each kind of UBL has its own set of dedicated enzymes, without overlapping between groups. In comparison to DUBs, in which around 100 different enzymes are known to cleave the isopeptide bond either between substrate and ubiquitin or between two ubiquitin moieties, 16 ULPs are described, reflecting the differences in abundance between UBLs and ubiquitin itself[67].

## 1.3. E3 ligases: the writers of the ubiquitin code

The fine-tuned regulation within the ubiquitin system is based, ultimately, on knowing when to modify a substrate and how it should be modified, hence giving it proper destination, either that meaning changing its activity or causing alteration in its stability.

The crucial step in defining who and when should be modified is made through protein-protein interactions between the substrates and the most abundant group in the ubiquitin system, the E3 ligases, involved in the last step in the conjugation of ubiquitin to the substrate.

In order to control a strict time-wise regulation of substrate modification, mammalian cells have equipped themselves with more than 600 different E3 ligases – bioinformatic analyses have estimated a precise number of 634[68]. Differences in structure and catalysis mechanisms render a division of E3 ligases in four major groups: RING, HECT, RBR and RCR E3 ligases[69] (Figure 3).

### 1.3.1. RING E3 ligases

Really Interesting New Gene (RING) E3 ligases form the most diverse subset of ligases, encompassing more than 600 enzymes that can work as monomers, dimers (either mono- or heterodimers) and also multi-subunit complexes, as the Cullin-RING ligases (CRLs)[69,70]. The classification of an E3 into the RING group rises from two points: the RING domain, present in all members of the family, and the particular mechanism of action.

Regarding their activity, their mechanism of substrate modification is based on the approximation between an E2 enzyme and the substrate, which causes the ubiquitin molecule to be

directly transferred, without the intermediate conjugation to an active site in the ligase – U-box ligases, which have the same mechanism of action, sometimes are included on the RING group, depending on the reference[69,70].

The lack of catalytic activity is compensated by their ability to bind an E2 enzyme and to "trap" the ubiquitin-linked E2 into a stable conformation that, associated to the binding of the E3 to the target substrate through its substrate receptor domain or subunit, allows the direct transfer of the ubiquitin moiety to its final destination[71]. In this regard and considering only the chain extending E2s, they play a major role in determining the linkage of the chain produced[18]. They can either be linkage-specific, such as the APC/C-associated UBE2S that produces only K11-linked chains[18], or promiscuous, which in principle can form any kind of chain; for this latter group, the E3 interaction is pivotal for definition of the linkage, as it holds the E2 in specific conformations that bias the E2 attachment to certain lysine residues of the acceptor ubiquitin[72].

The vast majority of RING E3 ligases are within the CRL subgroup, accounting for around half of the total members and nearly 20% of all the ubiquitination that is catalyzed in cells[71,73]. CRLs are basically composed of one Cullin (CUL1-9), a scaffolding protein that brings the complex together, and a RING-finger protein (either RBX1 or RBX2) – containing the hallmark domain of the family and interacting with the E2 enzyme. In addition, they either have two more subunits – an adaptor protein, that links Cullin to the substrate receptor, and the substrate receptor itself, that interacts with the target to be modified – or only one more subunit that is able to bind to both Cullin and substrate[69,73,74].

The first kind of CRL to have its structure determined, and maybe the most known subtype, was an SCF complex, specifically the SCF(Skp2)[75]. SCF's are composed of CUL1, RBX1, SKP1 as the adaptor protein between substrate receptor and Cullin, and a F-box motif containing protein, which interacts with SKP1 and the substrate[75]. CUL3 complexes, on the other hand, do not have an adaptor protein, but the substrate receptors BTB are capable of directly interacting with Cullin, due to a level of homology with SKP1[74].

One interesting remark about CRLs is the fact that the complexes themselves are modified by a PTM that highly stimulates its activity. Neddylation of Cullins, i. e. the modification of those subunits by the UBL NEDD8, is a conserved mechanism of activation of CRLs from fungi to humans, facilitating the interaction between Cullin and the RBX protein, which leads to interaction

with the E2 enzyme[74]. Although not necessary for their activity, it was seen to stimulate CRL1 (CRL based on CUL1) activity by 2000-fold[76].

### 1.3.2. HECT E3 ligases

Originally discovered by observation of the mechanism of infection by the human papillomavirus (HPV) that, together with the host E6-AP (nowadays known as UBE3A), targets p53 to proteasomal degradation, members of this family possess a unique structural feature in which all E3s contain a domain that is homologous to the E6-AP C-terminus (HECT), hence giving this family its name[77].

Differently from the RING family, the 28 members of the HECT group do not only recruit substrates and bring them to the proximity of E2, but form an intermediate state during the ubiquitin transfer in which they are covalently attached to ubiquitin itself through a thioester bond, later proceeding into transfer of the protein onto its target[77,78]. As the upstream enzymes in the ubiquitination cascade, these ligases possess a catalytic cysteine residue within their C-terminus that is responsible for this intermediate step in the process of substrate modification[69].

While their C-terminus lobe is a hallmark of the family by being the catalytic core of the enzyme, the N-terminus of these proteins is the binding domain, responsible for interaction with a ubiquitin-charged E2, when the ubiquitin moiety is transferred to the C-terminus lobe, and later for interaction with the respective substrate[78]. Furthermore, depending on the architecture of the N-terminus lobe, HECTs can be further subdivided into 3 groups: NEDD, HERC and the "other HECTs"[69,78].

All the 9 members of the NEDD subgroup are characterized by their C2 domains, which can bind to $Ca^{2+}$ ions and to phospholipid membranes, and the multiple WW domains, which contain tryptophan residues usually separated by circa 20 amino acids and that recognize their substrates by means of PPxY motifs (x indicating any residue)[69,78,79]. HERC, on other hand, share a common RLD (regulator of chromosome condensation 1 (RCC1) protein-like domains) among its 6 members in their N-terminal domain[78,79]. Lastly, the 13 HECT E3s that do not contain any of these specific domains but instead only share the typical HECT domain in their C-terminus are called "other HECTs"[78].

Another major difference from RING E3s is regarding the lysine specificity of these E3s when building ubiquitin chains. As discussed, RINGs rely heavily on E2s to determine, together, the chain produced. Alternatively, given that HECTs have a previous step when they covalently bind to ubiquitin, these E3s are the main enforcers of the conjugation that happens on the substrate, through means of their C-terminus lobe[18,80]. Therefore, different HECTs will have different linkage preferences – such as K48 for UBE3A, K63 for the NEDD4 enzymes or K29 for TRIP12[69,81]. Chimeric enzymes, in which the natural occurring HECT domain was substituted with a different linkage preference one, were seen to change the chain type formed in comparison to the wild type version[82].

An interesting remark about HECTs is regarding the regulation of their activity, which frequently occurs via protein-protein interactions, either within the same molecule, by formation of multimers of the same ligase or by attachment of co-factors. A baseline state of auto-inhibition is observed for ITCH and SMURF2, members of the NEDD subgroup. For ITCH, two WW domains directly interact with the HECT region, inhibiting the enzyme, which only goes to its active mode once the region between the C2 domain and the first WW is phosphorylated[83,84]. SMURF1 has a different relieving mechanism: its auto-inhibited form comprises a homodimer in which each C2 domain interacts with the HECT of the other molecule. By attachment of co-factors, it becomes monomeric and active[84,85]. Inorganic co-factors can also control the activation of HECTs; NEDD4 enzymes (NEDD4-1 and NEDD4-2), for instance, are inhibited by intramolecular interactions of the C2 domain with the HECT and, in presence of $Ca^{2+}$ ions, those bind to C2 domains and the ligase is activated[86].

### 1.3.3. RBR, RCR and RZ E3 ligases

RING-in-between-RING (RBR) family of E3 ligases form an intermediate structure and activity mode in relation to RING and HECT families[69]. Structurally, the 14 members of this family contain two RING domains separated by an IBR (in-between-RINGs) domain[87]. Although they use the RING1 domain to recruit ubiquitin-loaded E2s, their mechanism of action is dependent on the formation of a thioester bond between the RING2 domain and ubiquitin before the final transfer to the substrate, which resembles the catalytic property of HECTs[69,70,87]. Two of the main enzymes within the group are Parkin and HOIP: Parkin is central in coordinating events related to mitophagy

(as discussed in section 1.2.1), while HOIP – within the context of the LUBAC complex – is the main associated E3 ligase to the M1-linked/linear ubiquitin chains[88]. Similarly to HECTs, they can also undergo structural inhibition by other domains of their architecture, being released under specific conditions – for Parkin, for example, binding of phospho-Ub (Ser65) and its own phosphorylation at Ser65[88].

The RCR (RING cysteine relay) family of ligases utilizes an extended mechanism to those observed in HECTs and RBRs: not only it forms an intermediate species covalently binding a catalytic cysteine to ubiquitin but it extends the concept by possessing two catalytic cysteine residues that form a sequential two-step process before ubiquitination of final substrate[69,89]. The main protein in this group, MYCBP2, has been found to be involved in neurological development and maintenance from *Caenorhabditis elegans* to humans[90]. Although much is still open to understand about the activity of this group, MYCBP2 has an interesting feature of being selective for non-canonical ubiquitination, as it is an esterase targeting threonine residues[91].

Finally, the RZ family is still an emerging topic among E3 ligases, as the characteristic moiety for the group was only reported in 2021 from its best described member, RNF213, the largest E3 in humans[92,93]. This moiety encloses one primary sequence similar to a zinc-finger containing protein, which suggests a possible coordination with $Zn^{2+}$ ions – in addition, mutations within this region abolishes the ligase activity[92,93]. So far, their activity has been related to regulation of response against bacterial infection, being essential for recruitment of other complexes related to immune activity, such as the LUBAC ligase; furthermore, it has been observed to be able to ubiquitinate bacterial lipopolysaccharide (LPS) and to add ubiquitin in non-canonical residues such as serine and threonine[69,92,93].

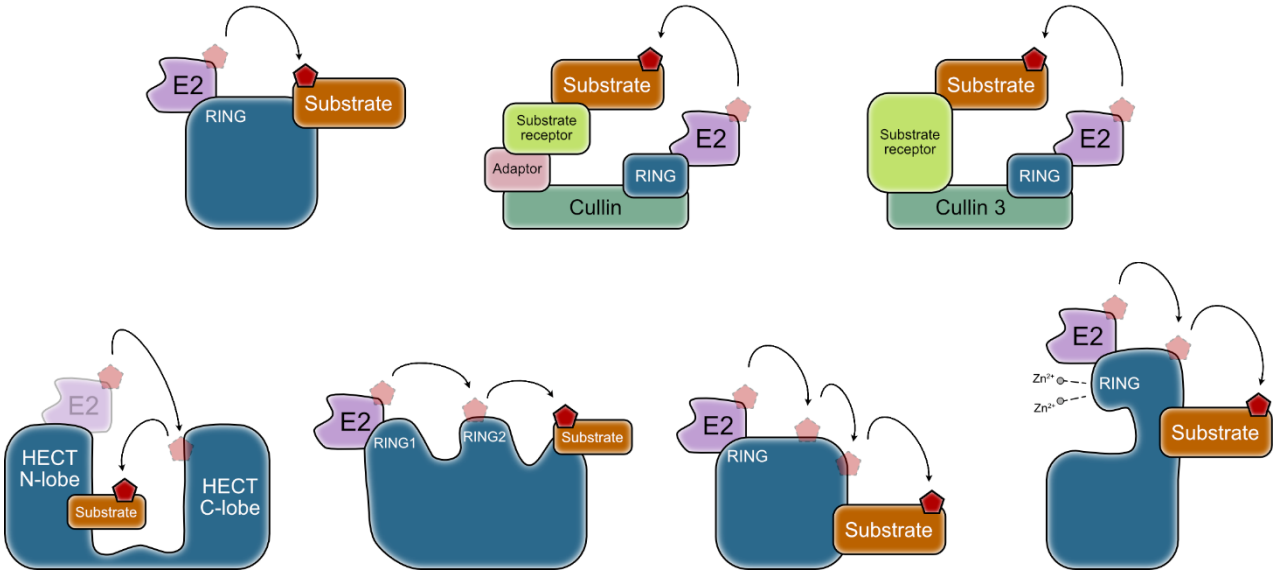


Figure 3: E3 ligase families and their basic mechanism of action.
From left to right and top to bottom: monomeric RING ligase; CRL RING (excluding CUL3-based) ligase; CUL3-based CRL RING ligase; HECT ligase; RBR ligase; RCR ligase; RZ ligase.

## 1.4. Ubiquitin binding proteins: the readers of the ubiquitin code

Ubiquitination of substrates, per se, does not generate an inherent signal that is capable of altering the substrate stability or cellular localization by itself. For that, the modification must be recognized and translated into an effective signal that will, ultimately, generate the outcome associated with it. Examples are the proteasomal-targeted K48 chains or the K63 within DNA damage repair; if there is no reader of this signal, downstream processes will not take place.

In order to recognize these signals, cells employ ubiquitin-binding domains (UBDs), which are not yet fully characterized, both quantitatively and qualitatively. There are around only 20 different types of UBDs known that are observed in different proteins, while few more are only encountered in unique factors. On top of that, the number of human proteins that contain UBDs is, by far, lower than the number of human E3 ligases, consequently lower than the number of ubiquitin-modified substrates[94,95].

The most common ubiquitin feature used by UBDs to recognize and bind ubiquitin is a hydrophobic patch on the protein surface around the residue Ile44, also encompassing residues

Leu8 and Val70[96]. This area, however, is not the only surface used for ubiquitin recognition: the surface in which residues Ile36, Leu71 and Leu73 are present is used to mediate the interaction between an E2 enzyme and a HECT-type E3 ligase, necessary for the ubiquitin transfer to the catalytic cysteine of the E3[97]. In addition, polar residues can also be recognized, as it is the case of the deubiquitinase A20, which uses the Asp58 residue to contact ubiquitin, alongside the Ile44 patch – interactions that are mediated through different UBDs in A20[96].

Given that ubiquitin itself, as a protein, can also be target of PTMs, its modification alters its interaction landscape due to variations in proteins and UBDs that are able to recognize modified ubiquitin. A study showed, for example, that phosphorylation of ubiquitin can induce conformational changes in its structure that causes a reduced binding to ubiquilin-1 UBA (ubiquitin-associated domain), one of the strongest UBD known[98].

When it comes to recognition of ubiquitin chains, different architectures on UBDs can also dictate their preference towards type of chain recognized. The UBAN domain, as an example, was the first to be characterized as a highly specific binder of atypical M1-linked ubiquitin chains; the UBD structure that forces interaction with C-terminus region of ubiquitin, plus protein dimerization, gives its specificity[99]. Even though most UBDs do not have an intrinsic linkage preference, this can be achieved by varied strategies. First, by using multiple binding sites that contact different ubiquitin moieties at the same time, restricting the chain architecture that can be bound; second by using other regions that enhance the binding towards a certain kind of chain, although isolated they would not have a preference; or third, by having more than one contact point in ubiquitin that only allows a certain type of chain to be tightly bound[100]. In case of UBDs that have specific chain preferences, a common mechanism is conformational alteration when in presence of the specific chain, either altering the UBD structure given the recognition or altering ubiquitin conformation[100].

One of the most common UBDs is the zinc finger domain (ZnF), a simple local conformation containing four β-strands that coordinates $Zn^{2+}$ ions and binds ubiquitin through the Ile44 hydrophobic patch[101]. This kind of fold is present in many domains – and many proteins – that, for example, contain the NZF domain (Npl4 ZnF), a structural feature identified in nuclear protein localization 4 (Npl4 in yeast, NPLOC4 in mammalians), from which the name derives[96,101].

In mammalians, NPLOC4 was characterized as forming a heterocomplex with UFD1L (UN) and p97. In this context, UN was seen involved in ubiquitin degradation pathway, and since most

of the endogenous staining of NPLOC4 was observed in the nucleus, the report suggested that it was involved with ubiquitin homeostasis in the nucleus. Later, it was shown NPLOC4 is the main responsible for ubiquitin binding within UN, in an NZF-dependent manner but without restricted linkage preference, since it was observed to bind both K63- and K48-linked chains[102–104].

### 1.4.1. Valosin-containing protein (VCP)/p97

Valosin-containing protein/VCP or p97 (Cdc48 in yeast) is a member of the AAA+ (ATPases associated with a variety of cellular activities), a class of proteins that shares a mechanism of cleaving ATP in order to perform mechanical activities in the cell. VCP is an extremely conserved protein across all domains of life, spanning from bacteria, archaea and all eukaryotes up to humans – with a sequence homology that can reach around 60% between the latter groups[105]. In addition, in some eukaryotes its abundance goes up to 1% of all proteins in the cytosol[106].

A common feature of AAA+, which is shared by VCP, is the formation of a ring-shaped structure that contains six monomers in a single complex that keeps a central opening in this barrel-like structure used for substrate translocation[106]. VCP contains four domains, the N-terminal (N-domain), followed by two sequential ATPase domains (D1 and D2) and the C-terminal domain. While D1 and D2 form two rings stacked on top of each other – D1 on top and D2 below –, N-domain has a higher flexibility due to the N-D1 linker, capable of adopting both a co-planar conformation while VCP is bound to ADP and an "up-conformation", above the D1 ring, when it is bound to ATP. D1 and D2 have the ability of hydrolyzing ATP, but the enzymatic activity of D2 is higher, while D1 is more related to the oligomerization of the hexamer. The N-domain works as a regulatory region of VCP, being able to control the ATPase function by its flexibility and to mediate interaction with ubiquitinated substrates and co-factors. Lastly, the C-terminal domain regulates both co-factor binding and the hexamer stability, being also necessary for its full enzymatic activity[107].

VCP is a major player within the ubiquitin-proteasome system (UPS). Its main activity is the recognition of ubiquitinated proteins and mechanical translocation of those through its central pore, unfolding these substrates and facilitating recognition and degradation by the proteasome. The main functions of VCP are linked to extraction of ubiquitinated substrates from cellular structures, which widely vary: a very well characterized pathway is ERAD, the endoplasmic

reticulum-associated degradation, in which proteins synthesized in ER that fail to properly fold become substrates of VCP and degraded by the proteasome[106]. In addition, VCP activity plays a role in ribosomal quality control, sensing aberrant translation and also stalling of ribosomes due to toxic stimuli that leads to crosslinks between proteins and RNA[108,109]. VCP can also extract proteins from the outer mitochondrial membrane for degradation, control the NF-κB signaling pathway by sending to proteasomal degradation inhibitors of the pathway and control formation of cellular endomembrane system[106]. Another cellular structure that is highly dependent on VCP for timely extraction of proteins is the chromatin. Several chromatin-related processes are seen to depend on the unfoldase activity of VCP, such as cell cycle, transcription and DNA repair[110–112].

Surprisingly, VCP itself has a low affinity for ubiquitin, so in order to recognize the PTM, it uses a panel of co-factors and associated proteins for binding, forming a multimeric heterocomplex[106,108]. The earliest reports about VCP co-factors showed a mutually exclusive interaction of VCP with either p47 or the pair UFD1L/NPLOC4[102,103]. More than 30 different co-factors, or adapters, have been described, commonly exhibiting a VCP-interacting domain that links them directly to the unfoldase. The interaction of some adapters to VCP, however, is also described to be dependent on other co-factors, such as the case of FAF1, that depends on UFD1L-NPLOC4 heterodimer to bind to VCP[113,114].

VCP adapters encompass a high functional diversity among the ubiquitin system; interaction with VCP not only means that these co-factors are able to recognize and bind ubiquitin but often are capable of modifying the substrates themselves. Within this subgroup, E3 ligases as CHIP, HOIP and UBE4B are found; in addition, different deubiquitinating enzymes are seen as VCP adapters, such as ATXN3, OTU1 and VCPIP1[113].

## 1.5. Deubiquitinases: the erasers of the ubiquitin code

One of the features of the ubiquitin system that makes it extremely resourceful as a controlling mechanism in several processes is its reversibility. The attachment of the PTM, either as single monomer or forming chains, is not a final sentence for its fate, either in terms of activity or in terms of stability. For that, another layer of control of ubiquitinated substrates is the removal of the signal, a task that is performed by deubiquitinating enzymes (DUBs).

The very own pool of free ubiquitin within the cell that is used to modify targets is maintained by DUBs. Ubiquitin protein synthesis does not occur by translation of individual molecules that become immediately available for activation and attachment – instead, it happens in a way that they are translated in tandem (either exclusively with other ubiquitin molecules or with ribosome subunits – Figure 1), which requires ultimately DUB activity to release ubiquitin moieties to be incorporated into the cascade[11,12,115].

Evolutionary distribution of DUBs varies significantly across organisms; for example, *Saccharomyces cerevisiae* has around 20 different enzymes, while this number increased strikingly for humans, that have around 100 DUBs expressed in cells[116,117]. Even though the ubiquitin system and cascade as we know was introduced in evolution from the eukaryotic emergence, bacteria also have related enzymes that can exert functions on the ubiquitin system, especially when interacting with defense mechanisms and guaranteeing a successful installation within host cells[118]. As one example, bacteria employ a family of enzymes called clippases, functionally similar to DUBs but with a very particular difference: instead of cleaving the bond between ubiquitin Gly76 and acceptor residue, they cleave between Arg74 and Gly75 of ubiquitin, making it not available for next round of conjugation due to removal of terminal GlyGly and leaving this remnant on the substrate acceptor residue[118].

Although sitting on the opposite side of the spectrum within the ubiquitin system, a pairwise activity between DUBs and E3 ligases often takes place to modulate cellular processes. Mass spectrometry approaches established consistent interactions between the two classes of enzymes, showing that this kind of phenomenon is not an isolated case, but instead a common event within cells[119]. Several examples of this association are known, either in which they form a pair that synergistically enhance each other or in a situation where they generate opposing outcomes. In the case of the MDM2-USP7 axis, the DUB USP7 counteracts the auto-ubiquitination of MDM2, stabilizing the ligase; the same relationship is seen between USP15 and CRL3(KEAP1), in which the USP15 removes the self-added ubiquitin on the ligase. On the other hand, in some cases the E3 destabilizes the DUB. PCNA is a substrate of USP1, and it is deubiquitinated by this enzyme. Upon DNA damage signaling – an event that triggers and requires PCNA ubiquitination –, USP1 can cleave itself by recognition of an internal GlyGly motif; this, however, leads to recognition by the E3 ligase CRL(KLHDC2), sending USP1 to degradation. Another example is OTUD5, which can remove ubiquitin from the E3 ligase UBR5 and stabilize its levels. In turn, ubiquitination of the

DUB by UBR5, in conjunction with a second E3, TRIP12, leads to OTUD5 proteasomal degradation[40,120].

DUB classification can occur through two different parameters: according to their catalysis mechanism or depending on their domain architecture (Figure 4). Firstly, looking at their catalysis mechanism, they can be divided into either metalloproteases, which require a coordinated $Zn^{2+}$ ion for the breakage of isopeptide bond, or cysteine proteases[121]. Although the sequence identity between DUBs may not be high and members within the same group would have very low sequence homology, the catalysis mechanism is well conserved and involves similar strategy between different enzymes, due to spatial arrangement of residues that participate in the catalysis.

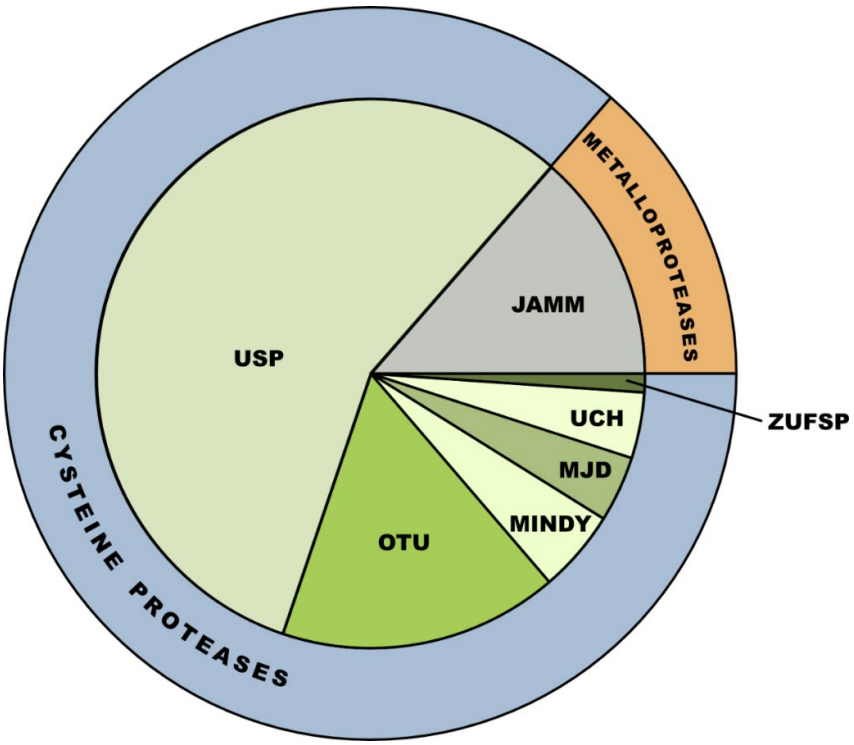


Figure 4: Distribution of mammalian DUBs according to catalysis mechanism and domain architecture.

## 1.5.1. Metalloproteases

The metalloproteases have a complex mechanism that involves several residues acting in concert with an inorganic factor. Two histidine and one aspartate residues coordinate one $Zn^{2+}$ ion; in addition, glutamate and serine residues also participate in the reaction. First, the zinc ion and

glutamate lateral chain stabilize a water molecule, which attacks the isopeptide bond and is hydrolyzed into a proton and a hydroxyl group. The proton is absorbed by glutamate lateral chain, which later deprotonates. The unstable intermediate is stabilized by the serine lateral chain until the hydroxyl group covalently replaces the isopeptide bond, causing the release of both ubiquitin moieties – interestingly meaning that this enzyme never form a covalent bond with ubiquitin[121].

The metalloproteases are all included in a single family, the enzymes with JAB1/MPN/MOV34 (JAMM) domains. There are 14 metalloprotease members and although the characteristic of the family is the coordination of zinc ions to perform their catalytic activity, reports suggest that only half, meaning seven members, are capable of coordinating the inorganic co-factor and, out of those, only six have ability to perform catalysis ($MPN^+$, opposite to the inactive $MPN^-$)[117].

Within the JAMM family, one of the most well studied enzymes is PSMD14/POH1 (or Rpn11 in yeast). PSMD14 is one of the three DUBs present at the lid of the proteasome, part of the 19S particle – and the only of those that is essential for whole proteasomal assembly –, responsible for controlling the entrance of clients into the proteolysis complex of the 20S core particle[115,121]. Although it does not bind or cleave ATP, the coupling to the AAA-ATPases present in the proteasome machinery are the source of energy for DUB activity[19]. Within the proteasome, PSMD14 is found in partnership with another JAMM member, the pseudo-DUB PSMD7 ($MPN^-$, Rpn8 in yeast). The dimer formation between PSMD14 and PSMD7 is essential for the full enzymatic activity of PSMD14, which only occurs when the 19S is integrated into the proteasome[122]. Interestingly, when associated with the proteasome, the spatial conformation that is adopted by PSMD14 suggests a removal of the ubiquitin molecules attached to the substrate as a block, cleaving the isopeptide bond between the substrate's lysine and the proximal ubiquitin molecule; moreover, the catalytic depletion of PSMD14 activity (by depletion of its levels or mutations in its active site) leads to a stalling in the insertion of ubiquitinated proteins into the proteasome, clogging the complex and reducing its ability to degrade modified substrates[19,117,121,123,124].

Just as the PSMD7/14 dimer that controls proteasomal activity, members of the JAMM family tend to be present in $MPN^+/MPN^-$ dimers, in which the non-catalytic member works as an allosteric activator of the catalytic one. Several other pairs have been described, such as subunits of the BRCA1-A complex and BRISC complex (BRCC36-ABRAXAS1/2, regulating DNA repair

and interferon signaling) or subunits of the COP9 signalosome (CSN5/6, regulating UBL PTMs as the activation of cullins in CRLs)[122,125].

## 1.5.2. Cysteine proteases

Cysteine proteases, as the name suggests, have a cysteine catalytic residue positioned within a group of three essential amino acids that allow breaking the bond between ubiquitin C-terminus and the upstream molecule[126]. Alongside cysteine, they contain one histidine and one residue that stabilizes histidine (often aspartate or asparagine)[121]. The catalysis occurs in a very straightforward manner, as the active cysteine attacks the isopeptide bond and the electrons released are absorbed by the histidine residue, which later receives a proton from a water molecule that is hydrolyzed to dissolve the bond between the cysteine and the carboxy terminus of ubiquitin, allowing the enzyme to be available for subsequent reactions[121].

The classification regarding domain structure divides the cysteine proteases into further 6 families (number of members in mammalians indicated): zinc finger with UFM1-specific peptidase domain (ZUFSP, 1 member), ubiquitin C-terminal hydrolase (UCH, 4 members), Josephin (4 members), MIU-containing novel DUB family (MINDY, 5 members), ubiquitin specific protease (USP, 58 members) and ovarian tumor related protease (OTU, 17 members)[117,125].

### 1.5.2.1. ZUFSP family

The newest family, and also the smallest, is the ZUFSP, which takes the name from its sole member. The enzyme was originally thought to be an inactive UBL peptidase, specifically UFM1 targeted. However, it contains the catalytic triad common among cysteine proteases (Cys, His and Asp) with an auxiliar Gln residue for the catalysis. Structural analysis of ZUFSP showed that the carboxy terminus of ubiquitin is able to sit within its catalytic domain, while UFM1 suffers from steric hindrance, thus the original conception that it was an inactive enzyme.

It was seen to be evolutionarily conserved, being present from yeast to humans, and to target specifically K63-linked, preferably containing four or more moieties. Given that, among other functions, K63-linked chains are an important signaling platform in DNA damage and DNA repair events, ZUFSP was tested in this context and seen to be involved in replication stress response,

interacting with RPA1 and possibly being involved in processes of genome stability maintenance[127,128].

### 1.5.2.2. UCH family

The UCH family contains four members – UCHL1, UCHL3, UCHL5 and BAP1[115], in which all members are linked with disease development.

UCHL1/3 were seen in high abundance within cells and the isoform 1 is one of the most abundant brain proteins, being highly associated with several neurological disorders and degenerative diseases[121]. Earlier reports from these two enzymes showed their relation with the processing of pro-ubiquitin genes, specially by co-translational cleavage of the tandem ubiquitin repeats (for UCHL1) and the fusion with ribosomal proteins (for UCHL3)[129]. UCHL3 has also been associated with cancer treatment resistance and DNA damage repair, as it is a target of one of the major kinases in the process, ATM, and reported to deubiquitinate RAD51, causing its binding to BRCA2[130].

A third member, BAP1, is the most common DUB mutated in cancer and its loss of function correlates with poor prognosis in malignant cancers[121,131]. On top of that, it was seen to be active towards one of the main ubiquitination signals in the nucleus, the histone H2A modification on Lys119, in a mechanism conserved from *Droshophila* to humans and that requires association with a co-factor – Asx in *Drosophila* and ASXL1 in humans.

Interestingly, association with co-factors is a common feature of UCH DUBs and exemplified further in the fourth member, UCHL5. It is involved in the regulatory particle of the proteasome, being the most active within the triad DUBs (requiring RPN13/ADRM1 as an allosteric activator[115]), although it is not a mandatory protein – as seen in *S. cerevisiae*, which contains no ortholog for this protein[19,121]. Even though earlier reports suggest that its DUB activity within the proteasome could avoid protein degradation and rescue the modified protein levels[19,117,132], recent evidence show that the trimming activity of UCHL5 against specifically branched chains enhances proteasomal activity[133].

### 1.5.2.3. Josephin family

The Josephin group consists of four enzymes, namely ATXN3, ATXN3L, JOSD1 and JOSD2, all exhibiting the catalytic Josephin domain that gives the name of this family[117]. Moreover, the name of the domain derives from the spinocerebellar ataxia type 3 (SCA3), also known as Machado-Joseph disease, a type of neurodegenerative disease associated with a CAG nucleotide expansion that generates poly-glutamine (polyQ) repeats in the protein sequence, such as Huntington disease (HD)[134]. In the case of SCA3, the gene in which the polyQ expansion happens is ATXN3, one of the DUBs in the family[121]. As in HD, the phenotypical outcome of the polyQ expansion of ATXN3 is the generation of protein aggregates, which in turn leads to cytotoxicity and eventually to neuronal cell death[134].

The Josephins can be separated into two subgroups within the family: ATXN3 and ATXN3L in one, JOSD1 and JOSD2 in the other. The difference between these two groups is the presence of ubiquitin-interacting motifs (UIM) in ATXN3 and ATXN3L (three in the former, two in the latter), while JOSD1/2 do not present those[135]. Evolutionarily speaking, these two groups seem to have arisen from two ancestral metazoan genes and duplications are suggested to have generated the four individual proteins present in humans – duplication event for *JOSD* ancestral happening during the emergence of jawed vertebrates and for *ATXN3* in primates[136].

ATXN3 is best described member of the family and shares a high sequence similarity to ATXN3L, with both being suggested to have *in vitro* activity against K63- and K48-linked ubiquitin chains. In terms of deubiquitinase activity, ATX3L was seen to have a higher catalytic activity, a property that was equalized when mutations were introduced in ATXN3 sequence and enhance it, which could suggest an evolution pressure on ATXN3 when duplication generated ATXN3L[137].

The ubiquitin linkage preference of ATXN3 has recently been put in perspective of branched chains instead of homotypic[138]. It was seen to have a much higher activity toward branched K63/K48 chains (containing at least 4 moieties) by cleaving the K63-linked portion and to associate with VCP, which would work downstream for recognition of K48-modified substrates[138].

Cellular activity of ATXN3L is not well understood, although it also targeted K63- and K48-linked chains *in vitro* and knockout of ATXN3 showed no visible phenotypes in animal models, which was suggested to be due, at least partially, to redundant activity with ATXN3L. In accordance to this hypothesis, ATXN3L was linked to regulate expression of the *PTEN*, similarly to ATXN3[137].

The second subgroup within the Josephin family is composed of two very similar enzymes, both from a primary structure perspective and in regard to domain architecture. Both have the family hallmark domain, the catalytic Josephin, however they lack, in comparison to ataxins, the UIM towards the enzyme C-terminus[135]. On the other hand, their cellular distribution and activation mechanism indicate their role does not overlap completely: while JOSD1 requires itself a ubiquitination to be active, this is not seen in JOSD2; in addition, when active JOSD1 is shuttled to the cell membrane, while JOSD2 is cytosolic[130,135].

A remarkable consideration about JOSD1/2 is their ability to cleave non-canonical ubiquitin from their substrates. Although these two members are the least described within Josephins, a recent non-lysine ubiquitination screen identified both with a high activity towards threonine- and serine-modified residues. On top of that, JOSD1 seems to have exclusively esterase activity (with suggestion it could be even more active towards cysteine modification in comparison to threonine-ubiquitin), while JOSD2 is capable of equally cleaving isopeptide and ester bonds, without noticeable differences[58].

#### 1.5.2.4. MINDY family

The five proteins within the MINDY family were described as the first deubiquitinating enzymes to contain motif interacting with ubiquitin (MIU), making them unique and a separate DUB family[117,139] – the same motif was later seen to be present also in the ZUFSP family[127].

Highly conserved within eukaryotes, members of this family exhibit an interesting variation in the cysteine proteases catalytic mechanism: instead of the common aspartate or asparagine residues that usually are found to stabilize the histidine in the triad, MINDY1/2 have a threonine residue that plays the role as the third residue within the catalytic core. As expected, mutation of this residue, in similarity to mutations of Cys/His, leads to disruption of their activity[140].

Out of the five members, four of them exhibit catalytic activity while MINDY4B is predicted to be a pseudo-DUB based on structural analysis[19]. On top of that, the four active members show a high specificity towards K48-linked chains, with a high preference of long ubiquitin chains and the almost lack of activity of MINDY1 when in presence of di-ubiquitin peptides[117,139].

Given its enhanced binding and cleavage of long chains, MINDY1 and MINDY2 were originally thought to be exo-DUBs, meaning they would trim the chain from the distal moiety

towards the proximal, with neglectable activity with shorter chains. However, further analysis showed that structural features of the enzymes make them able to bind to several ubiquitin moieties at the same time but to cleave the chain in a way to remove blocks of ubiquitin molecules, which would classify them as endo-DUBs[139,140]. This observation goes in line with the activity of the yeast ortholog of MINDY1, Miy1, which shows no preference for either exo- or endo-deubiquitination[139].

An interesting feature that separates MINDY2 from MINDY1 is that even though the cleavage activity is preferential towards K48-linked chains, its MIU binds to any kind of monotypic chain, in contrast to high selectivity of MINDY1 MIUs to K48. This observation led to the hypothesis that maybe MINDY2 would be able to recognize branched chains[141]; indeed, all the four active MINDYs were reported to cleave K48-linkages out of branched tetramers containing both K63/K48 isopeptide bonds – while no activity was observed towards other branches, such as K48-K11 or K48-K29[138].

#### 1.5.2.5. USP family

As the most abundant type of DUBs present in mammalians, with 58 enzymes containing the USP domain, the ubiquitin-specific protease family is involved in a plethora of processes within the cell, controlling the ubiquitin signaling in different compartments – and changing the outcome of the modified substrate in a high variety of events[115,117].

Description of USPs catalytic domains was first made for USP7 (or HAUSP), when authors observed a subdivision of the domain in three regions that were called Fingers, Palm and Thumb by the conformation they adopted in a substrate-free state. The intermediate region between Fingers and Thumb would comprise the ubiquitin binding area, while the boundary between Palm and Thumb would have the active cysteine within the catalytic cleft[142]. A finding that was observed back then and recently noted again – not only for USPs but also for other families, as MINDYs – is the structural differences between substrate-free and substrate-bound states for these DUBs. When in absence of ubiquitin binding, the catalytic triad residues sit far apart, not inferring any possibility of combined activity; on ubiquitin binding, however, a major structural change occurs so they come spatially together to accommodate the substrate and perform the isopeptide bond cleavage[142–144].

Although sharing the USP domain and the cysteine protease activity, structural features and catalysis mechanisms also vary among the family. The change in conformation observed for USP7 is observed in other members, such as USP40, but not a rule for all enzymes; USP15, for example, does not need ubiquitin to bring together its active residues, while USP4 does not have this misalignment in a substrate-free state[144].

In addition, there are some variations in terms of the residues that play a role in the catalysis for different members of USPs. As USP7 was the first description of the family, its three residues were taken as a hallmark for the whole family in terms of deubiquitination, although USP1 and USP48, as examples, require a fourth residue to perform its catalytic activity while USP15 behaves normally even in the absence of the third residue in the triad – of course, still requiring a Cys and a His residue to be active[144].

In general, USPs are seen to be non-selective enzymes, being able to target any kind of ubiquitin linkage chains. This is exemplified by USP16, which can cleave virtually all seven Lys-linked chains plus the linear type, and USP2, which recognized and use as substrate the seven internal linkages and is also able to recognize branched K63/K48 chains[138,145,146].

On the other hand, some members do show certain preferences in terms of linkage, with an example being USP30. In the context of mitophagy and ubiquitination of mitochondria by Parkin (discussed previously in section 1.2.1), USP30 counteracts Parkin activity, leading to diminished levels of mitochondrial recycling. This enzyme shows a marked preference for K6-linked chains – which is suggested to be due to preference binding to this type, although the catalytic domain is able, up to a certain degree, to digest other types of ubiquitin chains[147,148].

Furthermore, USPs can also cleave the proximal ubiquitin molecule tagged directly to the substrate. Controlling nuclear events related to DNA damage response, USP22 (subunit of the SAGA complex) can remove the monoubiquitination on histone H2B after double-strand breaks, allowing the signaling cascade to proceed[149]. In addition, USP1 has been reported to be able to counterbalance mono-ubiquitination of both FANCD2 and PCNA, respectively regulating cellular response to DNA interstrand crosslinks and the activation of translesion synthesis pathways after DNA damage[150,151].

Recycling of ubiquitin is also a process in which USPs are involved. USP3 and USP5, for example, are able to recognize unanchored ubiquitin chains through their terminal GlyGly motif and cleave the isopeptide bonds, impacting the control of signaling pathways but most importantly

the maintenance of free ubiquitin molecules available for conjugation, avoiding their depletion[19,152].

Lastly, a USP enzyme is the third member within the DUB triad that composes the 19S regulatory particle of the proteasome. USP14 was reported to remove ubiquitin signal from substrates in form of blocks, by cleaving the direct link between substrate lysine residue and the proximal ubiquitin. This event was seen to happen only to reduce the amount of ubiquitin chains present in an exemplary substrate modified in several lysine at once, independently on the linkage. In concert with PSMD4, this catalysis would facilitate the substrate entrance on the proteasome barrel[19,153].

#### 1.5.2.6. OTU family

The name of the family derives from a gene originally identified in *Drosophila melanogaster* as essential for oogenesis in that organism, named ovarian tumor (*Otu*). During characterization of the gene, it was noted a region that encoded for a domain of around 130 residues that were conserved from yeast to humans[154].

Today, we know 18 genes in humans that contain this domain, 17 of those that code for proteins and 16 of those that have the hallmark catalytic triad of the cysteine protease DUBs[155]. The different sizes of the OTU domain within the members can separate them into three groups: the OTUD, in which the hallmark domain ranges around 150 residues; otubains and OTULIN, where the catalytic domain has around 250 residues; and the A20 subgroup that has the biggest OTU domain, with a residue count higher than 300 amino acids. Phylogenetically, though, the otubains and OTULIN are individual groups, forming in total four subgroups among OTU enzymes[19,155].

An *in vitro* analysis of all the active deubiquitinases in the family revealed a marked characteristic: the members possess a high level of specificity in terms of the ubiquitin linkage they target for cleaving. When in presence of di-ubiquitin of all the 8 possible linkages, more than half of the family exhibited cleavage of only one or two types, showing that not only they have linkage restraints, but also different members have different directed specificities. On top of that, only one member was able to cleave linear chains, showing that the vast majority of the family prefers to cleave isopeptide bonds[155].

The striking ability of different members having particular preferences towards one or few kinds of linkages even led to the development of new tools for assessing the ubiquitin system by employing OTU enzymes. This is highlighted in UbiCRest, a panel of 9 DUBs, in which 7 are humans OTU DUBs, containing varied linkage preferences, enabling the evaluation of the linkage types that modify a certain substrate[156].

Preference of OTU DUBs towards specific linkages may arise by two independent manners, either by usage of ubiquitin binding domains that enhance their binding to certain chains or by the positioning of individual ubiquitin moieties along their structure in a way that imposes the cleavage between specific residues[116]. Interesting examples show these two different mechanisms: 1) OTUD1 contains two main ordered regions within its structure, the OTU catalytic domain and a ubiquitin-interacting motif (UIM), both close to the C-terminus of the enzyme. Cleavage analysis of the isolated OTU domain shows a lower processivity coupled with non-specificity in terms of linkage, which is generated by UIM; 2) OTULIN and Cezanne were the first enzymes identified with a high cleavage preference for linear and K11-linked chains, respectively. Even though in a substrate-free state, OTULIN structure is very similar to OTUB1 (a K48 specific DUB), OTULIN binding to a ubiquitin chain occurs in a way that the only linkage that positions the GlyGly terminal motif close to the active site is M1; Cezanne, on the other hand, strikingly changes its conformation only in presence of K11-linked ubiquitin molecules, leading to its catalytic activity[116,155,157–159].

OTULIN and Cezanne examples are also interesting to highlight the different contexts in which OTU DUBs play their role. By cleaving M1 chains, OTULIN acts as a balance to the chain-forming activity of LUBAC that, through a signaling cascade involving ubiquitination of other factors, leads to NF-κB induced expression of inflammatory genes – which poses OTULIN as an anti-inflammatory DUB[19,158]. Nevertheless, by targeting K11 chains – which are formed, for example, by the APC/C complex in conjunction with UBE2S for cell cycle regulation –, Cezanne is also a modulator of cycle progression, as it was observed to accumulate during mitosis and to oppose APC/C and UBE2S activity on some substrates, such as cyclin B[19,38,160].

#### 1.5.2.6.1. OTU domain-containing protein 5

Although some members of the OTU family have their specific functions within the cell thoroughly described, several enzymes still lack a full physiological characterization of their role, remaining their importance underscored.

One of these enzymes is OTUD5, originally described as deubiquitinating enzyme A (DUBA). Structurally, it is a simple enzyme, as its 571 residues long sequence contains the catalytic OTU domain relatively centered and the ubiquitin-interacting motif close to its C-terminus[161] (Figure *5*, upper panel). As evidenced by the disordering score of IUPred3[162] and by the visualization of the AlphaFold prediction (accession number Q96G74, Figure *12*), OTUD5 contains, apart from these forementioned domains, a high content of intrinsically disordered regions (Figure *5*, lower panel) – even in the case of AlphaFold prediction that suggests a long helix between residues 359-421, downstream of the OTU domain.

Upstream of its OTU domain, a pivotal residue for its activity is found: the serine at position 177 (Ser177/S177). Phosphorylation of this residue was identified in phosphoproteomics analysis from mammalian cells[163,164] and its importance was highlighted by *in vitro* studies that showed the inability of OTUD5 to perform its deubiquitinating catalysis in either absence of phosphorylated S177 or even with phospho-mimetics mutations S177D/S177E. Reconstitution of this phospho-site by incubation of OTUD5 with casein kinase II (CK2) generated fully active DUB, demonstrating the essentiality of pSer177 in the enzyme activity[155,165]. Interestingly, structural analysis of the catalytic domain with the upstream region containing S177 showed no difference when comparing substrate-free OTUD5 with either pS177 or S177. The major difference was when the OTU domain was incubated with ubiquitin, which showed that the phospho-site causes a structural change in OTUD5, apart from interacting with ubiquitin itself, that positions the C-terminal region of ubiquitin to sit closely to the catalytic Cys, promoting OTUD5 catalysis[165].

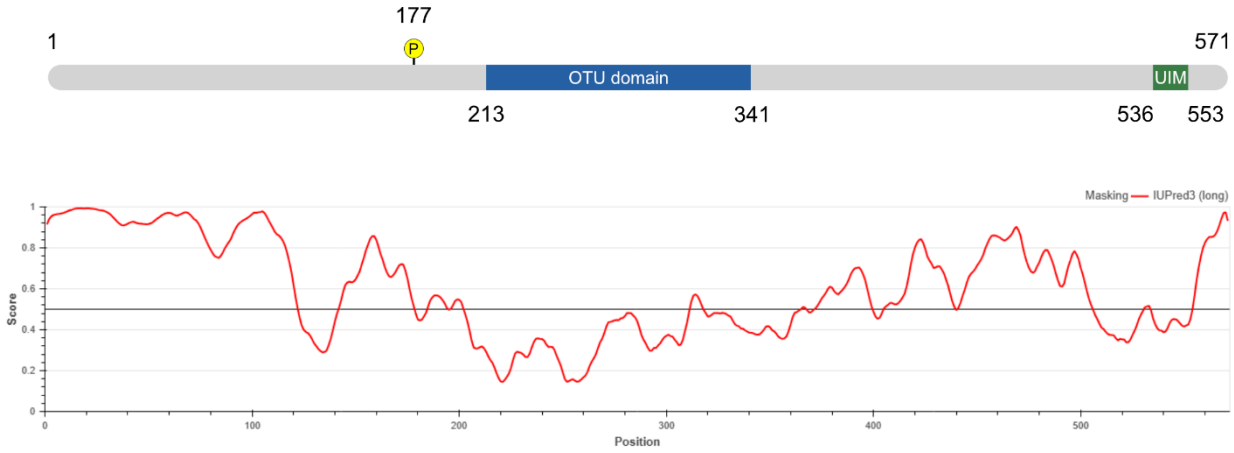


Figure 5: Structural architecture of OTUD5.
Top panel indicates the positioning of the two domains in OTUD5 in its primary sequence, with start and end residues below. The essential phosphorylation site is also indicated. Below, the disorder score obtained by IUPred[162]. Values above 0.5 (indicated by the solid line) suggest a high local disorder, while values lower than 0.5 suggest regions that adopt a more stable local structure.

As a cysteine protease, OTUD5 is also susceptible to environmental stimuli that alters chemical properties of cysteine lateral chain. Alkylation of thiol groups with N-ethylmaleimide (NEM) abrogated completely OTUD5 activity, while exposing it to oxidative stress conditions – such as in presence of hydrogen peroxide – caused an alteration in its catalytic cysteine, which could render the enzyme inactive[161,166].

As an OTU family member, OTUD5 also exhibits linkage preferences when it comes to ubiquitin chains. The first assessment of its preferences tested its activity against either K48- or K63-linked tetraubiquitin chains, which suggested only K63 to be cleaved[161]. Later reports testing its ability to cleave di-ubiquitin moieties reinforced its K63-linked cleavage but also showed a similar activity towards K48-linked ubiquitin – in addition to a residual activity towards K11[155,165]. These are corroborated by cellular model studies, in which both K63- and K48-linked chains were seen to be targeted by OTUD5[40,167,168]. Furthermore, a recent *in vitro* screen showed OTUD5 to potentially cleave K63/K48 branched tetraubiquitin chains[138], which yet needs *in vivo* confirmation.

OTUD5 was first implicated in modulation of immune response signaling. It was, then, described to cleave K63-linked ubiquitin chains from TRAF3, enhanced by its UIM, causing a dissociation of this factor from the downstream signaling that would lead to type I interferon synthesis, putting OTUD5 as a suppressor of immune signaling[161]. This view was further explored by a later report that showed its activity in controlling the synthesis of pro-inflammatory

interleukin-17A in immune cells. OTUD5 controls the stability of RORγt transcription factor, although possibly by an indirect mechanism: decreased levels of RORγt were caused by OTUD5-dependent stabilization of UBR5, the effector E3 ligase that ubiquitinated RORγt and led to decreased immune signaling[169]. On an opposite view, OTUD5 was seen to stabilize STING, in a catalytic-dependent manner, after activation of innate immunity following viral infection – a pro-inflammatory signal. Authors also showed that STING stabilization in a cancer background is dependent on OTUD5, opening a new perspective on understanding its activity[170].

In cancer context, OTUD5 has been put in the spotlight from opposing angles. Two reports showed that it stabilized p53 after DNA damage, generating a pro-apoptotic response, either by directly deubiquitinating it or by removing ubiquitin from PDCD5 – an inhibitor of the MDM2 E3 ligase that targets p53 for degradation[171,172]. In addition, OTUD5 was shown to target non-degradative ubiquitination in TRIM25, decreasing its activity and leading to an increased expression of tumor suppressor genes[167], while bioinformatics analysis suggested OTUD5 depletion to correlate with poor prognosis and higher metastasis rates[173]. On the other hand, OTUD5 was also reported as an inducer of cell proliferation by positively regulating mTORC1/2 signaling pathways, either by stabilizing RNF186 or β-TrCP1, leading to higher cell division rates[174,175].

Furthermore, OTUD5 has been implicated in modulating events related to chromatin homeostasis regulation and DNA damage response. It was seen to remove ubiquitin chains from Ku80/XRCC5, maintaining its association to chromatin for recruitment of DNA repair machinery, while OTUD5 depletion impaired overall repair[176]. In a similar outcome, OTUD5 was reported to form a complex with UBR5 and, in synergy, inhibit the activity of FACT complex (Facilitates Chromatin Transcription) nearby damaged regions, avoiding access of transcriptional complexes and conflicts between the two machineries[177]. OTUD5-UBR5 complex also controls transcription-replication conflicts, modulating FACT on chromatin by limiting its histone chaperone activity[178]. This DUB is also pivotal in chromatin homeostasis during development, as patients that exhibit mutations in its gene suffer from a severe developmental syndrome. *OTUD5* gene is highly sensitive to mutations and, given it is located in the X chromosome, single allele alterations are able to incapacitate its activity. This new syndrome, named LINKED (LINKage-specific deubiquitylation deficiency-induced Embryonic Defects), was described in humans due to lack of

enzymatic catalysis of OTUD5 towards K48-linked chains, leading to proteasomal degradation of chromatin remodelers and alteration in the normal developmental program[168].

OTUD5 involvement in immune response and cancer development still shows opposing conclusions coming from different reports. Its role in genome stability, however, points towards this DUB being a central actor in stability maintenance. So far, the number of high confidence substrates of this enzyme is limited, as only UBR5 was repeatedly reported as both interactor and substrate[168,169,177,178]. The unexplored landscape of OTUD5's substrates combined with its impact on cellular fitness makes the investigation of OTUD5 physiology essential, in order to uncover novel mechanisms by which cells maintain their nuclear homeostasis.

# 2. Aims of the study

In this work, we aim to systematically investigate the impact on nuclear homeostasis in response to the absence of OTUD5. For this purpose, we employ high-throughput mass spectrometry-based approaches to quantify the perturbations in the ubiquitin-modified and total proteome, hence identifying OTUD5 substrates. Considering its central role in the maintenance of genome stability, we intend to analyze the alterations in the nuclear environment by assessing the changes in chromatin proteome, as well as characterize the mechanism employed by OTUD5 to interact with its substrates. Furthermore, we aim to evaluate the cellular consequences of OTUD5 depletion through the analysis of phenotypical outcomes related to the lack of this enzyme. Ultimately, our goal is to comprehend, by an unbiased strategy, the spectrum of factors that are sensitive to OTUD5 loss, focusing on understanding the effects on chromatin homeostasis.

# 3. Materials and methods

## 3.1. List of reagents

Table 1: List of antibodies used in this study.

| ANTIBODIES | | | | |
|---|---|---|---|---|
| **Target** | **Catalog number** | **Supplier** | **Dilution** | **Application** |
| OTUD5 | 20087 | Cell Signaling | 1:1000 | WB |
| | | | 1:200 | PLA |
| | | | | MS |
| UBR5 | 65344 | Cell Signaling | 1:1000 | WB |
| SMC1 | 6892 | Cell Signaling | 1:1000 | WB |
| SMC2 | 5329 | Cell Signaling | 1:1000 | WB |
| SMC3 | 5696 | Cell Signaling | 1:2000 | WB |
| SMC4 | 5547 | Cell Signaling | 1:1000 | WB |
| p21 | 2947 | Cell Signaling | 1:1000 | WB |
| β-actin | A2228 | Sigma-Aldrich | 1:10000 | WB |
| Ubiquitin (P4D1) | sc-8017 | Santa Cruz | 1:500 | WB |
| VCP | 2649 | Cell Signaling | 1:1000 | WB |
| | MA3-004 | Thermo Fisher | 1:200 | PLA |
| NPLOC4 | HPA021560 | Atlas Antibodies | 1:2000 | WB |
| UFD1L | 10615-1-AP | Proteintech | 1:2000 | WB |
| | | | 1:200 | PLA |
| Cyclin E2 | 11935-1-AP | Proteintech | 1:1000 | WB |
| Cyclin A2 | ab181591 | Abcam | 1:2000 | WB |
| Vinculin | V9264 | Sigma-Aldrich | 1:10000 | WB |
| TPX2 | 8559 | Cell Signaling | 1:1000 | WB |
| IgG (anti-mouse)-HRP | P044701-2 | Agilent Technologies | 1:5000 | WB |
| IgG (anti-rabbit)-HRP | P044801-2 | Agilent Technologies | 1:5000 | WB |
| Alexa Fluor™ 647 azide | 10043964 | Fisher Scientific | 40 µM | MIC |

Table 2: List of oligonucleotides used in this study.

| OLIGONUCLETIDES – siRNA | | | |
|---|---|---|---|
| **Target** | **Sequence** | **Catalog number** | **Supplier** |
| Control (scrambled) | | D-001810-10-20 | Horizon Discovery Bioscience |
| UFD1L | GUGGCCACCUACUCCAAAU (S1)<br>AUUUGGAGUAGGUGGCCAC (AS1)<br>CUACAAAGAACCCGAAAGA (S2)<br>UCUUUCGGGUUCUUUGUAG (AS2) | | Sigma-Aldrich |
| NPLOC4 | CGUGGUGGAGGAUGAGAUU (S1)<br>AAUCUCAUCCUCCACCACG (AS1)<br>CAGCCUCCUCCAACAAAUC (S2)<br>GAUUUGUUGGAGGAGGCUG (AS2) | | Sigma-Aldrich |
| TRIP12 | GCAAUUUGAUUCGUUCAGATT (S)<br>UCUGAACGAAUCAAAUUGCCT (AS) | s17810 | Thermo Fisher |

Table 3: List of chemical inhibitors used in this study.

| INHIBITORS | | | |
|---|---|---|---|
| | **Catalog number** | **Supplier** | **Target** |
| TAK-243 | HY-100487 | MedChem Express | E1 enzymes |
| NMS-873 | S7285 | SelleckChem | VCP |
| DRB | D1916 | Sigma-Aldrich | RNA Pol II |
| PladB | SC-391691 | Santa Cruz | Spliceosome |
| Palbociclib | PZ0383 | Sigma-Aldrich | CDK4/6 |
| Sodium fluoride | S7920 | Sigma-Aldrich | Phosphatases |
| Sodium orthovanadate | S6508 | Sigma-Aldrich | Phosphatase |
| β-glycerophosphate | G5422 | Sigma-Aldrich | Phosphatase |
| N-ethylmaleimide | E3876 | Sigma-Aldrich | Cys-proteases |
| Protease inhibitor cocktail | P8340 | Sigma-Aldrich | Proteases |

Table 4: List of consumables used in this study.

| CONSUMABLES | | | |
|---|---|---|---|
| | **Catalog number** | **Supplier** | **Application** |
| Lipofectamine™ RNAiMAX | 13778150 | Thermo Fisher | Transfection |
| RNeasy Plus Mini | 74134 | Qiagen | RNA-Seq |
| Quick Start Bradford 1× Dye Reagent | 5000205 | Bio-Rad | Protein measurement |
| SulfoLink™ Coupling Resin | 20402 | Thermo Fisher | PD |
| Dynabeads™ Protein G | 10004D | Thermo Fisher | PD |
| NuPAGE™ 4-12% Bis-Tris Protein Gel | NP0321/NP0322/NW04125 | Thermo Fisher | SDS-PAGE |
| NuPAGE™ LDS Sample Buffer 4× | NP0007 | Thermo Fisher | SDS-PAGE |
| BLR BlueStar PLUS ProteinLadder Protein Marker | PL12.0500 | Diagonal & Co. | SDS-PAGE |
| Immobilon®-FL PVDF membrane | IPFL00010 | Sigma-Aldrich | WB |
| Immobilon ECL Ultra Western HRP Substrate | WBULS0500 | Merck | WB |
| SuperSignal™ West Pico PLUS Chemiluminescent Substrate | 34580 | Thermo Fisher | WB |
| Sequencing grade trypsin | 37283 | Serva | MS |
| Lysil endopeptidase (Lys-C) | 125-05061 | Wako | MS |
| PTMScan® Ubiquitin Branch Motif (K-ε-GG) | 5562 | Cell Signaling | MS |

| | | | |
|---|---|---|---|
| TMT10plex™ Label Reagent Set | 90309 (Lot XB318561) | Thermo Fisher | MS |
| TMTpro 16plex Isobaric Label Reagent Set | A44522 (Lot YC370078) | Thermo Fisher | MS |
| Colloidal Blue Staining Kit | LC6025 | Life Technologies | MS |
| L-lysine | L8662 | Sigma-Aldrich | MS |
| L-arginine | A6969 | Sigma-Aldrich | MS |
| L-lysine ($^{13}C_6/^{15}N_2$) | CNLM-291-H-1 | Cambridge Isotope Laboratories | MS |
| L-arginine ($^{13}C_6/^{15}N_4$) | CNLM-539-H-1 | Cambridge Isotope Laboratories | MS |
| Empore™ C18 47 mm disks | 66883-U | Supelco | MS |
| Empore™ Cation Exchange 47 mm disks | 66889-U | Supelco | MS |
| Sep-Pak C18 Classic Cartridge, 360 mg Sorbent | WAT051910 | Waters | MS |
| Sep-Pak C18 3 cc Vac Cartridge, 200 mg Sorbent | WAT054945 | Waters | MS |
| Duolink® In Situ Detection Reagent Red | DUO92008 | Sigma-Aldrich | PLA |
| Duolink® In Situ PLA® Probe anti-Mouse PLUS | DUO92001 | Sigma-Aldrich | PLA |
| Duolink® In Situ PLA® Probe anti-Rabbit MINUS | DUO92005 | Sigma-Aldrich | PLA |
| 5-ethynyl uridine (EU) | CLK-N002 | Jena Bioscience | MIC |
| Hoechst 33342 | B2261 | Sigma-Aldrich | MIC/PLA |
| ProLong™ Gold Antifade Mountant | P36934 | Thermo Fisher | MIC/PLA |

## 3.2. Mammalian cell line maintenance

Human retinal pigment epithelial cells (RPE-1), both wild type and knockout for OTUD5, were kindly donated by redacted (redacted). RPE-1 knockout for UBR5 was generated in our group (redacted, data not published). Cells were maintained in a humid incubation chamber at 37 °C and 85% humidity, containing 5% $CO_2$. Culturing was performed in Dulbecco's Modified Eagle Medium (DMEM), supplemented with 10% fetal bovine serum (FBS), 2 mM L-glutamine and 100 U/mL penicillin-streptomycin. For SILAC labelling, cells were maintained for at least four passages in SILAC DMEM, supplemented with 10% dialyzed FBS, 100 U/mL penicillin-streptomycin and either L-lysine and L-arginine or L-lysine ($^{13}C_6/^{15}N_2$) and L-arginine ($^{13}C_6/^{15}N_4$). Cells were routinely tested for *Mycoplasma* contamination by PCR.

## 3.3. Cell treatment and transfection

For different experiments, cells were treated with a selection of varied molecules. Inhibition of the ubiquitination cascade with TAK-243 was performed with 5 µM for different periods indicated in the respective result section and figures. NMS-873 was incubated also in a concentration of 5 µM for 4 hours. Treatment with 5,6-dichlorobenzimidazole-1-β-D-ribofuranoside (DRB) was performed for 3.5 hours with 100 µM, while cells were incubated with pladienolide B (PladB) in a concentration of 100 nM for 4 hours. UV-C irradiation on cells was performed using a custom-made equipment, with an energy density of 15 J/m$^2$. Palbociclib was used at 150 nM for 24 hours. DMSO negative controls consisted of the same volume used for the respective stimuli and incubation for the longest period of the experiment.

Small interference RNA (siRNA) transfection was performed based on manufacturer's instructions (Thermo Scientific), including the amount of oligos suggested for each scale. Oligos were diluted in Opti-MEM™ (Thermo Scientific) and after mixing with RNAiMAX, complexes were added onto cells. After 48 hours of incubation, cells were processed accordingly.

## 3.4. Protein extraction and pulldown

### 3.4.1. Whole cell lysate

All steps, otherwise indicated, were performed on ice. Before collecting protein extract, cells were washed twice with ice-cold PBS 1× and harvested while still in PBS. They were then centrifuged at 800 × *g* and then lysed in modified RIPA (mRIPA) buffer (50 mM Tris-HCl pH 7.5, 150 mM NaCl, 1 mM EDTA, 1% IGEPAL® CA-630 and 0.1% sodium deoxycholate) supplemented with 5 mM sodium fluoride, 1 mM sodium orthovanadate, 5 μM β-glycerophosphate, 10 mM N-ethylmaleimide and protease inhibitor cocktail. For optimal chromatin-bound protein extraction, NaCl concentration was raised to 500 mM and cellular suspension was sonicated for at least 3 cycles of 30 seconds on/off (Branson Ultrasonics™ 450 or Diagenode Bioruptor® Plus). Suspensions were then centrifuged at ≥ 17900 × *g*, 15 minutes at 4 °C and supernatant was collected. Protein concentration was measured with Quick Start Bradford 1× Dye Reagent.

### 3.4.2. Subcellular fractionation

Protein extraction from cytoplasmic, nucleoplasmic and chromatin-bound fractions was performed according to a previous report[179] and all steps, otherwise indicated, were performed on ice. After washing cells twice with ice-cold PBS 1×, they were first lysed in buffer SA (10 mM HEPES pH 7.9, 10 mM KCl, 1.5 mM $MgCl_2$, 0.34 M sucrose, 10% glycerol, 1 mM DTT) supplemented with 5 mM sodium fluoride, 1 mM sodium orthovanadate, 5 μM β-glycerophosphate, 10 mM N-ethylmaleimide, protease inhibitor cocktail and 0.1% Triton X-100. Suspensions were incubated for 15 minutes at 4 °C rotating and then centrifuged at 1300 × *g* for 5 minutes at 4 °C. Supernatant containing cytoplasmic fraction (S1) was separated from pellet (P1) and then cleared by centrifugation at 20000 × *g* for 5 minutes at 4 °C, in which the supernatant was collected as cytoplasmic fraction and pellet was discarded. P1 was then washed twice with ice-cold PBS 1× and lysed with buffer SB (3 mM EDTA, 2 mM EGTA, 1 mM DTT) supplemented with 5 mM sodium fluoride, 1 mM sodium orthovanadate, 5 μM β-glycerophosphate, 10 mM N-

ethylmaleimide and protease inhibitor cocktail rotating at 4 °C for 30 minutes. The solution was then centrifuged at 1700 × *g* for 5 minutes and 4 °C, after which the nucleoplasmic fraction (S2) was collected and separated from the pellet (P2). P2 was washed twice with ice-cold PBS 1× and then lysed in mRIPA supplemented with 5 mM sodium fluoride, 1 mM sodium orthovanadate, 5 μM β-glycerophosphate, 10 mM N-ethylmaleimide, protease inhibitor cocktail and with 1 mM DTT, being then sonicated for at least 3 cycles of 30 seconds on/off (Diagenode Bioruptor® Plus). Suspensions were then centrifuged at ≥ 17900 × *g*, 15 minutes at 4 °C and supernatant (S3) representing the chromatin-bound fraction was collected while pellet was discarded. Protein concentration was measured with Quick Start Bradford 1× Dye Reagent.

### 3.4.3. Immunoprecipitation

Cell lysis was performed in a modified way to preserve protein-protein interaction and all steps, otherwise indicated, were performed on ice. After washing and collecting cells in ice-cold PBS 1×, they were lysed in mRIPA supplemented with 5 mM sodium fluoride, 1 mM sodium orthovanadate, 5 μM β-glycerophosphate, 10 mM N-ethylmaleimide, protease inhibitor cocktail, 2.5 mM $MgCl_2$ and 1:1000 (v/v) of Sm Nuclease (IMB Protein Production Core Facility). Samples were left for 30 minutes rotating at 4 °C. Samples had NaCl concentration increased to 450 mM and left on ice for 15 minutes, with occasional vortexing, being later centrifuged for 15 minutes at 17900 × *g* and 4 °C. NaCl concentration was decreased back to 150 mM and protein quantification was performed with Quick Start Bradford 1× Dye Reagent.

Magnetic Dynabeads G (Thermo Scientific) were washed twice with mRIPA (supplemented with inhibitors but without $MgCl_2$ or Sm Nuclease) and incubated overnight with protein solution and antibodies, at 4 °C and rotating. Then, they were washed 3 times with mRIPA supplemented with inhibitors and samples were eluted with LDS 2× sample buffer supplemented with 1 mM DTT, followed by boiling at 95 °C for 10 minutes.

### 3.4.4. Pulldown of ubiquitinated proteins

Enrichment of a protein fraction containing ubiquitin-modified proteins was performed using a ubiquitin-binding domain from an *Orientia tsutsugamushi* DUB, named OtUBD[180].

OtUBD synthesis was performed by IMB Protein Production Core Facility and it was later conjugated to agarose beads – for each 1 mg of OtUBD probe, 1 mL slurry (1:1 ratio solution:beads) was used for conjugation. SulfoLink beads were first washed with four beads-bed volumes of coupling buffer (50 mM Tris pH 8.5, 5 mM EDTA). Then, the OtUBD probe was diluted in coupling buffer supplemented with 20 mM TCEP and incubated at room temperature for 30 minutes, rotating. Then, OtUBD solution was added onto the agarose beads and incubated for 1 hour at room temperature, rotating. Conjugated beads were then washed with three beads-bed volumes of coupling buffer and incubated for 30 minutes at room temperature, rotating, with cysteine solution (50 mM cysteine in coupling buffer). Afterwards, they were washed with 6 beads-bed volumes of 1 M NaCl for 4 times and once with column buffer (50 mM Tris pH 7.5, 150 mM NaCl, 1 mM EDTA, 0.5% Triton X-100, 10% glycerol), bring later stored, at 4 °C, in OtUBD storage buffer (column buffer supplemented with 0.05% $NaN_3$).

For the pulldown of ubiquitinated proteins, all steps were performed on ice unless otherwise indicated. Cells were first washed and harvested in ice-cold PBS 1×, being later lysed with OtUBD lysis buffer (50 mM Tris pH 7.5, 300 mM NaCl, 1 mM EDTA, 0.5% Triton X-100) supplemented with 5 mM sodium fluoride, 1 mM sodium orthovanadate, 5 μM β-glycerophosphate, 10 mM N-ethylmaleimide and protease inhibitor cocktail. Samples were left rotating at 4 °C for 30 minutes and then sonicated for at least 5 cycles of 30 seconds on/off (Diagenode Bioruptor® Plus). After centrifugation at 4 °C for 15 minutes at ≥ 17900 × *g*, protein quantification was performed with Quick Start Bradford 1× Dye Reagent. Beads were then washed once with column buffer and incubated overnight with protein extract (for each 1 mg of protein extract, 17.5 μL of bead-bed was used). Then, at room temperature, beads were washed 3 times with 15 beads-bed volumes of column buffer supplemented with 4 M urea and once with ultrapure water, which followed elution of ubiquitinated proteins with LDS 2× sample buffer supplemented with 1 mM DTT and boiling at 95 °C for 10 minutes.

## 3.5. Protein electrophoresis and Western blotting

Cell lysates containing 5-30 µg of protein were mixed with LDS sample buffer, supplemented with DTT and had their volumes adjusted equally. They were then boiled for 10 minutes at 95 °C and then resolved by SDS-PAGE on 4-12% gradient gels. For Western blotting, gels were then transferred to a polyvinylidene fluoride (PVDF) membrane of 0.45 µM pore size, for 90 minutes and 20 V applied in a wet tank system, which were subsequently stained with Ponceau S solution and then blocked with 5% (w/v) skim milk solution in PBST (PBS 1× supplemented with 0.1% Tween-20) for 1 hour at room temperature. Membranes were then washed three times for 5 minutes with PBST and primary antibodies were incubated overnight at 4 °C. Afterwards, membranes were again washed three times with PBST for 5 minutes and incubated with secondary antibodies (conjugated to horseradish peroxidase) diluted in a 5% (w/v) skim milk solution for 1 hour at room temperature. Another round of three 5 minutes washes with PBST was performed and then they were developed with either SuperSignal West Pico or Immobilon ECL Ultra Western HRP Substrate detection reagents, according to manufacturer instructions. Imaging for chemiluminescent signal detection was performed using a ChemiDoc MP system (Bio-Rad).

## 3.6. Proteomics analyses

### 3.6.1. Protein digestion and peptide clean-up

After cell lysis – indicated in section 2.3.1 – the protein extracts were precipitated by addition of ice-cold acetone to an at least 80% concentration and left overnight at -20 °C. Solution was then centrifuged in a swinging bucket centrifuge (Heraeus Multifuge X3R, Thermo Scientific) for 5 minutes at 2000 rpm and supernatant was discarded. Dry pellets were resuspended in denaturation buffer (6 M urea/2 M thiourea in 10 mM HEPES pH 8.0) by shaking at room temperature and proteins were then reduced with 1 mM DTT for 45 minutes at room temperature, shaking, followed by alkylation with 5.5 mM CAA for 30 minutes at room temperature, in the dark. Following a 4-fold dilution with ultrapure water to reduce urea/thiourea concentration, a second round of digestion was performed with proteomics grade trypsin (0.5 µg/µL in 50 mM ammonium

bicarbonate pH 8.0) in a ratio of 1:200, at room temperature, shaking, overnight. TFA was added to a final concentration of 0.5% and undigested proteins were pelleted incubating samples at 4 °C for 30 minutes followed by a 10 minutes/4000 rpm centrifugation in a swinging bucket centrifuge (Heraeus Multifuge X3R, Thermo Scientific). Peptides were then purified with C18 columns – previously activated with 100% ACN and washed 3 times with 0.1% TFA – and eluted with 50% ACN – after a round of 3 washes with ultrapure water.

### 3.6.2. OTUD5 endogenous interactome

Following the description from section 2.3.3, samples were alkylated with 5.5 mM CAA after boiling for 30 minutes at room temperature – in the dark – and loaded to be briefly resolved by SDS-PAGE on 4-12% gradient gels. Gels were then incubated for 10 minutes at room temperature in fixing solution (10% acetic acid, 50% methanol) and stained with colloidal blue according to manufacturer instructions (Life Technologies). After destaining overnight in water at 4 °C, lanes containing the pulldown material were cut into three fractions, had colloidal blue removed with destaining solution (40% ethanol, 25 mM ammonium bicarbonate pH 8.0, repeated 4 times) and dehydrated with 100% ethanol for 10 minutes at room temperature, shaking, twice. Gel pieces were then incubated overnight with 0.625 µg of proteomics grade trypsin at 37 °C. Afterwards, they were incubated twice, for 20 minutes and shaking at room temperature, with peptide extraction buffer (30% ACN, 3% TFA), followed by incubations in same conditions with buffer B* (80% ACN, 0.5% acetic acid) and with 100% ACN. Peptide solutions had their volumes reduced in a vacuum concentrator and followed for desalting – described in a later section.

### 3.6.3. Ubiquitin-remnant profiling

The procedure described in 2.5.1 had few extra steps for the particular identification of ubiquitin-modified peptides. As this quantification was performed by quantification of SILAC ratios, after lysis the protein extracts were mixed in a 1:1 (mg) ratio before acetone precipitation and before dilution with water they were digested with Lys-C protease (0.5 µg/µL in 50 mM ammonium bicarbonate pH 8.0) for 4 hours at room temperature, shaking, in a ratio of 1:200

(protease:protein) – extra information and details about individual steps were previously reported[181].

After obtaining the clean peptide solution in 50% ACN, 100 µL of IAP buffer 10× (500 mM MOPS pH 7.2, 100 mM $Na_3PO_4$, 500 mM NaCl) were added and the volume was reduced in a vacuum concentrator up to 1 mL of solution. Samples were then centrifuged for 10 minutes at 17900 × *g*. PTMScan® Ubiquitin Branch Motif beads (Cell Signaling) were washed three times with Wash Buffer II (IAP buffer 1×), which was followed by mixing beads with peptide sample and then solution was left for 4 hours rotating at 4 °C. Beads were then washed twice with Wash Buffer I (IAP buffer 1× supplemented with 150 mM NaCl and 0.5% IGEPAL® CA-630), twice with Wash Buffer II and twice with ultrapure water, afterwards being eluted with 0.15% TFA – 4 elution steps performed mixing all the eluates together.

### 3.6.4. Tandem Mass Tag (TMT) labelling for total and chromatin proteome measurements

After the protein extraction described in 2.3.1 – for full proteome – or 2.3.2 – for chromatin proteome – samples were processed according to 2.5.1 with a small adjustment of protein digestion with trypsin to a 1:50 ratio (trypsin:protein) and peptides being dried in a vacuum concentrator after elution with ACN.

Peptides were resuspended in 150 mM HEPES pH 8.5 containing 30% ACN and labelled with either TMT10plex or TMTPro (Thermo Scientific) in a ratio of 0.5 µg label/µg peptide, for 1 hour at room temperature. Labelling reactions were stopped by addition of 5% hydroxylamine solution, which was incubated with the labelled peptides for 15 minutes at room temperature[182]. Before full measurement of proteomes, a small aliquot (~3%) of each sample was taken, mixed and measured on the mass spectrometer to check the ratio between samples[183]. After mass adjustment across all samples, peptides were cleaned up by C18 columns as described in section 2.5.1. Then, they were fractionated and desalted as described in later section.

### 3.6.5. Micro tip-based strong cation exchange chromatography (Micro-SCX) and peptide desalting

Once peptides were either enriched from di-glycine pulldown or TMT-labelled for full and chromatin proteome analyses, samples were fractionated by Micro-SCX[184,185]. In both these cases and for all other mass spectrometry measurements described, peptides were also desalted before loaded on the equipment, based on previous reports[186].

For Micro-SCX, a cation 47 mm extraction disk was washed sequentially with methanol and then twice with SCX elution buffer (40% ACN, 60% SCX concentrated buffer – 40 mM acetic acid, 40 mM boric acid, 40 mM phosphoric acid with pH steps of 4.0, 5.0, 6.0, 7.0, 8.5 and 11.0) corresponding, respectively, to the lowest and highest pH steps. Disks were then washed with SCX wash buffer (40% ACN, 60% TFA 0.1%) and peptides were loaded onto the disks. Fractionation was then performed by eluting peptides with SCX elution buffers, from the lowest to the highest pH steps, which was followed by removal of ACN and volume reduction by a vacuum concentrator. Peptides were then acidified to reach a pH of around 2.0 and then proceeded into desalting.

For desalting, C18 filter disks were first washed with 100% methanol, followed by one wash with buffer B (80% ACN, 0.1% FA) and two washes with buffer A' (3% ACN, 1% TFA). Then, the acidified peptides were loaded and disks were further washed once with buffer A (0.1% FA). Afterwards, elution buffer (50% ACN, 0.1% FA) was used to collect peptides into a 96-well plate and once again samples had their volumes reduced and ACN removed by a vacuum concentrator.

### 3.6.6. Measurement of peptides by LC-MS/MS

The parameters used for the MS measurements are summarized in Table 5. Analysis of the data generated was done with MaxQuant[187] (from version 1.5.2.8 on) and both parent ions and MS2 spectra were searched against a reference proteome database of human protein sequences (UniProtKB, from version 2020_02 on), using the Andromeda search engine[188]. Search consisted of strict trypsin specificity (and, when used for previous digestion, Lys-C specificity), allowing maximum of 2 missed cleavages. Cystein carbamidomethylation was used as a fixed modification, while methionine oxidation, N-terminal acetylation and N-ethylmaleimide modification of

cysteines (mass difference to cysteine carbamidomethylation) were used as variable modifications – in addition of di-glycine remnant in lysine residues for ubiquitinome profiling. Maximum number of modifications peptides was set to 5 and dataset was then filtered based on posterior error probability (PEP) in order to arrive at a false discovery rate (FDR) of ≤ 1%, estimated using a target-decoy approach[189].

Table 5: Equipment settings for mass spectrometry measurements.

| Experiment | **Ubiquitin-remnant profiling** | **Proteome** | **Chromatin-bound proteome** | **Interactome** |
|---|---|---|---|---|
| Labelling strategy | SILAC | TMT10plex | TMTPro | LFQ |
| **LC** | | | | |
| Device | EASY-nLC 1200 | EASY-nLC 1200 | Vanquish Neo | EASY-nLC 1200 |
| Column | 55 cm length, 75 mm inner diameter | 55 cm length, 75 mm inner diameter | 45 cm length, 75 mm inner diameter | 55 cm length, 75 mm inner diameter |
| Gradient | 2.4 to 32% ACN, 90 minutes | 2.4 to 33.6% ACN, 120 minutes | 1.6 to 34.4% ACN, 100 minutes | 2.4 to 32% ACN, 60 minutes |
| **MS** | | | | |
| Device | Orbitrap Exploris 480 | Orbitrap Exploris 480 | Orbitrap Astral | Orbitrap Exploris 480 |
| **MS1 scan** | | | | |
| *m/z* range | 300-1650 | 300-1650 | 350-1500 | 300-1650 |
| Resolution | 60000 | 60000 | 120000 | 60000 |
| Target value (%) | 300 | 300 | 300 | 300 |
| Maximum injection time (ms) | 40 | 28 | 20 | 28 |
| **MS2 scan** | | | | |
| Dependent scans | 15 | 20 | 50 | 15 |
| Normalized collision energy (%) | 30 | 33 | 33 | 30 |
| Resolution | 15000 | 15000 | - | 15000 |
| Target value (%) | 100 | 100 | 100 | 100 |
| Maximum injection time (ms) | 40 | 28 | 15 | 28 |
| Isolation window (*m/z*) | 1.4 | 0.8 | 0.5 | 1.4 |

## 3.7. RNA sequencing

Extraction of RNA was performed with the RNeasy Plus Mini kit (Qiagen) according to manufacturer's instructions and samples (quadruplicates for each cell line) were eluted from columns with RNAse free water and kept at -80 °C. NGS library prep was performed with Illumina's Stranded mRNA Prep Ligation Kit following Stranded mRNA Prep Ligation Reference Guide (June 2020) (Document # 1000000124518 v00). Libraries were prepared with a starting amount of 1000 ng and amplified in 10 PCR cycles. Libraries were profiled in a HS DNA chip on a 2100 Bioanalyzer (Agilent Technologies) and quantified using the Qubit dsDNA HS Assay Kit, in a Qubit 2.0 Fluorometer (Life Technologies). All 8 samples were pooled in equimolar ratio and sequenced on 1 NextSeq500 Highoutput FC, SR for 1× 80 cycles plus 10 cycles for the index read and 1 dark cycle upfront Read 1.

## 3.8. Cell based assays

### 3.8.1. Proximity ligation assay (PLA)

For each cell line, $3 \times 10^5$ cells were seeded onto glass coverslips in 6-well dishes. The day after, they were washed with PBS 1× and fixed with 4% PFA for 30 minutes at room temperature, washed again with PBS 1× and permeabilized with 0.25% Triton X-100 for another 30 minutes at room temperature, followed by another PBS 1× wash. The processing of samples was then according to the manufacturer's instructions (Duolink®, Sigma-Aldrich). In the end, samples were incubated with 2 µg/mL Hoechst 33342 for 30 minutes at room temperature and before mounting on glass slides they were washed twice with PBS 1× and once with ultrapure water. Imaging of samples was performed with the Stellaris 8 FALCON (Leica) and analysis performed with Fiji[190], isolating nuclei regions and counting PLA foci in those regions.

### 3.8.2. Global transcriptional evaluation by 5-ethynyluridine (EU)

Cells were seeded either as in 2.6.1 or in 96-well black-wall microplates with clear bottom at a density of $5 \times 10^4$ cells per well. After presenting the stresses for the indicated times, the media was refreshed in order to remove the chemical stressor (or, in case of UV-C irradiation, media was removed before irradiation and fresh DMEM was added on cells after it) and cells were returned to the incubator. For the last 30 minutes of the recovery period, cells were then treated with 100 μM of EU, which was followed by removal, three washes with PBS 1× and fixation with 4% PFA for 20 minutes at room temperature. After another set of three PBS 1× washes, cells were blocked and permeabilized with BP buffer (0.2% BSA, 0.1% Triton X-100 in PBS 1×) for 20 minutes at room temperature. Fluorophore conjugation to EU was performed by diluting AF647-azide to 40 μM in click solution (2 mM $CuSO_4$, 10 mM L-ascorbate in PBS 1×) and incubating samples for 45 minutes at room temperature, in the dark. Later, samples were washed twice with PBS 1× and stained with 1 μg/mL of Hoechst 33342 for 30 minutes at room temperature, in the dark, followed by washing cells twice with PBS 1× – and in case of glass coverslips, a final wash with ultrapure water before mounting on glass slides. Sample imaging was performed with the Opera Phenix (Revvity) and analysis for AF647 intensity performed with the Harmony software.

### 3.8.3. Cellular growth rate

Wild type and OTUD5 knockout cell lines were seeded at a density of $10^4$ cells per well in a 24-well dish and incubated for 72 hours in the IncuCyte SX5 (Sartorius). After imaging wells for the indicated period, well confluence was measured by the predefined “Adherent Cell-by-Cell” pipeline from the IncuCyte software itself.

### 3.8.4. Cell cycle profiling

Both cell lines were seeded at a number of $10^6$ cells in 10 cm dishes and the protocol followed a previous literature report[191]. After 16 hours of seeding, cells were treated for the next 24 hours with 150 nM of Palbociclib, which was followed by a triple wash with PBS 1× for the

time points collected after release. By the end of the release time points – as well as for cells not released after treatment or for the asynchronous samples –, cells were harvested by trypsinization, had their numbers equalized throughout all samples to a final amount of $10^6$, washed with PBS 1× and resuspended in 0.5 mM EDTA in PBS 1×. Afterwards, they were fixed with 4% PFA for 20 minutes and washed twice with 2% BSA in PBS 1×. Then, they were resuspended in FC buffer (0.1% Triton X-100, 2% BSA in PBS 1×), incubated 10 minutes at room temperature, had the supernatant removed after another 5 minutes/800 × *g* centrifugation and had a last resuspension step in 2% BSA in PBS 1× containing 5 µg/mL Hoechst 33342. The acquisition was performed in an LSRFortessa flow cytometer (Becton Dickinson) with the UV laser operating at an excitation wavelength of 355 nm with the 450/50 band pass filter for detection. Analysis was performed with FlowJo software (v10.10), gating for individual cells based on FSC/SSC and later determining cell cycle stage of those via the Watson model for cell cycle[192] based on nuclear staining.

## 3.9. AlphaFold model predictions

For the AlphaFold3 predictions of protein pair model, 5 recycles and all 5 model parameter sets were used; ranking was performed by the internal confidence metrics (pLDDT and pTM/ipTM) and the for analysis the best ranked models were used[193]. MSAs were constructed by the pipeline's default database searches, and structural templates were disabled unless stated. Confidence was evaluated by per-residue pLDDT and global pTM/ipTM, while a cutoff of < 50 was established to filter segments for further mechanistic inference[194,195]. Complexes were modeled with AlphaFold-Multimer and ranked by (ipTM + pTM), prioritizing models by the interface confidence; alternative stoichiometries were explored by varying seeds[196]. AlphaFold Protein Structure Database[197,198] was used to collect the entries OTUD5 (accession number AF-Q96G74-F1) and NPLOC4 (accession number AF-Q8TAT6-F1). Predictions were treated as testable hypotheses[199] and interpreted in association with non-*in silico* methods. Visualization of the prediction models and for deposited structures was performed with ChimeraX[200] (version 1.9).

## 3.10. Data analysis and visualization

Raw data coming from MaxQuant calculations was analyzed either with R software (from version 4.0.4 on) in the RStudio environment, also used for data visualization, or with Perseus[201] (version 2.0.6.0). Filtering of mass spectrometry data was performed by removing hits identified as potential contaminants, reverse, or only identified by site. Peptides with lysines identified as modified by a di-glycine remnant were filtered so only those with a localization probability higher than 0.75 were used for downstream analysis. LFQ data analyzed in Perseus had the missing values imputed based on a normal distribution using the standard software parameters. Statistical significance was calculated either with a standard two-tailed *t*-test or with the LIMMA linear model[202]. Gene ontology enrichment was performed with the pathfindR[203] package for R environment.

Quantification of Western blotting signal intensities was performed with Fiji[190]. Statistical significance for these differences, for PLA quantifications and for global transcriptional evaluation was obtained either by two-tailed *t*-test or by one-way analysis of variance (ANOVA) with GraphPad Prism software (version 9.4.1).

# 4. Results

## 4.1. Depletion of OTUD5 leads to alteration of ubiquitin-modified proteome

In order to elucidate protein substrates of OTUD5 and which set of factors have their ubiquitination status impacted by the absence of this DUB, we employed the ubiquitin-remnant profiling strategy[204], which enables us to identify endogenous ubiquitination sites across the proteome. We combined this strategy with stable isotope labeling by amino acids in cell culture (SILAC)[205], allowing us to quantitively compare by mass spectrometry relative levels of the ubiquitin-modified proteome between OTUD5 knockout to wild type conditions (Figure 6A).

We measured more than 11000 endogenous ubiquitination sites – coming from 3403 different proteins – and quantified 1179 of those as being more abundant in the condition of OTUD5 depletion in comparison to wild type state – originating from 578 unique proteins. On the other hand, 384 sites were more abundant in wild type – coming from 209 proteins (Figure 6B). We also evaluated the variation of different ubiquitin chain linkages based on OTUD5 absence. We observed only minor alterations in the global linkage landscape, indicating that the individual knockout of OTUD5 does not cause a significant redistribution of ubiquitin linkages or accumulation of certain types of chains (Figure 6C).

We then focused our attention on the subset of ubiquitination sites that exhibited an increased level of ubiquitination upon OTUD5 depletion. Given that our model is based on the depletion of a deubiquitinating enzyme, we expected its substrates to have a higher abundance of the modification. For understanding the processes in which OTUD5 is involved, we performed a Gene Ontology (GO) analysis of the putative substrates of OTUD5. Our results showed a high enrichment for chromatin-associated processes and nuclear-associated terms, highlighting OTUD5 relation with these essential cellular pathways (Figure 6D).

On the other hand, when performing the GO-term analysis for the subset of proteins that exhibited a decreased level of ubiquitination in OTUD5 knockout condition, we observed a general weaker enrichment, based on the respective statistical significance, and lower number of terms

associated with nuclear processes (Figure 6E), which could represent secondary effects of OTUD5 depletion.

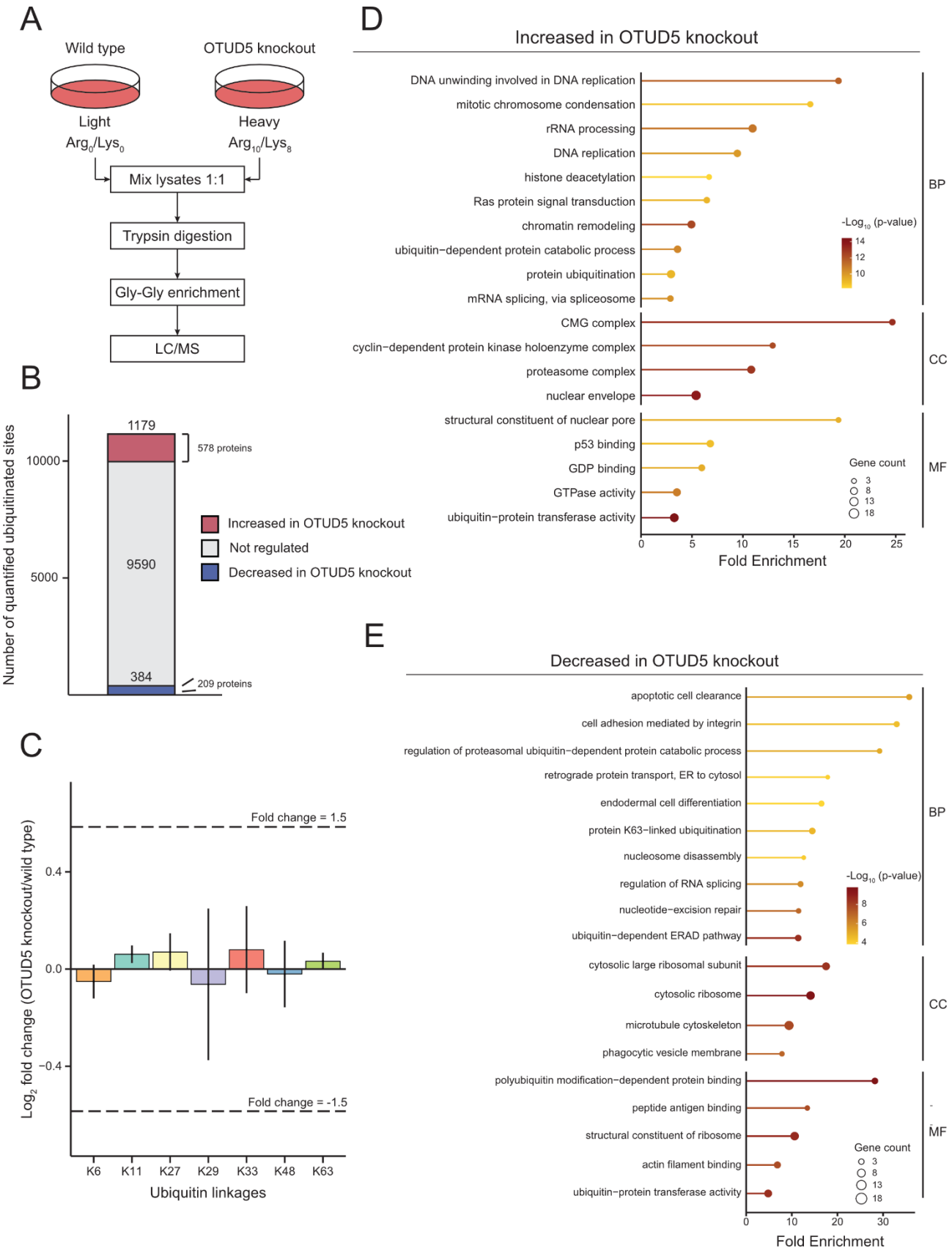
A
Wild type
OTUD5 knockout
Light
Arg0/Lys0
Heavy
Arg10/Lys8
Mix lysates 1:1
Trypsin digestion
Gly-Gly enrichment
LC/MS
B
Number of quantified ubiquitinated sites
10000
5000
1179
578 proteins
9590
384
209 proteins
Increased in OTUD5 knockout
Not regulated
Decreased in OTUD5 knockout
C
Log2 fold change (OTUD5 knockout/wild type)
Fold change = 1.5
Fold change = -1.5
0.4
0.0
−0.4
K6
K11
K27
K29
K33
K48
K63
Ubiquitin linkages
D
Increased in OTUD5 knockout
DNA unwinding involved in DNA replication
mitotic chromosome condensation
rRNA processing
DNA replication
histone deacetylation
Ras protein signal transduction
chromatin remodeling
ubiquitin−dependent protein catabolic process
protein ubiquitination
mRNA splicing, via spliceosome
CMG complex
cyclin−dependent protein kinase holoenzyme complex
proteasome complex
nuclear envelope
structural constituent of nuclear pore
p53 binding
GDP binding
GTPase activity
ubiquitin−protein transferase activity
BP
CC
MF
-Log10 (p-value)
14
12
10
Gene count
3
8
13
18
0
5
10
15
20
25
Fold Enrichment
E
Decreased in OTUD5 knockout
apoptotic cell clearance
cell adhesion mediated by integrin
regulation of proteasomal ubiquitin−dependent protein catabolic process
retrograde protein transport, ER to cytosol
endodermal cell differentiation
protein K63−linked ubiquitination
nucleosome disassembly
regulation of RNA splicing
nucleotide−excision repair
ubiquitin−dependent ERAD pathway
cytosolic large ribosomal subunit
cytosolic ribosome
microtubule cytoskeleton
phagocytic vesicle membrane
polyubiquitin modification−dependent protein binding
peptide antigen binding
structural constituent of ribosome
actin filament binding
ubiquitin−protein transferase activity
BP
CC
MF
-Log10 (p-value)
8
6
4
Gene count
3
8
13
18
0
10
20
30
Fold Enrichment

Figure 6: Characterization of the ubiquitin modified proteome in OTUD5 knockout cells.
A) Outline of the ubiquitin-remnant profiling experiment performed to quantify endogenous ubiquitination sites comparing wild type cells to OTUD5 knockout, performed in triplicates and applying SILAC label switching between replicates. B) Number of quantified ubiquitination sites (on the right side of the bar, number of proteins that had ubiquitination sites detected) in the experiment described in A. In order to be considered quantified, each site had to be identified in at least two out of the three replicates. Categorization into increased or decreased in OTUD5 knockout was based on the proposed cutoffs of fold change $\geq \pm 1.5$ and p-value $< 0.05$ calculated by LIMMA linear model[202], while not regulated did not surpass one or both cutoffs. C) Quantification of ubiquitin linkages in the experiment outlined in A. Each of the linkages (excluding M1-linked chains) is indicated, with bars representing the average value of the three quantifications and lines representing the standard deviation. Dashed lines indicate the fold change cutoff. D) GO-term enrichment for the subset of proteins that contained ubiquitination sites upregulated after OTUD5 knockout (enrichment performed with package patfindR[203]) (BP = biological process; CC: cellular compartment; MF: molecular function). E) GO-term enrichment for the subset of proteins that contained ubiquitination sites downregulated after OTUD5 knockout (enrichment performed with package patfindR[203]) (BP = biological process; CC: cellular compartment; MF: molecular function).

## 4.2. Transcriptional regulators and chromosome organization factors are substrates of OTUD5

Based on our results showing the functional enrichment for GO-terms related to transcription, DNA replication, chromatin organization and mitosis within the subset of proteins that have their ubiquitination increase by OTUD5 depletion, we investigated the group of factors that generated enrichment of these terms (Figure 7A).

Regarding the transcription process, we observed the enrichment of the terms "transcription elongation by RNA polymerase II promoter" (GO:0006368) and "histone monoubiquitination" (GO:0010390), associated to factors such as subunits of the Polymerase Associated Factor 1 (PAF1) complex (PAF1, CTR9, CDC73), members of the DRB sensitivity-inducing factor (DSIF) (SPT4 and SPT5) and the ubiquitin E3 ligase RNF20 (Figure 7B).

The PAF1 complex (PAF1C), originally described in *S. cerevisiae* and conserved from yeast to humans, directly binds to the RNA Pol II and assists the transition from the pausing state during first steps of transcription to the elongation state[206–208]. In order to bind effectively to the RNA Pol II complex, PAF1C requires the presence of the DSIF subunit SPT5[209], which collectively form a recruitment signal for RNF20, the E3 ligase responsible for the monoubiquitination of the histone variant H2B at lysine residue 120 (in humans), an epigenetic marker associated to gene transcription[206,209,210]. Altogether, our results indicate an important role of OTUD5 in regulation of the ubiquitination status of several essential modulators of transcriptional processes.

Our analysis also showed enrichment of terms "chromatin remodeling" (GO: 0006338) and "histone deacetylation" (GO: 0016575), in which we observed the presence of subunits from the NuRD complex (nucleosome remodeling and histone deacetylation), such as the HDAC1/2 (histone deacetylases) and MTA1/2 (Figure 7B). The activity of the complex is marked by its ability of altering epigenetic markers on histones and consequently to perform chromatin remodeling[211]. HDACs, in particular, are the subunits responsible for the removal of acetyl groups from histones, which is commonly associated with gene repression, and in higher eukaryotes are critical for regular embryonic development, as their activity are associated to correct developmental gene expression programme[212,213].

Furthermore, we noted enrichment of terms associated to DNA replication ("DNA unwinding involved in DNA replication" – GO: 0006268 –, "DNA replication" – GO: 0006260" – and "regulation of DNA replication" – GO: 0006275), coming from essential factors in such processes (Figure 7C). Mini-chromosome maintenance (MCM) proteins are part of the CMG helicase complex, a major player during S phase of the cell cycle and responsible for the unwinding of the DNA double helix to allow for the replisome machinery to properly generate a copy of cellular DNA[214]. In parallel, we also observed factors such as RPA1 and RFC3, directly involved in this nuclear process. RPA1 is a single-strand DNA (ssDNA) binder, essential in protecting displaced DNA strands from harmful stimuli and, when bound to ssDNA, working as a platform to recruit other members of the replication machinery[215,216]. RFC3, on the other hand, is part of the factors known to recruit, and associate to, sliding clamps, such as PCNA in eukaryotes, which in turn increases the processivity of DNA polymerase complexes during DNA replication[217].

Lastly, coming from the "mitotic chromosome condensation" (GO: 0007076) term, we observed the structural maintenance of chromosomes (SMC) proteins 2 and 4 among putative substrates of OTUD5 (Figure 7D), but also other SMCs, 1 and 3, associated to other terms. SMC1-4 are ATPases and the main subunits of cohesin (SMC1/3) and condensin (SMC2/4) complexes, which both are known to form ring-like structures around DNA[218]. The main function they are related to are formation of chromosomes during mitosis, in which cohesins are responsible for maintaining sister chromatids together until their separation during anaphase, while condensins work in order to generate full compaction of chromosomes to guarantee that both daughter cells will receive identical DNA from the dividing cell[218,219].

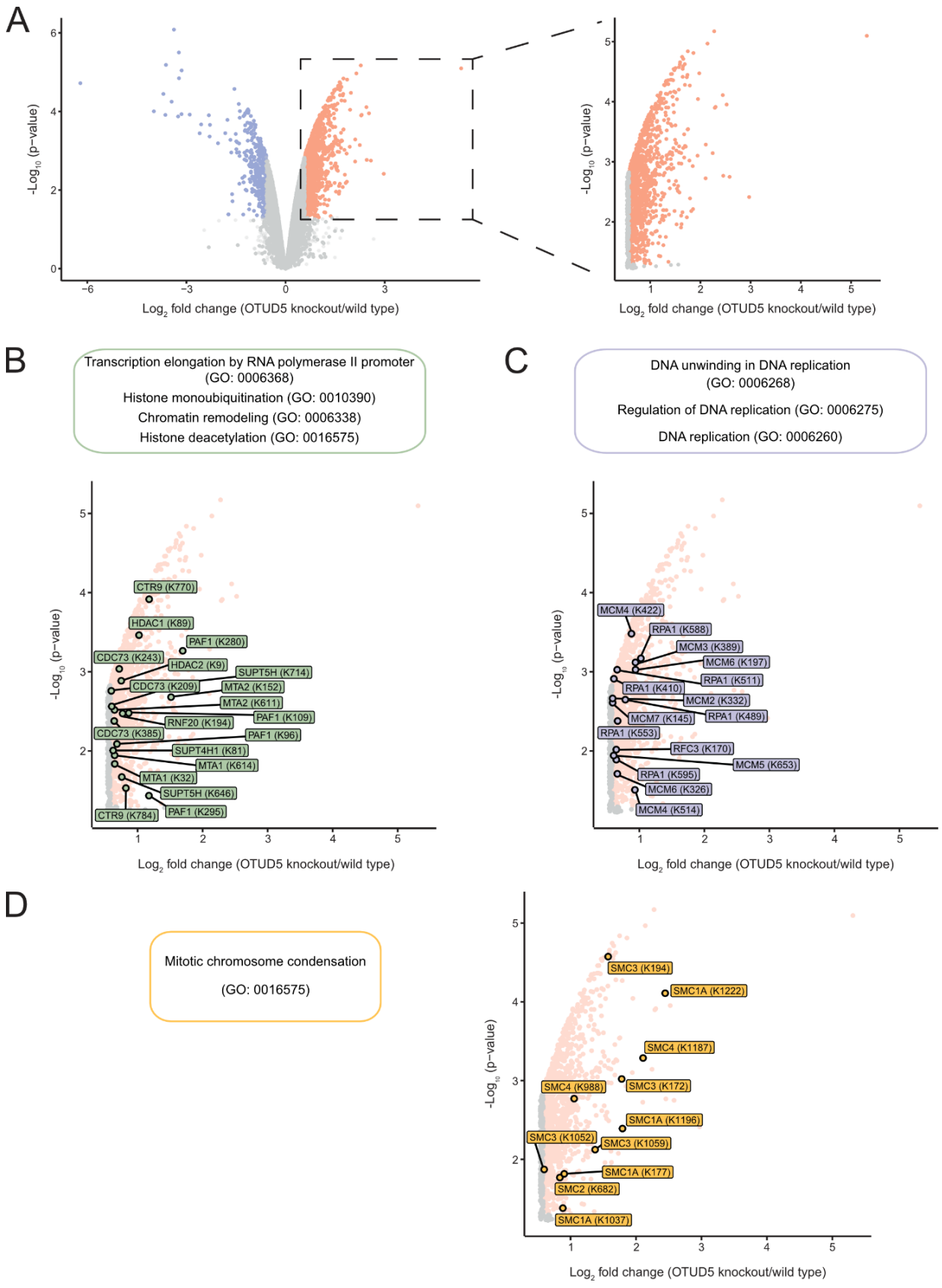
A
-Log10 (p-value)
Log2 fold change (OTUD5 knockout/wild type)
B
Transcription elongation by RNA polymerase II promoter (GO: 0006368)
Histone monoubiquitination (GO: 0010390)
Chromatin remodeling (GO: 0006338)
Histone deacetylation (GO: 0016575)
CTR9 (K770)
HDAC1 (K89)
PAF1 (K280)
CDC73 (K243)
HDAC2 (K9)
SUPT5H (K714)
CDC73 (K209)
MTA2 (K152)
MTA2 (K611)
PAF1 (K109)
RNF20 (K194)
CDC73 (K385)
PAF1 (K96)
SUPT4H1 (K81)
MTA1 (K614)
MTA1 (K32)
SUPT5H (K646)
CTR9 (K784)
PAF1 (K295)
C
DNA unwinding in DNA replication (GO: 0006268)
Regulation of DNA replication (GO: 0006275)
DNA replication (GO: 0006260)
MCM4 (K422)
RPA1 (K588)
MCM3 (K389)
MCM6 (K197)
RPA1 (K511)
RPA1 (K410)
MCM2 (K332)
MCM7 (K145)
RPA1 (K489)
RPA1 (K553)
RFC3 (K170)
MCM5 (K653)
RPA1 (K595)
MCM6 (K326)
MCM4 (K514)
D
Mitotic chromosome condensation (GO: 0016575)
SMC3 (K194)
SMC1A (K1222)
SMC4 (K1187)
SMC4 (K988)
SMC3 (K172)
SMC1A (K1196)
SMC3 (K1052)
SMC3 (K1059)
SMC1A (K177)
SMC2 (K682)
SMC1A (K1037)

Figure 7: Essential regulators of nuclear processes are substrates of OTUD5.
A) Volcano plot of the ubiquitin remnant profiling experiment comparing wild type cells to OTUD5 knockout condition. Red and blue dots indicate the significantly enriched ubiquitinated sites in OTUD5 knockout (upregulated) and in wild type (downregulated) with inlet of the upregulated sites indicating putative substrates of OTUD5 (p-value < 0.05; fold change ≥ ± 1.5, as described in Figure *6*Figure *6*: Characterization of the ubiquitin modified proteome in OTUD5 knockout cells.).
B-D) Set of GO-terms associated with transcriptional (B), replication (C) or cohesion and condensation (D) processes (first panel) and inlet of the volcano plot from A with highlight for the upregulated ubiquitination sites (second panel) coming from proteins that generated the term enrichment presented in the upper panel.

Given OTUD5 has previously been associated with transcription and replication events, we focused on this novel regulation on cohesin and condensin complexes. In order to validate the higher levels of ubiquitination caused by OTUD5 depletion on SMCs, we performed an ubiquitin-modified protein enrichment by using the OtUBD probe – a high-affinity probe capable of binding both mono- and polyubiquitinated proteins even under denaturing conditions such as urea[180] – and detected ubiquitinated species of SMCs. We observed a higher level of ubiquitination of SMC1-4 in OTUD5 knockout condition when compared to wild type (Figure 8A, eluate lanes 1 and 5), indicating that absence of OTUD5 generates an increasing amount of ubiquitination on these proteins.

To further confirm the impact of OTUD5 in their ubiquitination status, we performed the inhibition of the ubiquitination cascade by treating cells with TAK-243 (MLN7243), an inhibitor of the E1 activating enzyme (UAE)[220]. Our strategy was based on performing a time course series of treatment with this inhibitor and to assess the ubiquitination levels for SMC proteins along the time points. We observed that under inhibition of the ubiquitin cascade, SMCs ubiquitination levels remained more stable under OTUD5 depletion in comparison to wild type (Figure 8A – eluate lanes 2-4 and 6-8 – and Figure 8B), although TAK-243 treatment after 2 hours has already depleted most of total ubiquitin signal (Figure 8A). As a control, we compared SMC ubiquitination to UBR5, a known substrate of OTUD5[40], which exhibited a similar pattern of maintained levels of ubiquitination after OTUD5 knockout. In conclusion, our observations indicate that SMC proteins subunits of cohesin and condensin complexes are confident novel substrates of OTUD5.

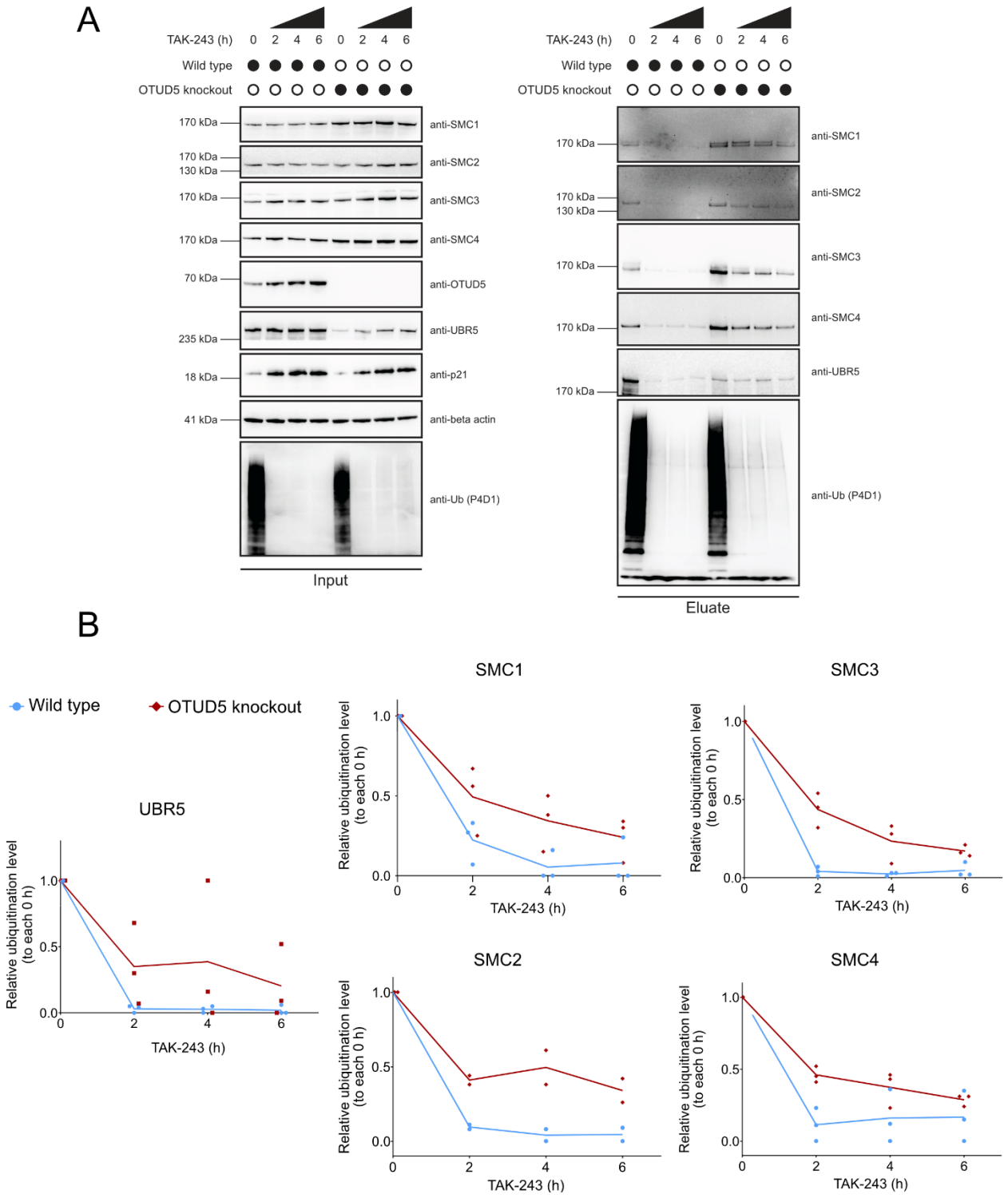


Figure 8: Cohesin and Condensin subunits SMC1-4 are high confidence novel substrates of OTUD5.

A) Representative Western blot from the pulldown of ubiquitinated proteome with OtUBD probe from both wild type and OTUD5 knockout cells after treatment with TAK-243 for the indicated times, performed in triplicates. B) Quantification of the Western blot signal intensity from eluate samples for the indicated four SMC subunits and UBR5, represented in relative fold variation.

Experiment was performed in triplicates and all quantifications were normalized to the control (0 h) sample of each condition. Lines indicate the mean value of each time point and dots each replicate value.

## 4.3. Proteome-level changes due to OTUD5 depletion are not mirrored by gene expression alterations

After our assessment of the ubiquitination changes upon OTUD5 knockout, we further evaluated the total proteome variation in the same conditions (Figure 9A). We quantified a total of 5637 proteins, of which 476 had their total levels increased and 478 were considered downregulated after OTUD5 depletion (each subset representing around 8.5% of the total proteins identified) (Figure 9B).

Surprisingly, when we observed the impact of OTUD5 absence on total protein levels, we noted that several of the substrates we identified had their total levels increased upon depletion of the DUB. Regarding transcription associated factors – PAF1C, NuRD and DSIF members, alongside with the histone ubiquitin ligase RNF20 – showed a significant increase above our proposed cut-offs (fold change $\geq 1.2$; p-value $< 0.05$) (Figure 9C). On the other hand, among the factors involved in the replication machinery, we only saw a significant variation for RPA1 (Figure 9C), while subunits of the MCM complex and RFC3 did not show a major variation in their total amounts. The trend was also observed when we evaluated chromosome structural factors SMC1-4: proteins that compose cohesin complexes (SMC1/3) had a greater elevation in their levels, while condensin subunits (SMC2/4) also showed the same tendency, although not so strongly (Figure 9C).

These variations in protein total levels made us wonder whether the changes in the proteome were a consequence of changes in gene expression levels due to OTUD5 knockout. In order to address this question, we performed RNA-sequencing and assessed transcriptional variations between the two conditions.

We were able to quantify over 18000 unique transcripts in both cell lines (Figure 9D, left panel), without observing any global tendency of either increase or decrease of gene transcription in the OTUD5 knockout condition when comparing gene's FPKM (fragments per kilobase of transcript per million fragments mapped). When we looked specifically into OTUD5 substrates, we observed that the vast majority of those had a very similar FPKM number in both cell lines, indicating marginal changes in expression levels of these proteins in comparison of OTUD5 knockout to wild type (Figure 9D, right panel).

We then further compared the magnitude of variation in the expression levels to the observed alteration in proteome levels for OTUD5 substrates. Our results showed that, for the most proteome-level changing substrates (such as PAF1C subunits, RNF20 and cohesin subunits), the increase observed in their protein amount did not correspond directly to changes in their gene expression, which were marginal when compared to the higher variation in the proteome. Even for SMC3, which exhibited a higher increase in its gene expression, the proteome variation was higher than the former (Figure *10*). Altogether, our data suggests OTUD5 controls its substrates levels in a post-translational manner.

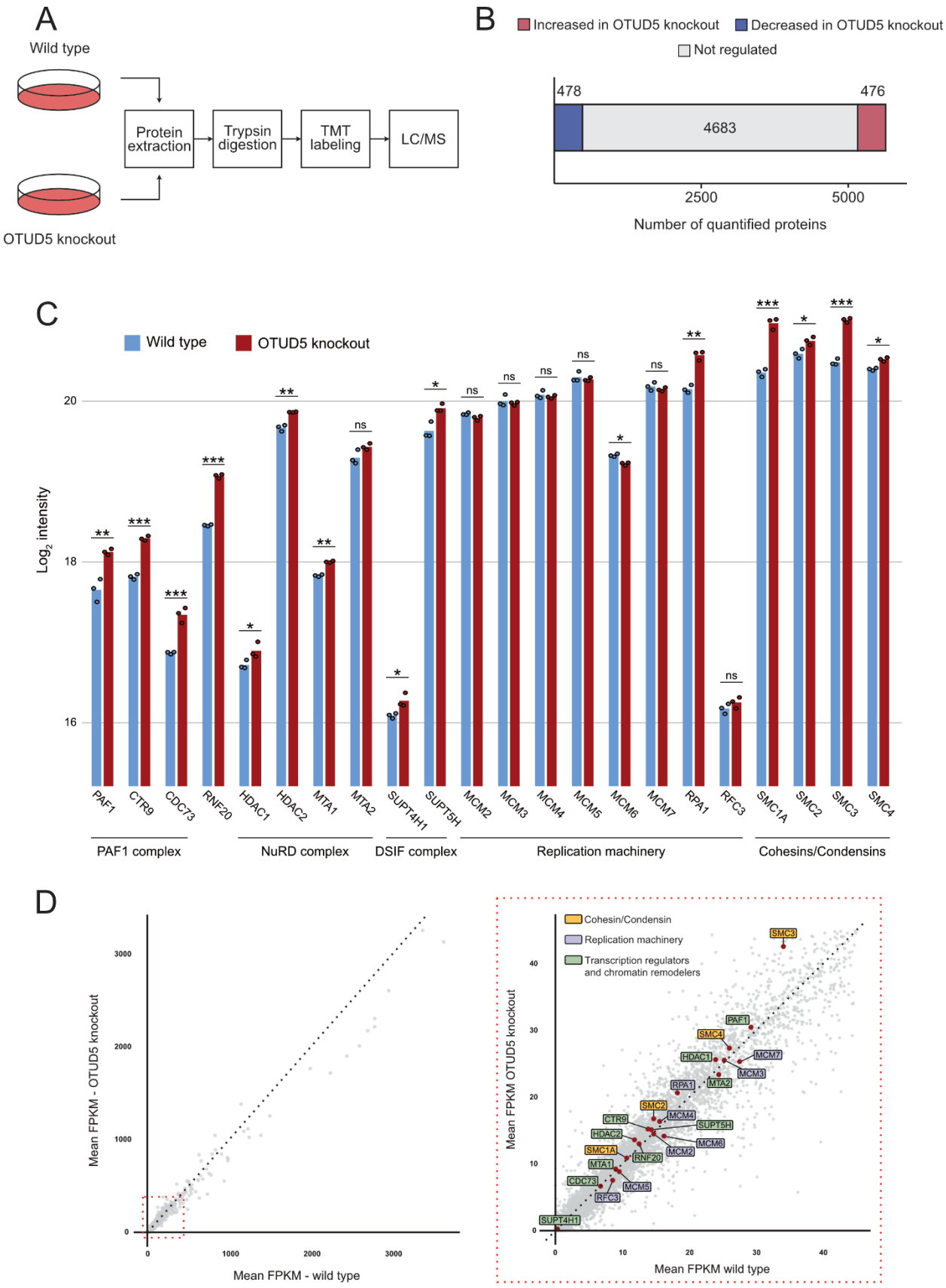
A
Wild type
Protein extraction
Trypsin digestion
TMT labeling
LC/MS
OTUD5 knockout
B
Increased in OTUD5 knockout
Decreased in OTUD5 knockout
Not regulated
478
476
4683
2500
5000
Number of quantified proteins
C
Wild type
OTUD5 knockout
Log2 intensity
20
18
16
PAF1
CTR9
CDC73
RNF20
HDAC1
HDAC2
MTA1
MTA2
SUPT4H1
SUPT5H
MCM2
MCM3
MCM4
MCM5
MCM6
MCM7
RPA1
RFC3
SMC1A
SMC2
SMC3
SMC4
PAF1 complex
NuRD complex
DSIF complex
Replication machinery
Cohesins/Condensins
D
Mean FPKM - OTUD5 knockout
Mean FPKM - wild type
Cohesin/Condensin
Replication machinery
Transcription regulators and chromatin remodelers
Mean FPKM OTUD5 knockout
Mean FPKM wild type

Figure 9: OTUD5 substrates exhibit increased protein levels upon its depletion, but not gene expression levels.
A) Experimental design of the total proteome measurements performed in triplicate to compare protein levels of wild type and OTUD5 knockout cells. B) Overview of total proteome measurements indicating number of proteins quantified and subsets of increased or decreased in OTUD5 knockout. In order to be categorized in either subset, proteins needed to be significantly regulated according to cutoffs proposed (fold change $\geq \pm 1.2$, FDR $< 0.05$). If a protein would not surpass one or both cutoffs, it was considered not regulated. C) Bar plots of the $\log_2$-transformed intensities measured in the experiment outlined in A for proteins associated with transcription processes, replication processes or part of cohesin and condensin complexes. Bars represent the average intensity measured while dots the individual replicate values. Statistical significance was obtained by the LIMMA model[202] and is indicated as asterisks. *: FDR $< 0.05$; **: FDR $< 1 \times 10^{-3}$; ***: FDR $< 1 \times 10^{-5}$; ns: not significant. D) Scatter plots of the mean FKPM value (fragments per kilobase of transcript per million fragments mapped) of wild type and OTUD5 knockout conditions derived from RNA-sequencing, performed in triplicates. On the left, all values measured in the experiment. On the right, inlet from left panel highlighting OTUD5 substrates – color code indicated in the figure.

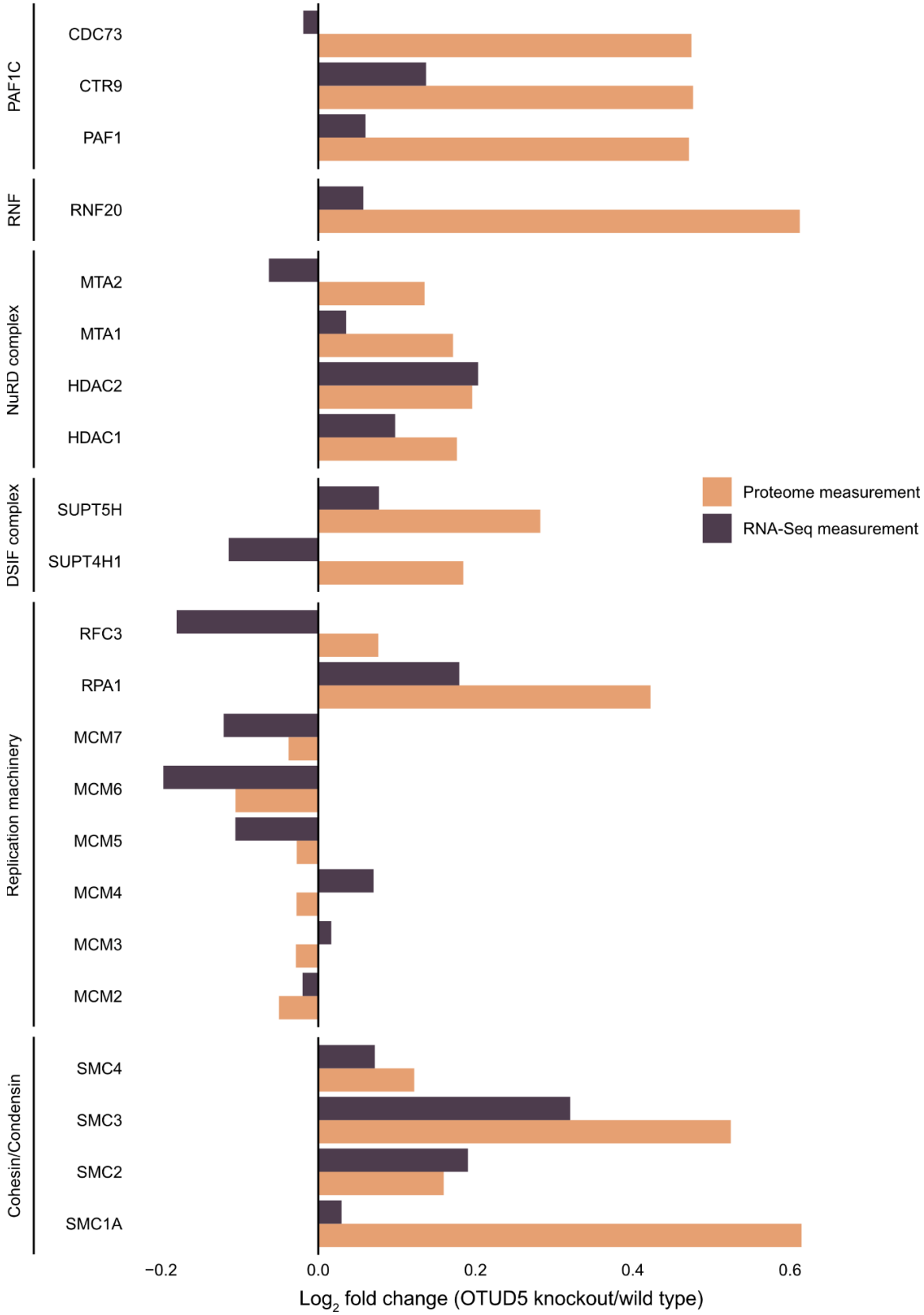
PAF1C
CDC73
CTR9
PAF1
RNF
RNF20
NuRD complex
MTA2
MTA1
HDAC2
HDAC1
DSIF complex
SUPT5H
SUPT4H1
Replication machinery
RFC3
RPA1
MCM7
MCM6
MCM5
MCM4
MCM3
MCM2
Cohesin/Condensin
SMC4
SMC3
SMC2
SMC1A
Proteome measurement
RNA-Seq measurement
−0.2
0.0
0.2
0.4
0.6
Log2 fold change (OTUD5 knockout/wild type)

Figure 10: Comparison of gene expression and protein abundance in wild type and OTUD5 knockout cells.
Bar plot indicating the average $log_2$-transformed fold change between OTUD5 knockout and wild type from full proteome and RNA-sequencing analyses, described in Figure 9.

## 4.4. OTUD5 knockout leads to increased loading of its substrates on chromatin

Given we had observed chromatin-associated factors as substrates of OTUD5, we then investigated their abundance in a chromatin-loaded state. Binding to chromatin is a highly dynamic process, not only for specialized and transiently binding proteins, – such as transcription factors and replication machinery subunits – but also for structural and architectural proteins, such as cohesin components[221–223]. Although strongly bound proteins, as linker and core histones, disassociate from chromatin at a much slower rate than other binders, they are still part of a dynamic environment that constantly exchange molecules from a bound to unbound state, modulating chromatin behavior.

In order to evaluate the impact OTUD5 has on controlling chromatin binding dynamics, we performed subcellular fractionation, isolating the chromatin-bound fraction of the cell – even from the remaining soluble nucleus – and measured protein levels by mass spectrometry (Figure 11A). Taking into account that controlling the homeostasis of ubiquitinated factors that are bound to chromatin is one of the several functions of VCP, we also treated both cell lines with NMS-873, an allosteric inhibitor[224] that causes defects in extraction of ubiquitinated substrates from chromatin and its own trapping in a chromatin-bound state[225].

Our results showed that, in general, OTUD5 absence did not have a global effect on the abundance of its putative substrates on chromatin (Figure 11B, first row). Proteins that are more ubiquitinated upon OTUD5 knockout varied in their loading in chromatin, with groups exhibiting a higher level of abundance in a chromatin-bound state, while other groups were seen to have their levels downregulated. However, when focusing on the novel substrates we identified, some interesting patterns were observed (Figure 11C).

First, as a control of our conditions, we noticed a severe depletion of UBR5 on chromatin, which could be interpreted as a consequence of its total levels being decreased in absence of OTUD5. Moreover, we also noted an increase in the abundance on chromatin of cohesin and condensin factors (SMC1-4) (Figure 11C, first row). All four subunits showed an upregulation when comparing OTUD5 knockout to wild type. Their levels already presented a trend of increase in chromatin abundance when wild type cells were treated with NMS-873 (Figure 11C, third row),

showing a dependence in VCP activity to control their levels on chromatin, but not comparable to OTUD5 absence, which showed a higher impact. On top of that, treatment of OTUD5 knockout cells with NMS-873 did not present an additive effect, suggesting that OTUD5 activity has a stronger effect than VCP inhibition on controlling SMC proteins levels on chromatin. Western blotting samples also showed the same trend, since NMS-873 treatment did not have such a strong effect as OTUD5 depletion (Figure 11D).

Another point to be considered was related to non-SMC proteins of cohesin and condensin complexes. These are not only formed by the main SMC factors, but the ring-shaped structure on DNA is only possible due to other components within these complexes. Although they do not possess ATPase activity, they play an essential role as bridges for the two main subunits of each complex (kleisin proteins; RAD21 for cohesin, CAP-H/NCAPH for condensin I and CAP-H2/NCAPH2 for condensin II) and as accessory proteins, the HAWK subunits[219]. Within the cohesin subunits, only the main SMC1-3 showed significant upregulation due to OTUD5 depletion, which was also observed for condensin I complex (SMC2-4 associated to CAP-H/NCAPH and accessory proteins CAP-D2/NCAPD2 and CAP-G/NCAPG). Notably, for condensin II subtype, not only the ATPases were observed to be more abundant on chromatin, but also all the non-SMC components of the complex, including the CAP-H2/NCAPH2 HAWK protein and the accessory factors CAP-D3/NCAPD3 and CAP-G2/NCAPG2.

Furthermore, a very interesting effect was observed regarding VCP itself. As previously reported[225], inhibition of VCP ATPase activity causes it to be “stuck” in a chromatin-bound state, even when it cannot process its substrates anymore – and our results indeed showed a higher abundance of VCP on chromatin after treatment with NMS-873 in both cell lines (Figure 11C – rows three and four – and Figure 11D). However, when looking at the comparison of VCP levels on chromatin in OTUD5 knockout cells to wild type, we noticed a marked decrease (Figure 11C – rows one and two – and Figure 11D) that only marginally was rescued by treatment with NMS-873. Our experiments showed that OTUD5 controls not only its substrates binding to chromatin but also VCP levels in a chromatin-bound state. We also evaluated these variations for VCP adaptors UFD1L and NPLOC4 and obtained less striking, yet similar, results, as NMS-873 caused a higher accumulation of those in chromatin in both cells lines although OTUD5 knockout showed a slight reduction of their levels when compared to wild type.

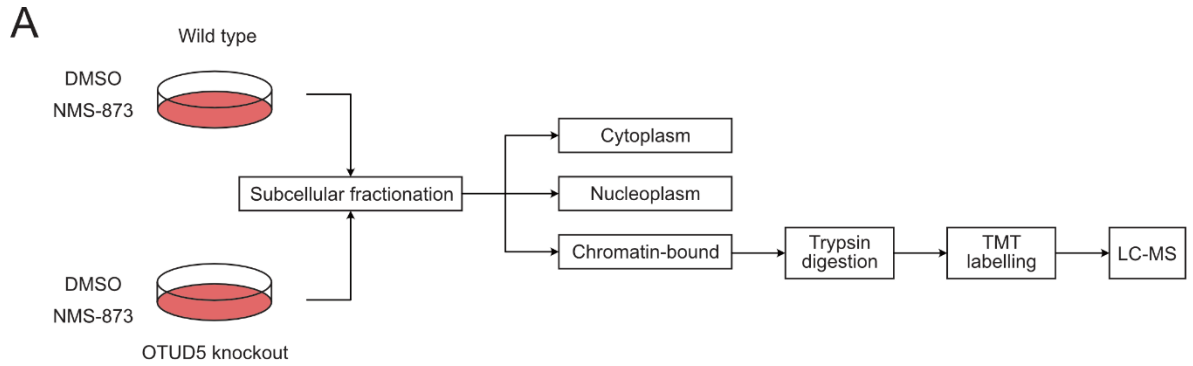
A
Wild type
DMSO
NMS-873
Subcellular fractionation
Cytoplasm
Nucleoplasm
Chromatin-bound
Trypsin digestion
TMT labelling
LC-MS
DMSO
NMS-873
OTUD5 knockout

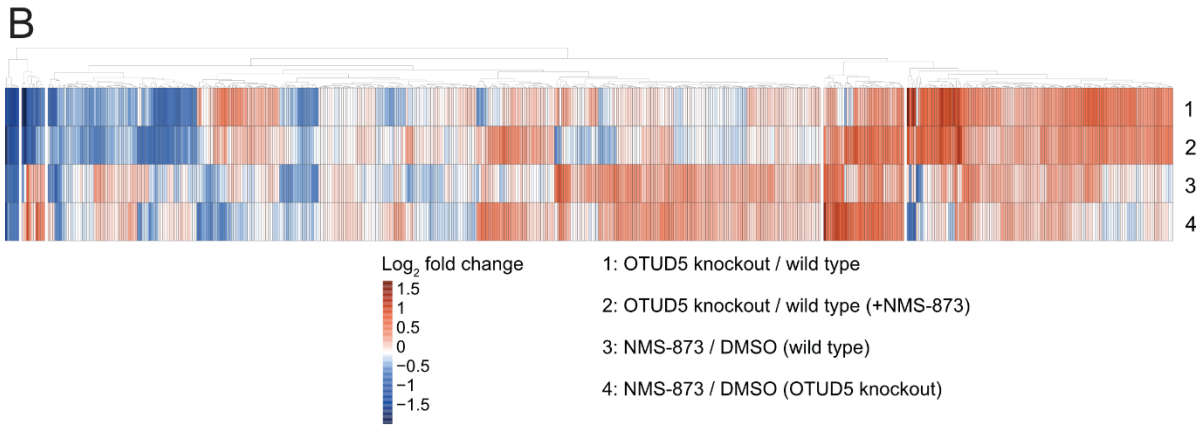
B
1
2
3
4
Log2 fold change
1.5
1
0.5
0
−0.5
−1
−1.5
1: OTUD5 knockout / wild type
2: OTUD5 knockout / wild type (+NMS-873)
3: NMS-873 / DMSO (wild type)
4: NMS-873 / DMSO (OTUD5 knockout)

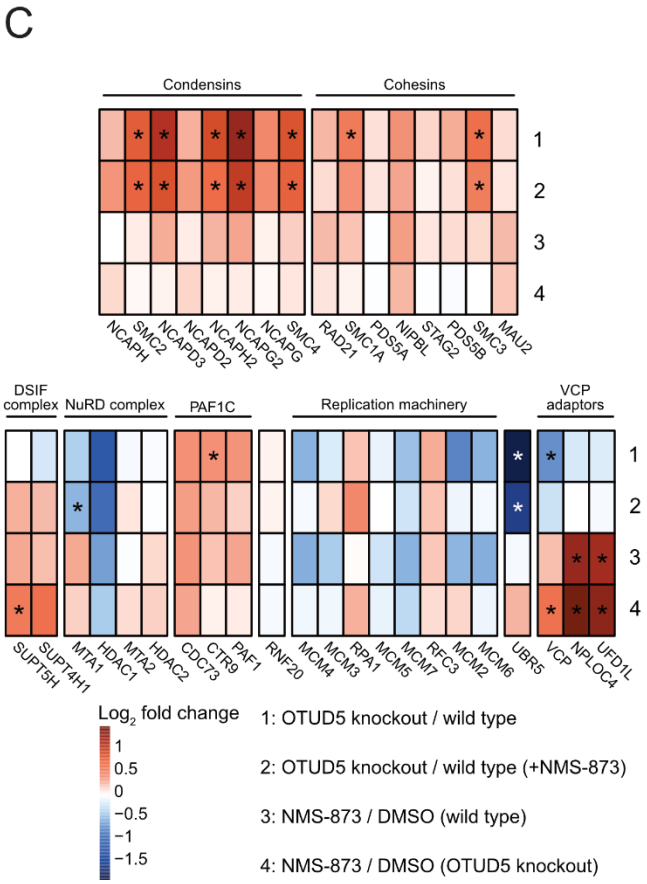
C
Condensins
Cohesins
NCAPH
SMC2
NCAPD3
NCAPD2
NCAPH2
NCAPG2
NCAPG
SMC4
RAD21
SMC1A
PDS5A
NIPBL
STAG2
PDS5B
SMC3
MAU2
DSIF complex
NuRD complex
PAF1C
Replication machinery
VCP adaptors
SUPT5H
SUPT4H1
MTA1
HDAC1
MTA2
HDAC2
CDC73
CTR9
PAF1
RNF20
MCM4
MCM3
RPA1
MCM5
MCM7
RFC3
MCM2
MCM6
UBR5
VCP
NPLOC4
UFD1L
Log2 fold change
1
0.5
0
−0.5
−1
−1.5
1: OTUD5 knockout / wild type
2: OTUD5 knockout / wild type (+NMS-873)
3: NMS-873 / DMSO (wild type)
4: NMS-873 / DMSO (OTUD5 knockout)

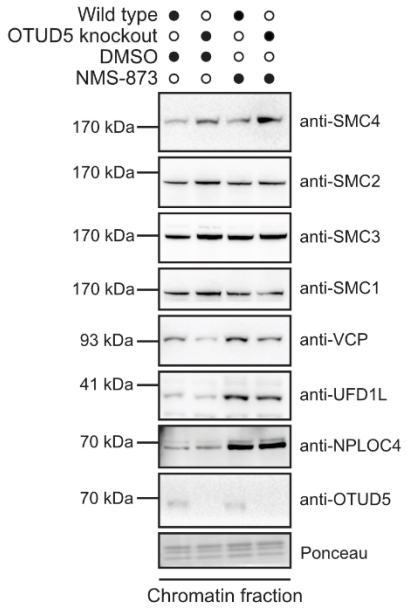
D
Wild type
OTUD5 knockout
DMSO
NMS-873
170 kDa
anti-SMC4
170 kDa
anti-SMC2
170 kDa
anti-SMC3
170 kDa
anti-SMC1
93 kDa
anti-VCP
41 kDa
anti-UFD1L
70 kDa
anti-NPLOC4
70 kDa
anti-OTUD5
Ponceau
Chromatin fraction

Figure 11: OTUD5 knockout induces a higher chromatin loading of its substrates, while decreases VCP and its adapters abundance in a chromatin-bound state.
A) Outline of the experiment performed to investigate the chromatin-bound levels of proteins in both wild type and OTUD5 knockout conditions, in presence or absence of VCP inhibitor NMS-873 (5 μM, 4 hours). Cell fractions representing cyto- and nucleoplasm were separated from proteins bound to chromatin and this last fraction was analyzed by mass spectrometry. Experiment was performed in quadruplicates. B) Heatmap of the quantified chromatin-bound levels (represented in $log_2$-transformed fold change between conditions indicated in the figure) for all OTUD5 putative substrates. C) Heatmap of the quantified chromatin-bound levels (represented in $log_2$-transformed fold change between conditions indicated in the figure) for OTUD5 substrates related to transcriptional and replication processes and part of cohesin and condensin complexes (and respective accessory proteins), alongside UBR5, VCP and its adaptors. Asterisks indicate statistical significance obtained by LIMMA linear model[202] (q-value < 0.01). D) Representative Western blot of the four conditions analyzed by mass spectrometry probed against the proteins indicated (n = 4).

## 4.5. OTUD5 and VCP form a novel identified nuclear interaction mediated by NPLOC4

Based on our new described substrates of OTUD5 and detection that some of these factors exhibited a higher abundance in a chromatin-bound state, we decided to investigate the interactome of OTUD5 to potentially observe these novel substrates interacting with this DUB. We performed a pulldown of OTUD5 from wild type cells, using a targeted antibody against OTUD5 – and a non-specific IgG as a control –, and quantified the enriched proteins via mass spectrometry (Figure 12A).

Although the number of proteins significantly enriched (fold change $\geq 1.5$; p-value $< 0.05$) after OTUD5 pulldown was not high, as we quantified 39 proteins in comparison to the IgG control pulldown, some interesting factors were co-immunoprecipitated with OTUD5. First, we observed a very high enrichment of our bait, which would be expected in our experimental design, and alongside we noted UBR5 being pulled down, a known interactor of OTUD5. Furthermore, we also noticed the presence of ubiquitin itself (represented by gene names "RPS27A; UBC; UBB; UBA52"), which given the enzymatic activity of the DUB also suggested that we confidently enriched true partners of OTUD5 (Figure 12B).

Surprisingly, among OTUD5 interactors, we observed presence of VCP, indicating a possible partnership between these two proteins. In order to validate this finding, we performed a proximity ligation assay (PLA) that would both validate the interaction but also indicate the subcellular compartment in which this interaction would occur. The technical controls of our experiment showed the expected results. We did not see any signal coming from wild type cells either not probed with antibodies targeting any protein or probed with just one antibody as well as no signal observed from OTUD5 knockout cells probed against the pair OTUD5-VCP. On the other hand, we noted a high number of PLA foci in cells probed against VCP and UFD1L, which form a well-known pair. (Figure 12C).

When assessing for the OTUD5-VCP interaction in wild type cells, we noticed the signal coming from PLA foci across the cell – but mainly concentrated in the nucleus, where our data indicates that OTUD5 performs its main functions –, confirming the novel interaction we identified between OTUD5 and VCP (Figure 12C).

We then evaluated how this interaction would behave if we depleted the adaptors UFD1L and NPLOC4 from the cell. Our results indicated that even in the RNA (siRNA)-based knockdown of either of these two adaptors, the interaction of OTUD5 with VCP was still visible. Quantification of nuclear foci derived from PLA signal, however, showed that in the condition where NPLOC4 was depleted, interaction of OTUD5 and VCP was perturbed and significantly reduced (Figure 12D). On the other hand, knockdown of UFD1L showed a significantly increased PLA signal, which could indicate that in absence of UFD1L, VCP hexameric ring could be more available for the interaction with OTUD5 (Figure 12D).

The next question we asked was if UBR5 and TRIP12 would have any impact on the interaction between OTUD5 and VCP. For that, we also performed PLA in scenarios where UBR5 was knocked out and/or TRIP12 had its levels decreased via knockdown. Our results did not show any reduction of the signal, both in individual or combined depletions of the two E3 ligases, but instead showed a significantly increased number of nuclear PLA foci in these conditions (Figure 12E).

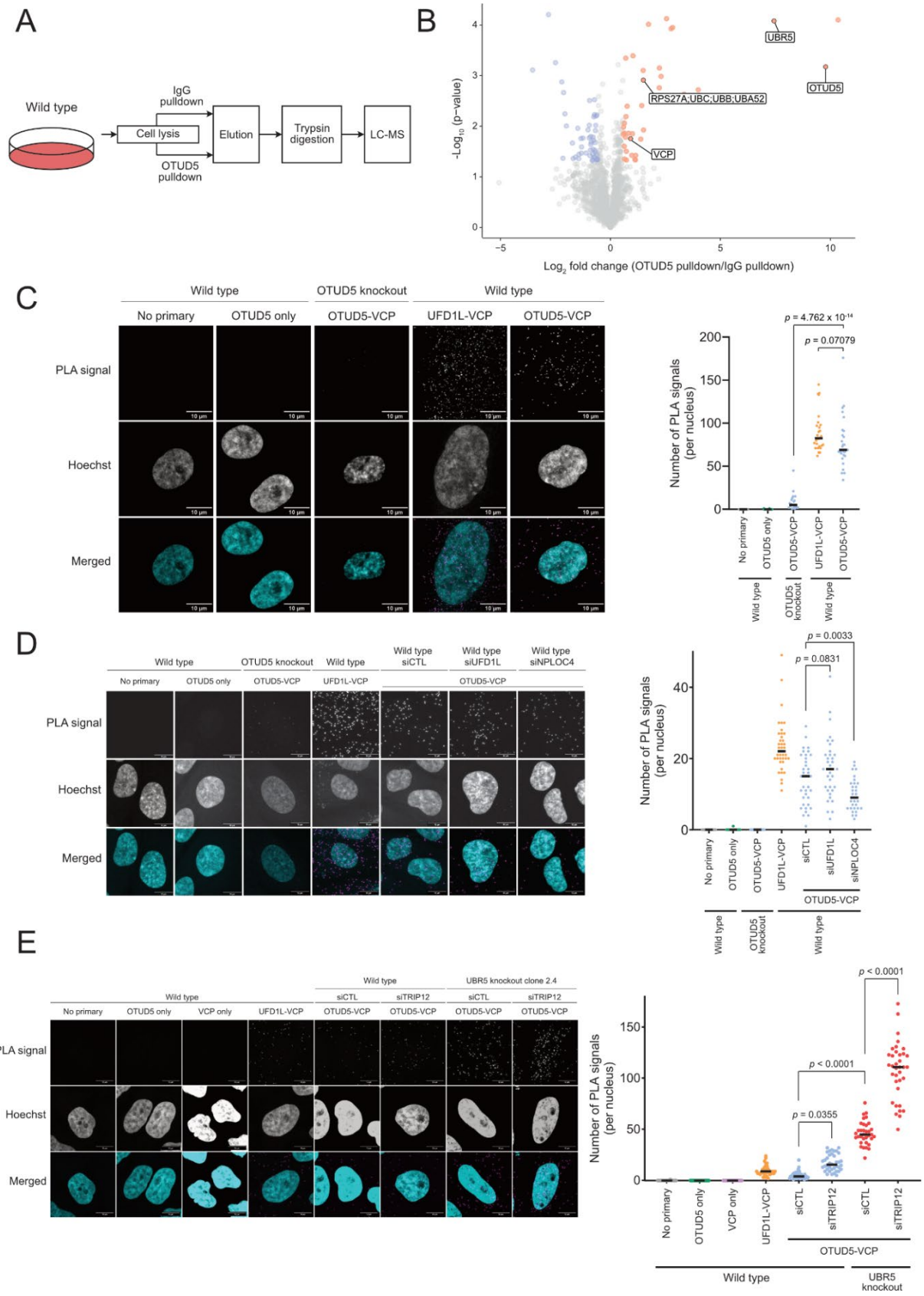
A
Wild type
IgG pulldown
Cell lysis
Elution
Trypsin digestion
LC-MS
OTUD5 pulldown
B
UBR5
OTUD5
RPS27A;UBC;UBB;UBA52
VCP
-Log10 (p-value)
Log2 fold change (OTUD5 pulldown/IgG pulldown)
C
Wild type
OTUD5 knockout
Wild type
No primary
OTUD5 only
OTUD5-VCP
UFD1L-VCP
OTUD5-VCP
PLA signal
Hoechst
Merged
p = 4.762 x 10-14
p = 0.07079
Number of PLA signals (per nucleus)
D
Wild type
OTUD5 knockout
Wild type
Wild type siCTL
Wild type siUFD1L
Wild type siNPLOC4
No primary
OTUD5 only
OTUD5-VCP
UFD1L-VCP
OTUD5-VCP
PLA signal
Hoechst
Merged
p = 0.0033
p = 0.0831
Number of PLA signals (per nucleus)
siCTL
siUFD1L
siNPLOC4
E
Wild type
UBR5 knockout clone 2.4
siCTL
siTRIP12
siCTL
siTRIP12
No primary
OTUD5 only
VCP only
UFD1L-VCP
OTUD5-VCP
OTUD5-VCP
OTUD5-VCP
OTUD5-VCP
PLA signal
Hoechst
Merged
p < 0.0001
p < 0.0001
p = 0.0355
Number of PLA signals (per nucleus)
UBR5 knockout

Figure 12: OTUD5 forms a protein complex with VCP mediated by NPLOC4.
A) Experimental design of the immunoprecipitation of OTUD5 followed by measurement of enriched proteins via mass spectrometry. Targeted OTUD5 pulldown was performed in triplicates and compared to a control IgG from the same host species. B) Volcano plot indicating the results of the experiment described in A. Red and blue dots indicate the significantly enriched proteins either by OTUD5 specific pulldown or control IgG according to the cutoffs proposed (fold change $\geq \pm 1.5$ and p-value $< 0.05$, derived from a two-tailed *t*-test). OTUD5, as well as known partner UBR5, ubiquitin (RPS27A; UBC; UBB; UBA52) and novel interactor VCP are indicated in the figure. C-E) PLA of the pair OTUD5-VCP. On the left, representative microscopic images of each condition analyzed (indicated on image) for each channel imaged and their merged image (scale bar = 10 μm). On the right, quantification of the number of PLA foci in cell nuclei for conditions shown on the left ($n \geq 30$, p-value derived from a two-tailed *t*-test).

Next, we decided to explore this possibility of NPLOC4 being the factor mediating the interaction between OTUD5 and VCP by performing AlphaFold predictions for the relationship between these two factors. First, by analyzing the individual models of OTUD5 and NPLOC4, we noticed a high disordered content for the deubiquitinase, as its prediction showed large stretches of residues forming loops without presence of stable secondary structures (Figure 13A). NPLOC4, on the other hand, exhibited a higher content of structured regions and a more diverse local secondary structure arrangements (Figure 13B).

Interestingly, when performing a prediction of both proteins in order to observe a possible interaction *in silico*, we observed a notable insertion of OTUD5 N-terminus in a cleft in NPLOC4 structure, which has a high content of negatively charged residues (Figure 13C). However, having in mind the highly disordered tertiary structure of the DUB, we decided to generate a new prediction model containing only the N-terminus of OTUD5, ranging from residues 1-30, that we identified as a promising interacting region of the DUB and, again, we could observe the insertion of this region of OTUD5 in NPLOC4 cleft in the same way as for the full length (Figure 13D). Considering in parallel the residue composition of OTUD5 N-terminus (Figure 13E), we observed the presence of positively charged residues in this region, such as the stretch of three lysine residues, which could mediate the interaction between the DUB and NPLOC4 to this pocket, as this last one has a predominant negative charge.

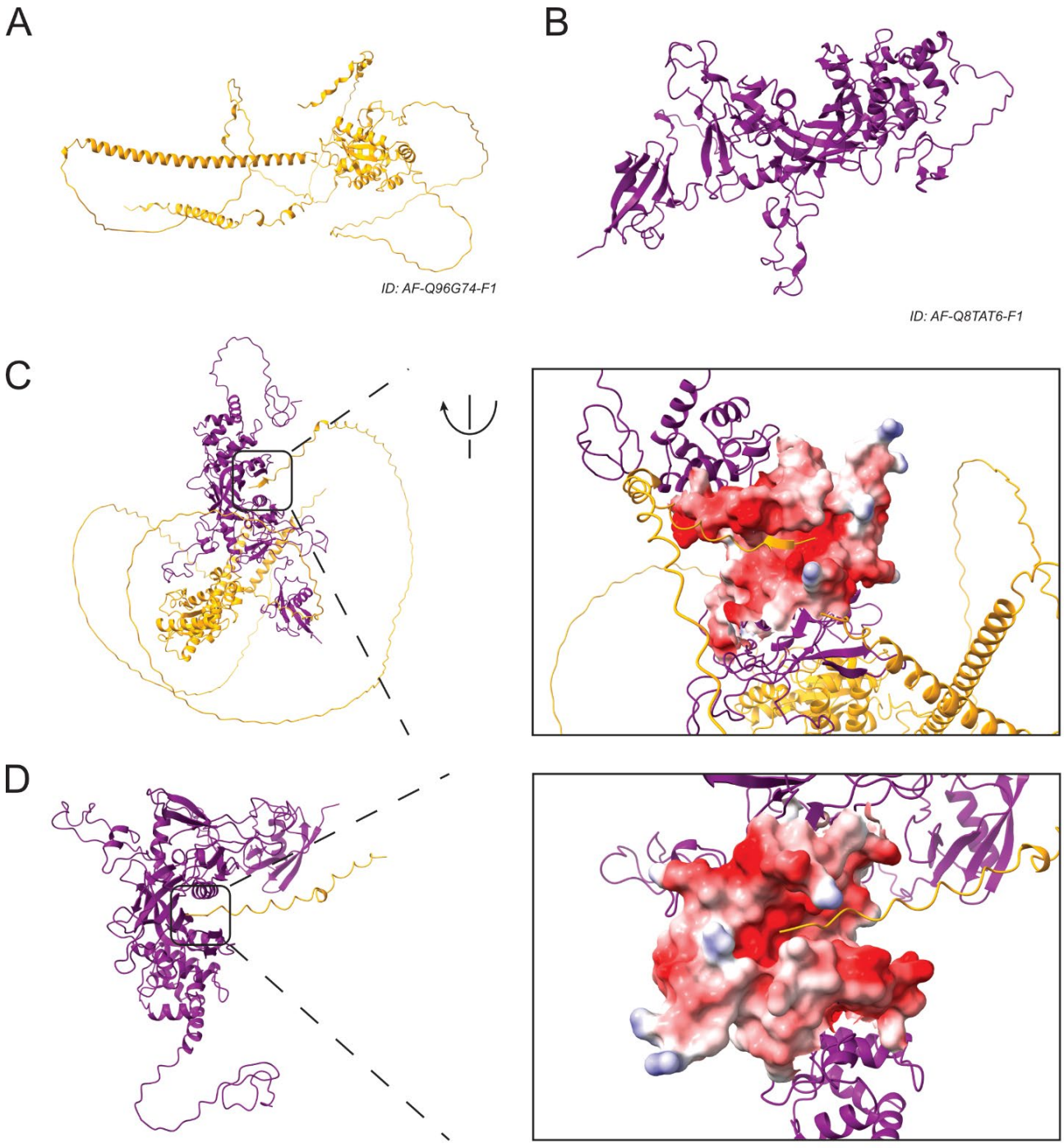
A
ID: AF-Q96G74-F1
B
ID: AF-Q8TAT6-F1
C
D
E
hOTUD5
M T I L P K K K P P P P D A D P A N E P P P P G P M P P A P
1.....10.....20.....30
Hydrophobic residue
Positively-charged residue
Polar residue
Prolines
Negatively-charged residue
Glycine

Figure 13: AlphaFold prediction model indicates the N-terminus of OTUD5 to interact with NPLOC4 pocket.
A) AlphaFold prediction model of OTUD5 (ID: AF-Q96G74-F1). B) AlphaFold prediction model of NPLOC4 (ID: AF-Q8TAT6-F1). C-D) On the left, prediction model of interaction between full length OTUD5 (C) or first 30 residues in OTUD5 N-terminus (D) (orange) and NPLOC4 (purple). On the right, inlet showing the insertion of OTUD5 in a negatively charged pocket of NPLOC4. E) Primary sequence of the selected OTUD5 peptide for prediction in D, with colors indicating the residue characteristic (following Clustal X default coloring scheme).

## 4.6. OTUD5 knockout cells exhibit physiological alteration in nuclear processes

Our previous results led us to question whether we could observe variations in phenotypes associated with the biological processes that OTUD5 was seen to be involved in.

First, we then assessed the global transcriptional activity of OTUD5 depleted cells by means of measuring incorporation of EU into RNA[226]. Working similarly to BrU, EU is a uridine analog that can be incorporated into newly synthesized RNA during transcription and labels exclusively RNA. As one advantage of the method, it can be easily detected by means of the so called "click chemistry", which is based on a Copper (I)-catalyzed reaction between the alkyne group present in EU with a reactive azide group linked to a fluorophore[227,228], making it possible to be quantified by microscopy.

We measured not only the incorporation of EU comparing wild type to OTUD5 knockout cells in unstressed conditions but also under different physicochemical stresses (Figure 14A), such as UV-C irradiation and chemical inhibitors DRB and PladB. UV-C irradiation generates lesions on DNA (cyclobutene-pyrimidine dimers and 6-4 pyrimidine-pyrimidone photoproducts) and triggers inhibition of both initiation and elongation steps of transcription, which can eventually lead to degradation of RNA Pol II complex itself[229–232]. DRB is a chemical inhibitor of the P-TEFb complex subunit CDK9, a regulator of RNA Pol II pausing-release and elongation, that is required for RNA Pol II complex phosphorylation and subsequent activation[233,234]. Lastly, PladB targets SF3b complex, part of the splicing machinery, impairing its activity[235,236].

When assessing the comparative results for wild type condition between un-/stressed conditions, we observed that all stimuli we presented to cells decreased the global transcriptional activity significantly (Figure 14B-C). Similarly, OTUD5 knockout cells also exhibited lower transcriptional levels upon treatment with different stressors. Furthermore, our results showed that although in an untreated manner the general level of transcription was similar between wild type and OTUD5 knockout, the DUB depleted cells exhibited significantly higher levels of global transcriptional activity after one hour of release from the physicochemical stresses (Figure 14B-C).

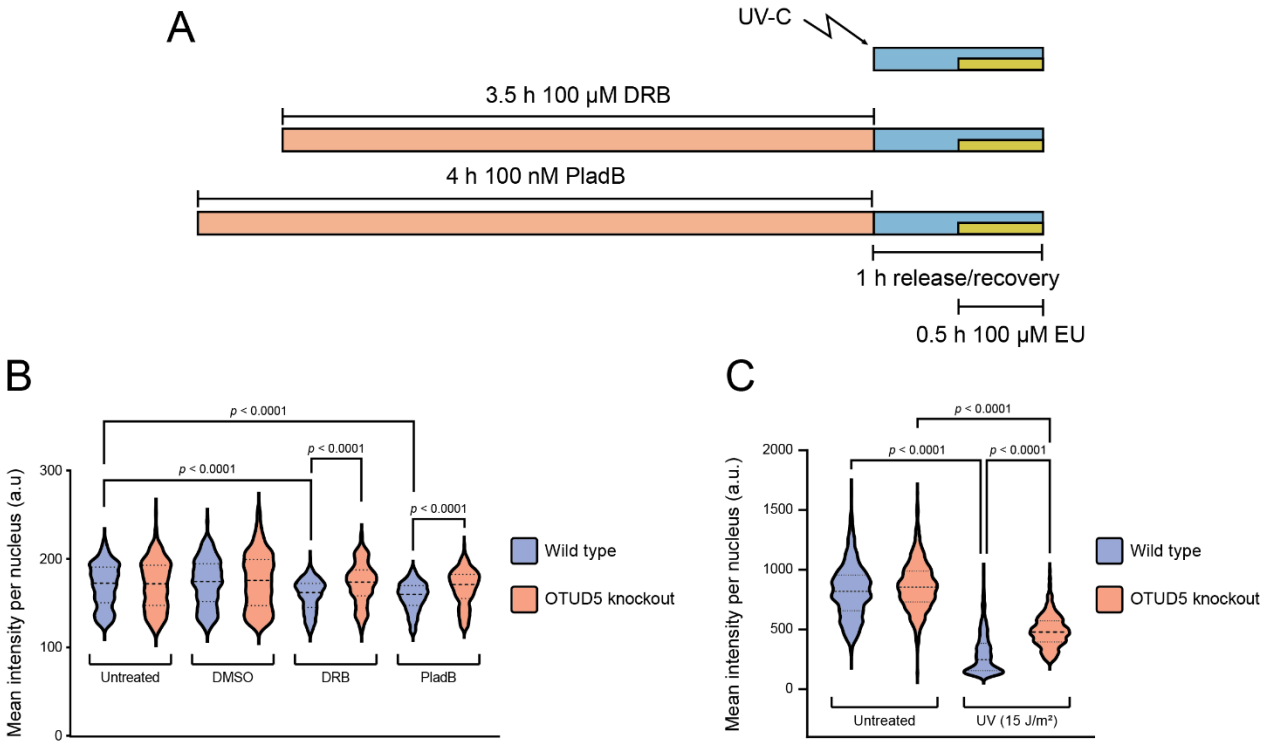


Figure 14: OTUD5 depletion impacts recovery of global transcriptional activity after physicochemical stress.
A) Overview of transcription perturbation experiment performed to evaluate global transcriptional levels in wild type and OTUD5 knockout cells, indicating the physicochemical stresses used and for how long cells were treated, as well as recovery time and period of EU incorporation (100 µM). Experiment was performed three times and values for all individually measured nuclei were included. B-C) Violin plots of the measured mean intensity per nucleus of the EU conjugated to fluorophore (arbitrary units, a. u.) in both cell lines and different stresses, indicated. Statistical significance was calculated via analysis of variance (ANOVA one-way) and p-values are indicated.

In addition to the transcriptional levels assessment, the observation that processes related to DNA replication and mitosis were also enriched in our ubiquitin-remnant profiling GO-term analysis made us question whether there would be growth differences between the two cell lines and whether they would show alterations in their cell cycle progression profile.

The results we obtained for cell growth indicated that from the early timepoints assessed, OTUD5 knockout cells had a slower growth rate compared to wild type condition. Both cell lines were seeded with the same amount and during the whole time course of our analysis, from the first time point collected (8 hours) to 72 hours after cell seeding, wild type cells exhibited a higher level of confluence in comparison to OTUD5 depleted cells. Final time point evaluated indicated a variation of around 40% in confluence between two cell lines (Figure 15).

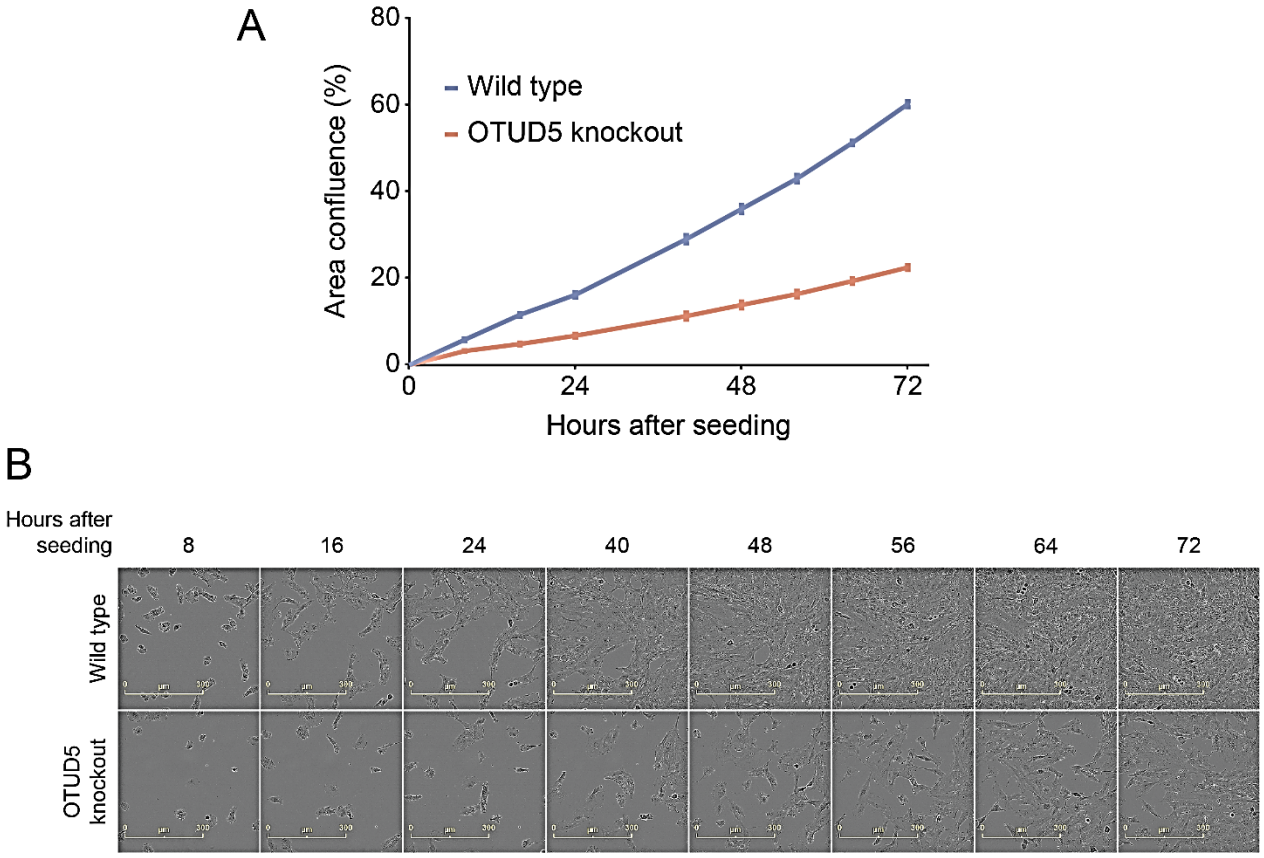


Figure 15: OTUD5 knockout cells exhibit a slower growth rate.
A) Growth curve of wild type and OTUD5 knockout cell lines after tracking the confluence area – represented by percentage of the well covered by cells – for 72 hours. Both cell types were seeded with same cell number per well (1 x $10^4$ cells) and assessment was performed in quadruplicates. Error bars indicate the standard error of the mean. B) Representative images of the quantifications exhibited in A for each of the time points for both cell lines. Scale bar = 300 µM.

On top of the observed decreased cell growth when cells are in absence of OTUD5, we evaluated the cell cycle progression profiles of wild type and OTUD5 knockout cells. For that, we compared them both in a asynchronous manner but also under arrest and release from palbociclib (PB), a CDK4/6 inhibitor that induces cellular arrest during G1 stage of the cell cycle by inhibiting the kinases activity towards the retinoblastoma protein (Rb) and preventing the formation of phospho-Rb, consequently inhibiting progression from G1 to S phase[191,237]. PB has also been used in the clinic as a breast cancer treatment, causing a high sensitivity for endocrine receptor-positive (ER+) and human epidermal growth factor receptor 2 (HER2)-amplified subtypes[238].

When first comparing the cell cycle stage distribution from asynchronous cells, we observed a very similar behavior between wild type and OTUD5 depleted cells. Both cell lines had around 40-45% of cells in G1 stage, around 40% in S phase and between 14-17% in G2, with a slightly

increased number of cells in G1 for OTUD5 knockout condition while a slightly higher proportion of wild type cells in G2 (Figure 16A-B).

Moreover, when comparing the arrested cells without any release from PB treatment (time point 0 h), we observed also a similar general behavior between cell lines, with the majority of cells in G1 and lower proportions in S and G2 stages, respectively. The first time point after release (2 hours) also showed similar trends, with a slight increase in S phase for both cell lines accompanied by a decrease in G1, while G2 remained stable. From the 6 hours time point on, the behavior of the two cell lines started to differ more prominently. While the distribution of cell cycle stages in the wild type condition was similar to previous reports using the same cell line, same arrest strategy and same time points[191], the distribution for OTUD5 knockout condition differed (Figure 16C). OTUD5 depleted cells only had their peak of S phase after 12 hours of release from PB arrest (while that happened after 6 hours for wild type) and after 15 hours of release, they reached the highest accumulation of G2 within the experiment, while wild type cells had already reached that point after 12 hours of release and after 15 hours showed indications that their cycle had already restarted (Figure 16C-D).

In addition to the flow cytometry measurements, we also analyzed via Western blotting the protein levels during different release time points across the cell cycle. In order to observe the sequential stages of the cycle, we used as markers cyclins E2 and A2, which are respectively associated with S phase – peaking at this stage for its participation during transition from G1 to S – and G2/M stages – when peak of cyclin A2 happens due to its role in the induction of entry into mitosis[239]. On top of those two markers, we also assessed levels of TPX2, a known spindle assembly regulator during mitosis, that undergoes an increase in its levels during later time points of the cycle and being degraded during the mitotic process so cells can restart cycling[240].

First, we assessed levels of OTUD5 and UBR5 during the release time points after PB inhibition. Both proteins showed quite stable levels throughout the time course, with no major variations during any stage of the cycle that could indicate that their activity is restricted to certain step(s) (Figure 16E-F). Even in OTUD5 knockout, which exhibited the marked severe decrease in UBR5 levels, we did not see any variations in the ligase levels, going in line with our observations in the wild type condition (Figure 16E-F).

Our results showed in wild type cells an expected variation in cycle markers, such as both cyclins and TPX2 (Figure 16E-F). We observed the previously reported increase in Cyclin E2 after

6 hours of release from PB arrest, which should be related to cells being in S phase, and its later decrease during the expected G2/M stages and cycle restart after 12 and 15 hours of release, respectively. Cyclin A2 peaked after 12 hours of release, in line with cells being at G2/M transition, but already had its levels diminished at 15 hours, suggesting the cycle restarted.

On the other hand, when we looked at OTUD5 knockout cells, we observed differences from wild type cells that were similar to our flow cytometry measurements. We noted the marked increase of cyclin E2 after 6 hours of release but with strikingly higher levels in comparison to wild type, suggesting an abnormal progression of these cells when entering S phase, in parallel with a maintenance of its levels in later time points, indicating possible deregulations of the cycling. Cyclin A2 also showed maintained levels after its increase, consistent with an inability of these cells to conclude and restart the cycle at the same time as wild type cells (Figure 16E-F).

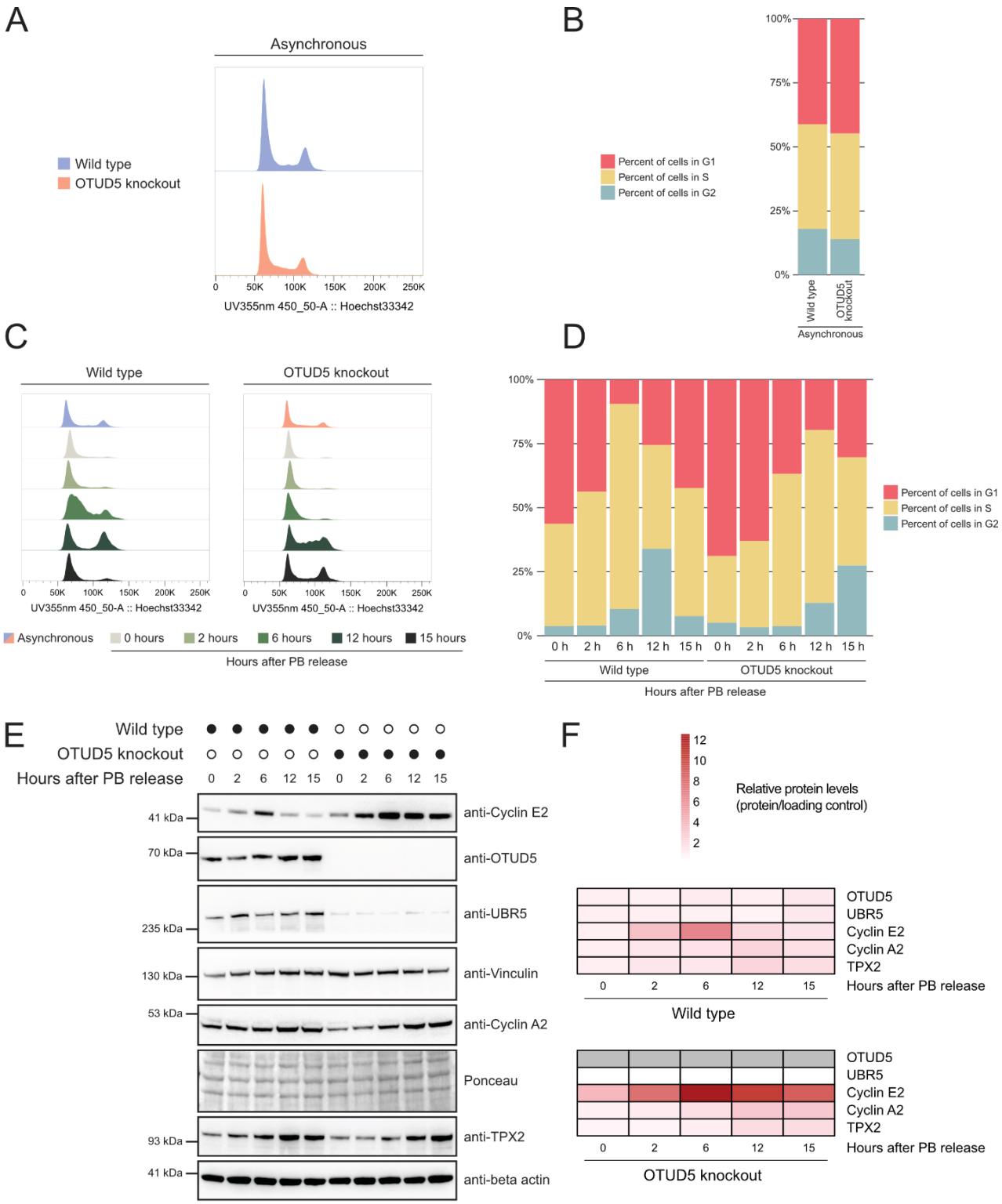


Figure 16: OTUD5 knockout delays cell cycle progression and exhibits abnormalities in cycle markers.

A) Histograms of flow cytometry measurements of asynchronous wild type and OTUD5 knockout cell lines indicating cell count and Hoechst 33342 intensity. Experiment was performed in triplicates and one is represented as example. B) Distribution of cells in each cell cycle stage from

measurement shown in A for both asynchronous cell lines. Percentages were obtained using the Watson model for cell cycle in FlowJo software and indicate the average of three individual measurements. C) Histograms of flow cytometry measurements for wild type and OTUD5 knockout cell lines indicating cell count and Hoechst 33342 intensity, for either asynchronous cells or after arrest with PB and release from treatment (indicated in the figure). Cells were treated with PB for 24 hours/150 nM, and then collected either without washing out the inhibitor or with the time points indicated (at least 7000 events). Measurements were performed in three independent replicates. D) Distribution of cell cycle stage for the measurements shown in C. Percentages were obtained using the Watson model for cell cycle in FlowJo software and represent the average of the three measurements. E) Representative Western blot of the samples measured by flow cytometry in C for arrested cells after PB treatment and sequential release time points. Probed proteins are indicated in the figure, together with loading controls. F) Quantification of the Western blot signal intensity from the proteins probed in E, represented in relative fold variation. All quantifications were normalized to the first time point collected (0 h after release) of wild type. Western blots were performed three times derived from the three samples generated for flow cytometry measurements and the average relative protein level is shown.

# 5. Discussion

## 5.1. OTUD5-dependent ubiquitination status and proteome alterations

Mass spectrometry-based approaches have been shown to be a very powerful tool to determine substrates of deubiquitinases. Association between these approaches and enrichment of ubiquitin-remnant modified peptides – e. g., the di-glycine tryptic remnant[204] or the 13 residues long Lys-C remnant[241] – enabled the identification of endogenous ubiquitin sites that had their ubiquitination increased in the absence of DUBs such as USP7, USP30 and USP32[242–244] or those responsive to cysteine protease chemical inhibition, also causing their ubiquitination status to be elevated[245].

Our strategy, making use of the anti-K-ε-GG for enrichment of tryptic ubiquitin remnant[204], uncovered 787 proteins that had their ubiquitination status impacted by OTUD5 knockout. Among those, we focused our attention on the subset that exhibited a higher ubiquitination upon OTUD5 absence, in which we observed a high enrichment in our GO-term analysis in terms related to the nucleus, for both biological process and cellular compartment (Figure 6C). Furthermore and in line with our observations, previous reports have indicated that OTUD5 is involved in the regulation of nuclear mechanisms, as control of DNA replication activity[178] and control of transcriptional activity, by interaction with transcriptional regulators or by modulating their levels[168,177].

As an internal control of our experiment, we assessed the ubiquitination levels of UBR5 sites, as it was one of the first validated substrates of OTUD5[169]. Although UBR5 experiences a severe depletion in its levels when OTUD5 has its levels decreased (refs. [169,177] and Figure 8A), we still observed increased levels of ubiquitinated peptides coming from this E3 ligase in the condition of OTUD5 knockout. This example of UBR5 being more ubiquitinated although its levels are depleted led us to question whether the changes in ubiquitination status would be an outcome of increased protein levels for the putative substrates of OTUD5. We then measured the full proteome of OTUD5 knockout cells and normalized our ubiquitinome data with the proteome data (Figure 7) – i. e., we subtracted the proteome variations from the ubiquitination variations –, which gives

us a higher confidence that the alteration in ubiquitination levels was not a simple consequence of changes in total protein levels.

Given the novelty of seeing chromosome structural regulators among putative substrates of OTUD5, we focused on validating their increased ubiquitination status upon depletion of the DUB. We confirmed our data by performing a TAK-243 chase assay, in which we inhibited the ubiquitination cascade[220], and observed the removal (or maintenance) of the ubiquitin signal by pulling down a ubiquitin-modified enriched fraction of the proteome[180] and immunostaining for these specific targets (Figure 8). Our observations showed an increased ubiquitination for all the four SMC proteins analyzed in a non-stressed state, while the total ubiquitin signal was similar, going in line with our mass spectrometry data. Furthermore, we noticed a more stable maintenance of the ubiquitinated species of the four targets in the OTUD5 knockout state in comparison to wild type after inhibition of the ubiquitin cascade. The maintenance for those was similar to what is observed for UBR5, as the absence of the DUB causes it to remain ubiquitinated after TAK-243 treatment. It is also worth noting that the signal after 6 hours of treatment is not the same as in the DMSO control, which makes us speculate that OTUD5 might not be the only deubiquitinase acting on those proteins – as well for UBR5. However, it is clear that the absence of OTUD5 directly impacts the ubiquitination of those factors. In conclusion, we uncovered SMC1-4 as novel high confidence substrates of OTUD5.

The full proteome data also led to another interesting observation: OTUD5 substrates, when in absence of the DUB, exhibit an increased abundance when in comparison to wild type cells. Historically, ubiquitin attachment to target proteins and formation of chains were seen as signal for degradation[27,246]. Hence, the removal of the ubiquitin signal by DUBs can lead to stabilization of their substrates, which was observed by previous reports involving DUBs from the OTU family[160,247] and even from OTUD5 – in the context of embryonic development[168]. Our results, on the other hand, showed an opposite effect in which OTUD5 depletion led to an elevated level of its substrates (Figure 9), which suggests that OTUD5 activity on these proteins is not a simple case of rescuing them from proteasomal degradation. *In vitro* reports showed OTUD5 has activity towards K48- and K63-linked ubiquitin chains[155] and that it is also capable to cleave these linkages in the context of branched K48/K63 chains[138]. Altogether, one speculation that could be raised is that OTUD5 could be recognizing and cleaving branched chains from these substrates, which in turn would be a mechanism that would facilitate their degradation, therefore explaining the augmented

levels we observed. However, we have not explored so far linkage composition and chain architecture present on these substrates that are dependent on OTUD5 activity – which would be an interesting point to elucidate in the future.

## 5.2. Regulation of substrate abundance on chromatin and VCP recruitment

Ubiquitination is a very well-known mode of controlling both function and homeostasis of chromatin-associated proteins. Histone 2A (H2A), for example, has a range of 5 to 15% of its pool in a ubiquitinated form, making it the most ubiquitin modified protein in the nucleus of mammalian cells and one of the most ubiquitinated proteins in the cell – apart from the fact that it was the first example of a protein to be ubiquitinated[248,249]. Literature does not indicate a universal correlation of changes in chromatin-binding to changes in ubiquitination status. For histone 2B (H2B), for example, an increase in ubiquitination leads to higher levels of association with chromatin[250]; on the other hand, other factors can be ubiquitinated as a signal to have their pool of molecules bound to chromatin removed, such as PARP1[251] and the DNA replication complex DNA polymerase α/Primase[252].

When looking at the chromatin-binding status of the substrates of OTUD5 (Figure 11C), we noticed a trend among PAF1 complex (Figure 11C) and specially for cohesin/condensin subunits (Figure 11C-D) to be in a higher abundance bound to chromatin when OTUD5 is depleted. It does not seem to be a general mechanism of action for OTUD5 as other substrates did not show the same pattern regarding their chromatin-bound levels: UBR5, HDAC2 or HCF1[168] had either similar or significantly reduced levels in OTUD5 knockout (appendix, Figure 18A). Ku80/XRCC5, another described substrate of OTUD5[176], in our hands showed – similarly to the literature – that increased ubiquitination – caused by OTUD5 absence – decreases its chromatin-bound abundance (appendix, Figure 18A). In the case of the MCM proteins, these subunits of the CMG helicase also showed a marked decrease in chromatin loading upon OTUD5 knockout – going in line with reports showing them to be removed from chromatin upon increase of their ubiquitination while removal of this signaling would stabilize them in this state[253]. Altogether, our results indicate that the OTUD5-

dependent ubiquitination status of high confident novel substrates SMC1-4 directly impact their chromatin-bound abundance, causing them to be more bound to chromatin in OTUD5 depletion.

A second interesting observation was that in absence of OTUD5, we noted a decreased amount of VCP in chromatin (Figure 11C-D). When compared to wild type, our mass spectrometry data shows that VCP exhibits almost a 2-fold reduction in its chromatin-bound levels. Although its decrease was reduced to a lesser extent, this observation was still visible in the comparison between the two cell lines when VCP was inhibited with NMS-873. NMS-873 itself caused VCP to be trapped in a chromatin-bound status for both cell lines, going in line with previous observations[252,254,255] – as well as its two main nuclear adaptors UFD1L and NPLOC4. Both co-factors exhibited a much lower variation in their chromatin levels in OTUD5 knockout condition, while allosteric inhibition of VCP elevated in a similar manner in both cell lines their loading.

VCP recruitment to chromatin has been shown to be an important mechanism in the nucleus to maintain protein homeostasis, being able to recognize and extract, in combination with its several co-factors, ubiquitinated proteins. *In vitro* systems combined with cellular models showed that VCP is responsible for removing Ku80 from a chromatin-bound state[255] – a previously described substrate of OTUD5[176]. Furthermore, *S. cerevisiae* models showed that VCP, together with Ufd1 and Npl4, modulates cycles of (un-)loading of condensin complexes from a chromatin-bound state, showing specifically a lower diffusion for Smc4 in cells depleted of Cdc48[256] (VCP ortholog in yeast) –, while in mammalians a report that explored the VCP-dependent ubiquitination showed SMC4 to exhibit upregulated sites upon VCP inhibition with NMS-873[257].

Collectively, we observed that the OTUD5-dependent increase in ubiquitination of its novel substrates correlates with an increase in chromatin loading of these proteins, while on the other hand OTUD5 modulates the recruitment of VCP to chromatin, as this unfoldase was seen to have its chromatin levels depleted upon OTUD5 knockout.

## 5.3. OTUD5 interaction with VCP mediated by NPLOC4

The presence of VCP among the quantified proteins and significantly enriched by OTUD5 pulldown (Figure 12B), in combination with our observation of changes in the chromatin proteome, raised the possible interpretation that the combined activity of both proteins would be important for regulating the chromatin loading of the novel OTUD5 substrates, working together in a novel

protein-protein interaction pair, since DUBs are a class of proteins known to function as partners of VCP[113]. In order to explore this partnership, we performed PLA experiments and observed, once again and confirming the interaction, *in vivo* proximity between OTUD5 and VCP, occurring in the whole cell area but, more importantly, in the nucleus (Figure 12C).

One line of interpretation of this result would be that OTUD5 and VCP would interact as a consequence of OTUD5 itself being ubiquitinated and hence a substrate of VCP. OTUD5 is known to be a substrate of two different E3 ligases that together modify this DUB: UBR5 and TRIP12[40]. Hence, we performed the same assay in the absence of either one or both ligases (Figure 12E). Our results showed a cumulative effect of the depletion of UBR5 and TRIP12 in the number of nuclear foci indicating the interaction between OTUD5 and VCP, which could be explained by the increased total levels of OTUD5 when these ligases, individually or in combination, have reduced amount in cells – observation from our group (redacted, unpublished data) and others[40]. Although this evidence does not rule out the possibility of OTUD5 to be a substrate of VCP, it shows that the interaction does not depend on OTUD5 to be ubiquitinated, as it is observed still when OTUD5 ubiquitination is decreased. On the other hand, when assessing the impact of VCP co-factors UFD1L and NPLOC4, we observed a significant reduction in the interaction between OTUD5 and VCP when NPLOC4 was depleted, decreasing the number of nuclear foci in around a 2-fold manner (Figure 12D). Interestingly, no perturbation was noted in the case of UFD1L depletion, as we observed even a tendency of upregulation of the interaction in this scenario.

Since we noticed NPLOC4 interfering in the interaction between OTUD5 and VCP, we hypothesized that NPLOC4 could be a bridging factor, mediating the formation of the pair. If this were true, then we would be able to observe the interaction of OTUD5 also with NPLOC4. In the endogenous OTUD5 interactome we performed, VCP was seen as a significantly enriched protein after OTUD5 pulldown. Although NPLOC4 did not surpass the cutoff proposed for fold change ($\geq \pm 1.5$), we still observed this factor to be more strongly co-immunoprecipitated with OTUD5 than with IgG control (fold change = 1.33, p-value = 0.02; appendix, Figure 18B), further suggesting a multi-protein interaction.

Furthermore, we explored the possible partnership between OTUD5 and NPLOC4 via AlphaFold predictions. OTUD5 has a high content of intrinsically disordered regions, containing only the OTU domain, characteristic of its family of DUBs, and a ubiquitin interacting motif in a higher degree of local structural organization. Given that, we prepared predictions for both full

length and N-terminus only of OTUD5, as in our first prediction OTUD5 had this region inserted in a cleft in the MPN domain of NPLOC4 – which we again observed when modelling with only a peptide of OTUD5 (Figure 13C-D).

Using the orthologs of *S. cerevisiae* and *Chaetomium thermophilum*, recent structural studies of Cdc48 (VCP ortholog) bound to its co-factors Npl4 (NPLOC4 ortholog) and Ufd1 showed Npl4 forming a tower-like structure on top of the hexameric ring of Cdc48, as its UBXL domain, present in its N-terminus, would interact with the N-domain of one Cdc48 molecule. Cdc48 domain would sit right below it and would be the primary step for maintaining the interaction between the two partners[258,259]. The interacting surface would be between the zinc-finger (zf)-Npl4 domain of the adaptor and the D1 domain of Cdc48, still allowing the central pore of the ring to be open in order to unfold its substrates.

In the resolved structure without the presence of a ubiquitinated substrate[258], Npl4 was seen to form the tower-like structure and the cleft, that in our prediction would accommodate OTUD5 N-terminus peptide, sits towards the outside part of the tower, which would not imply any steric hindrance for OTUD5 positioning. When a polyubiquitin chain was added to the structure[259], it was seen that at least three ubiquitin moieties would be accommodated alongside Npl4 structure, in which the first would be unfolded by Npl4 to enter Cdc48 pore. This, however, would be in an internal interface of Npl4 while, extrapolating from our models, OTUD5 would sit in the opposite surface as the ubiquitin monomers – from this, given OTUD5 highly flexible structure, one hypothesis that could be raised is that its OTU domain would be directed towards Npl4 C-terminal domain (CTD) to cleave the isopeptide bonds available.

A third report was able to determine the structure considering the presence of Ufd1 in the complex[260]. In their model – in which the positions of ubiquitin moieties, Npl4 and Cdc48 agrees with past literature –, the Npl4 binding motif (NBM) of Ufd1 interacts to a segment of Npl4 close to the cleft we identified as a possible surface interaction between NPLOC4 and OTUD5. However, the Ufd1 peptide resolved in this structure was positioned in the opposite side of the cleft that our model predicted OTUD5 peptide to exit it (Figure 13D) – which would still allow for both proteins to interact with NPLOC4 at the same time. Nevertheless, experiments exploring the impact of OTUD5 N-terminus and presence of UFD1L modulating interaction between OTUD5 and NPLOC4 – and NPLOC4 mediating interaction between OTUD5 and VCP – are still needed to understand the relationship between these factors.

Lastly, the suggestion that the N-terminal peptide of OTUD5 mediates the interaction with NPLOC4 raises another interesting interpretation: the first 17 residues in OTUD5 primary structure were reported to also mediate the interaction between this DUB and UBR5[177], one of the ligases responsible for its ubiquitination and for the homeostasis of its total levels[40]. Considering that UBR5 has been linked to orphan quality control, a mechanism that leads to protein degradation whenever subunits of a complex are unpaired[261], we could speculate that there is a competition between NPLOC4 and UBR5 for binding to OTUD5 N-terminus. This competition would either lead to proteasomal processing of the DUB or to a higher interaction between OTUD5 and the VCP-NPLOC4 complex – as we observed *in vivo* – due to the higher availability of the deubiquitinase (Figure 12D). Associated with the previous outlook of investigating whether this region is important for OTUD5-NPLOC4 (and consequently VCP) relationship, the behavior of OTUD5 lacking this N-terminal peptide in comparison to the wild type from the UBR5 degradation perspective would also be a path to be explored.

## 5.4. Changes in cellular phenotype in response to OTUD5 depletion

Given the effects we observed on a protein level in relation to OTUD5's substrates ubiquitination status, total amount and their binding to chromatin, we set out to investigate the physiological outcomes of these alterations in OTUD5 knockout cells.

First, when looking at the transcriptional activity, we observed a higher global transcriptional rate in comparison to wild type after recovery from physicochemical stresses (Figure 14B-C). While wild type cells had not yet fully recovered from the transcription inhibition after 1 hour of recovery, in all conditions OTUD5 knockout cells exhibited a significantly increased rate in comparison to wild type – even in the UV-C irradiation when also OTUD5 depleted cells had not return to baseline levels. OTUD5 was shown to directly interact with FACT, a histone chaperone complex, and to inhibit its activity when close to DNA lesion sites – hence preventing active transcription nearby those regions[177]; this relationship was also shown to be relevant to prevent transcription-replication conflicts, as OTUD5 inhibition of FACT avoids excessive transcriptional activity that would generate these conflicts[178]. In addition, when looking at our chromatin proteome

data (Figure 11C), we observed a higher loading of PAF1C subunits when OTUD5 is depleted. PAF1C was reported to positively modulate transcription elongation, as a decrease in its levels – consequently a lower loading on chromatin – would lead to decreased elongation rates[262,263]. Although further experiments are necessary to conclude that PAF1C is responsible for the increased global transcriptional activity, we observed a higher load of this complex on chromatin that could be associated with the higher transcriptional rates seen in OTUD5 knockout.

On a second look at cellular physiology, we observed that OTUD5 levels are constant throughout different stages of the cell cycle, without any major alteration in the amount of the DUB in any phase (Figure 16E), although we observed a distinct pattern of progression between wild type cells and OTUD5 knockout (Figure 16C). One possible causal relationship for this effect may come from condensins. Although they share the main SMC subunits SMC2-4, mammalian condensins are present in two different subtypes, condensin I and condensin II, which differ not only in complex composition but also in cellular localization, as the subtype I is cytoplasmic during interphase and then is recruited to chromosomes, while subtype II is nuclear and associated to chromatin during whole cycle[264]. In yeast – which have only one type of condensin –, one of HAWK proteins (Ycg1) was seen as the limiting factor for condensin recruitment to chromatin, and increased abundance of this subunit bound to chromatin recruited the other subunits of the complex, increasing their chromatin-bound state[265]. Interestingly, this change in homeostasis caused a slower transition between G1 and S[265], an observation that goes in line with what we observed in OTUD5 depletion, for both the increased binding to chromatin of condensin II subunits and the cycling perturbations. In *D. melanogaster*, an organism that exhibit two independent condensins subtypes as in mammalians, elevated levels of the CAP-H2 subunit on chromatin caused nuclear structural aberrations, such as inhibition of centromere dispersion or high chromosome compaction during interphase, some of the phenotypes that were rescued by depletion of either CAP-H2 itself or SMC2[266,267]. Similarly, decreased condensin levels was reported to increase chromatin mobility during interphase in yeast[268]. Considering the phenotypes observed when condensin II is more abundant on a chromatin-bound state, it will be extremely interesting to assess global chromatin organization in OTUD5 knockout cells, in order to evaluate if we can recapitulate these phenotypes in a similar way as we recapitulate the delay in cell cycle progression, in parallel to higher chromatin abundance of specifically condensin II complex.

Another angle of OTUD5 impact on cell cycle comes from an indirect perspective. One of the regulators of G1/S transition is the tumor suppressor Rb, a transcriptional modulator that inhibits progression of the cell cycle and is normally degraded, which allows cells to enter S-phase. UBR5 was seen to be an E3 ligase for Rb, being able to ubiquitinate and degrade Rb – consequently, in depletion of this ligase, Rb levels were maintained high and cells transitioned slower from G1 to S[269]. As one of the effects of OTUD5 depletion is a parallel reduction in UBR5 levels, OTUD5 would indirectly modulate Rb stability, causing a further decrease in the rate of cell cycle progression.

Our Western blot analysis also showed perturbed levels for the two cycle markers we looked at, cyclin A2 and cyclin E2 (Figure 16E-F). Cyclin A2 changes are more subtle and the main difference comes from the later timepoints where there was a persistent elevated level of this cyclin in OTUD5 knockout (detailed quantification in appendix, Figure 18C). One hypothesis to explain this observation would be a delayed resolution of the cycle, and given cyclin A2 association with G2 and mitotic stages[239], this effect could be seen as an outcome of this extension in cycling times. Cyclin E2, on the other hand, although we observed general higher amounts of the protein, the pattern in its levels across the timepoints showed a similar behavior for OTUD5 knockout when compared to wild type (timepoints quantifications in appendix, Figure 18D), showing that its characteristic S-phase associated peak happens also in OTUD5 depletion. Literature reports cyclin E2 to be a target of Myc transcription factor, which induces its expression[270]. Considering UBR5 was seen to ubiquitinate and target Myc for degradation[271,272], one possible speculation would be that lack of UBR5 induced higher levels of cyclin E2 due to Myc increased abundance, in general, although the cycling pattern of the former is still observable. Unfortunately, neither Myc nor cyclin E2 were quantified in our full proteome analysis. Finally, the perturbation in cycle progression we observed in OTUD5 depleted cells, which show a delay in completion of the cycle – in the timepoints we analyzed, we were not able to observe a full G1 restart –, would imply and generate an expectation of limited growth and slower rates of cell division in comparison to wild type. Indeed, in line with other observations, we noted that OTUD5 knockout cells have a decreased cellular division rate than wild type cells (Figure 15).

# 6. Concluding remarks and outlook

In this study, we aimed to investigate the processes in which OTUD5 is involved, by looking at the changes in the ubiquitination landscape of the human proteome when OTUD5 is absent in the cell, in order to infer the protein substrates of this deubiquitinase, being able to uncover novel substrates of OTUD5. In addition, we explored the consequences of this alteration in ubiquitination patterns of its substrates, showing that OTUD5 absence causes an increase in their levels, also affecting their abundance in a chromatin-bound state, which could be directly linked to the phenotypical effects we observed in cell cycle progression, cellular growth and global transcriptional activity. Furthermore, we noted OTUD5 to be a novel partner of the VCP/UFD1L/NPLOC4 complex, interacting via NPLOC4 and modulating its recruitment to chromatin.

These observations led to a working model in which OTUD5 targets and removes ubiquitin moieties from the condensin II subunits, causing the extraction of this complex from chromatin through VCP activity (Figure 17A). In its absence, highly ubiquitinated forms of SMC2/4 are more stably present in a chromatin-bound state and less accessible for the VCP-mediated extraction. In turn, this would interfere in normal cell cycle progression and delay in stage transitions, finally causing slower growth rate in OTUD5 knockout cells (Figure 17B).

Although we bring to light novel mechanisms by which cells ensure proper nuclear homeostasis by means of using ubiquitin as a signaling platform for these processes, further questions are still to be elucidated. Which ubiquitin chain topology is targeted by OTUD5 in these new substrates? Is OTUD5 N-terminus in the center of a balance between UBR5 recognition and NPLOC4 interaction *in vivo*, which would control OTUD5 levels and activity? What are the structural consequences in chromosome organization of OTUD5 depletion? These are some examples of open questions that we expect to clarify in the upcoming future.

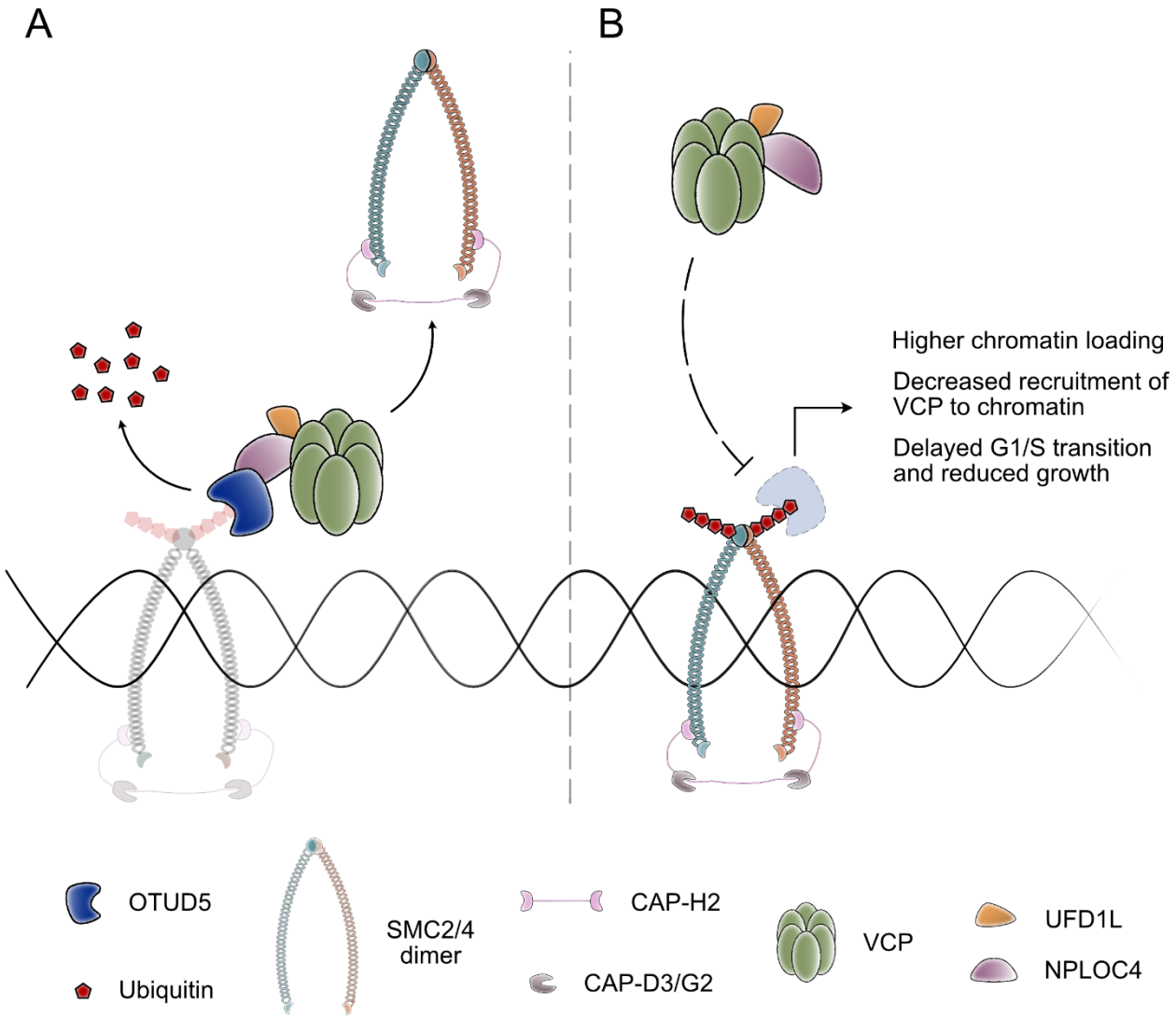


Figure 17: Current working model.
A) In regular cell homeostasis, OTUD5 removes ubiquitin molecules from the SMC2/4 dimer and enables recognition and extraction of the condensin II complex from chromatin. B) In OTUD5 depletion, SMC2/4 remains bound to chromatin, in a high ubiquitination state, while VCP recruitment is compromised, leading to the phenotypical effects observed.

# LIST OF ABBREVIATIONS

| | |
|---|---|
| **19S** | Regulatory particle of the 26S proteasome |
| **20S** | Core particle of the 26S proteasome |
| **A/Ala** | Alanine |
| **A20** | Deubiquitinase OTUD7C |
| **AAA** | ATPases associated with diverse cellular activities |
| **ABRAXAS (followed by subtype)** | BRCA1-A complex subunit Abraxas |
| **ACN** | Acetonitrile |
| **ADRM1** | Adhesion-regulating molecule 1 |
| **AF647** | Alexa Fluor 647 |
| **ANOVA** | Analysis of variance |
| **APC/C** | Anaphase-promoting complex/cyclosome |
| **APF-1** | ATP-dependent proteolysis factor 1 |
| **Asx** | Protein additional sex combs |
| **ASXL1** | Additional sex combs-like protein 1 |
| **ATG (followed by subtype)** | Autophagy-related protein (followed by subtype) |
| **ATM** | Ataxia telangiectasia mutated kinase |
| **ATP** | Adenosine triphosphate |
| **ATPase** | Adenosine triphosphate phosphatase |
| **ATXN3** | Ataxin-3 deubiquitinase |
| **ATXN3L** | Ataxin-3-like deubiquitinase |
| **BAP1** | BRCA1-associated protein 1 |
| **BP** | Biological process |
| **BRCA (followed by subtype)** | Breast cancer type (subtype) susceptibility protein |
| **BRCC36** | BRCA1/BRCA2-containing complex subunit 36 |
| **BRISC** | BRCC36-containing isopeptidase complex |
| **BrU** | 5-bromouridine |
| **BSA** | Bovine serum albumin |

| | |
|---|---|
| **β-TrCP** | F-box/WD repeat-containing protein 1A |
| **C/Cys** | Cysteine |
| **CAA** | Chloroacetamide |
| **CAP/NCAP (followed by subtype)** | Chromosome-associated protein (subtype) |
| **CC** | Cellular compartment |
| **CCCP** | Carbonyl cyanide m-chlorophenyl hydrazone |
| **Cdc48** | Cell division control protein 48 |
| **CDC73** | Cell division cycle protein 73 homolog |
| **CDK (followed by subtype)** | Cyclin dependent kinase (followed by subtype) |
| **CHIP** | Carboxy terminus of Hsp70-interacting protein |
| **CK2** | Casein kinase 2 |
| **CMG** | CDC45-MCM-GINS replicative helicase |
| **COP9** | COP9 signalosome complex subunit 9 |
| **COPS5/CSN5** | COP9 signalosome complex subunit 5 |
| **CRL** | Cullin-RING ubiquitin ligase |
| **CSN6** | COP9 signalosome complex subunit 6 |
| **CTD** | C-terminal domain |
| **CTR9** | RNA polymerase-associated protein CTR9 homolog |
| **CUL** | Cullin |
| **D/Asp** | Aspartate |
| **DMEM** | Dulbecco’s modified Eagle medium |
| **DMSO** | Dimethylsulfoxide |
| **DNA** | Deoxyribonucleic acid |
| **Doa4** | Ubiquitin carboxyl-terminal hydrolase 4 |
| **DRB** | 5,6-Dichloro-1-β-D-ribofuranosylbenzimidazole |
| **dsDNA** | Double-stranded DNA |
| **DSIF** | DRB sensitivity inducing factor |
| **DTT** | Dithiothreitol |
| **DTX3L** | Protein deltex-3-like |

| | |
|---|---|
| **DUB** | Deubiquitinase |
| **DUBA** | Deubiquitinating enzyme A |
| **E/Glu** | Glutamate |
| **E1** | Ubiquitin activating enzyme |
| **E2** | Ubiquitin conjugating enzyme |
| **E3** | Ubiquitin ligase |
| **E6-AP** | Human papillomavirus E6-associated protein |
| **EDTA** | Ethylenediaminetetraacetic acid |
| **EGTA** | Ethyleneglycol-bis(β-aminoethyl ether)-N,N,N′,N′-tetraacetic acid |
| **ER** | Endoplasmic reticulum |
| **ER+** | Estrogen receptor-positive |
| **ERAD** | Endoplasmic reticulum associated protein degradation |
| **EU** | 5-ethynyl-uridine |
| **FA** | Formic acid |
| **FACT** | Facilitates chromatin transcription complex |
| **FANCD2** | Fanconi anemia group D2 protein |
| **FAT10** | Ubiquitin-like protein FAT10 |
| **FBS** | Fetal bovine serum |
| **FDR** | False discovery rate |
| **FPKM** | Fragments per kilobase of transcript per million mapped reads |
| **FSC** | Forward scatter |
| **FUBI** | FAU ubiquitin like and ribosomal protein S30 fusion |
| **G/Gly** | Glycine |
| **GDP** | Guanosine diphosphate |
| **GO** | Gene ontology |
| **GTPase** | Guanosine triphosphate phosphatase |
| **H/His** | Histidine |
| **H2A** | Histone H2A |
| **H2B** | Histone H2B |

| | |
|---|---|
| **HAUSP** | Ubiquitin carboxyl-terminal hydrolase 7 |
| **HCF1/HCFC1** | Host cell factor 1 |
| **HD** | Huntington's disease |
| **HDAC (followed by subtype)** | Histone deacetylase (followed by subtype) |
| **HECT** | Homologous to the E6-AP carboxyl terminus |
| **HER2** | Human epidermal growth factor receptor 2 |
| **HERC** | HECT domain and RCC1-like domain-containing protein |
| **HEPES** | 4-(2-hydroxyethyl)-1-piperazineethanesulfonic acid |
| **HOIL-1** | RanBP-type and C3HC4-type zinc finger-containing protein 1 |
| **HOIP** | HOIL-1-interacting protein |
| **HPV** | Human papillomavirus |
| **HRP** | Horseradish peroxidase |
| **IBR** | In-between RING |
| **I/Ile** | Isoleucine |
| **IAP** | Immunoaffinity purification |
| **IgG** | Immunoglobulin G |
| **(i)pTM** | (Interface) predicted template modelling score |
| **ISG15** | Ubiquitin-like protein ISG15 |
| **ITCH** | HECT-type E3 ubiquitin transferase Itchy homolog |
| **JAMM** | JAB1/MPN/Mov34 metalloenzymes |
| **JOSD (followed by subtype)** | Josephin domain-containing protein (followed by subtype) |
| **K/Lys** | Lysine |
| **KEAP1** | Kelch-like ECH-associated protein 1 |
| **KLHDC2** | Kelch domain-containing protein 2 |
| **L/Leu** | Leucine |
| **LC** | Liquid chromatography |
| **LFQ** | Label-free quantification |
| **LPS** | Lipopolysaccharide |
| **LINKED** | Linkage-specific-deubiquitylation-deficiency-induced embryonic defects syndrome |

| | |
|---|---|
| **LUBAC** | Linear ubiquitin chain assembly complex |
| **Lys-C** | Endopeptidase Lys-C |
| **M/Met** | Methionine |
| **MAU2** | Cohesin loading complex subunit SCC4 homolog |
| **MCM (followed by subtype)** | Minichromosome maintenance (followed by subtype) |
| **MDM2** | RING-type E3 ubiquitin transferase Mdm2 |
| **MF** | Molecular function |
| **MHC** | Major histocompatibility complex |
| **MIC** | Microscopy |
| **MINDY** | Motif interacting with Ub-containing novel DUB family |
| **MIU** | Motif interacting with ubiquitin |
| **Miy1** | Ubiquitin carboxyl-terminal hydrolase Miy1 |
| **MJD** | Machado-Joseph deubiquitinases |
| **MOPS** | 3-(N-morpholino)propanesulfonic acid |
| **MS** | Mass spectrometry |
| **MTA (followed by subtype)** | Metastasis-associated protein MTA (followed by subtype) |
| **mTORC (followed by subtype)** | Mammalian target of rapamycin complex (followed by subtype) |
| **Myc** | Myc proto-oncogene protein |
| **MYCBP2** | Myc-binding protein 2 |
| **NBM** | Npl4 binding motif |
| **NEDD4** | Neural precursor cell expressed developmentally down-regulated protein 4 |
| **NEDD8** | Neural precursor cell expressed developmentally down-regulated protein 8 |
| **NEM** | N-ethylmaleimide |
| **NF-κB** | Nuclear factor κ-light-chain-enhancer of activated B cells |
| **NGS** | Next generation sequencing |
| **NIPBL** | Nipped-B-like protein |
| **Npl4** | Nuclear protein localization protein 4 |
| **NPLOC4** | Nuclear protein localization protein 4 homolog |
| **NuRD** | Nuclear remodeling and deacetylase complex |

| | |
|---|---|
| **NZF** | Npl4 zinc finger |
| **OMM** | Outer mitochondrial membrane |
| **OTU (followed by subtype)** | Ovarian tumor (followed by subtype) |
| **P/Pro** | Proline |
| **p21** | Cyclin-dependent kinase inhibitor 1 |
| **p47** | Platelet 47 kDa protein |
| **p53** | Cellular tumor antigen p53 |
| **p97** | Transitional endoplasmic reticulum ATPase |
| **P-TEFb** | Positive transcription elongation factor b |
| **PAF1** | RNA polymerase II-associated factor 1 homolog |
| **PAF1C** | PAF1 complex |
| **PARP1** | Poly(ADP-ribose) polymerase 1 |
| **PB** | Palbociclib |
| **PBS** | Phosphate-buffered saline |
| **PBST** | Phosphate-buffered saline with Tween-20 |
| **PCNA** | Proliferating cell nuclear antigen |
| **PCR** | Polymerase chain reaction |
| **PD** | Pulldown |
| **PDB** | Protein data bank |
| **PDCD5** | Programmed cell death protein 5 |
| **PDS5B** | Sister chromatid cohesion protein PDS5 homolog B |
| **PFA** | Paraformaldehyde |
| **PEP** | Posterior error probability |
| **PEX5** | Peroxisomal targeting signal 1 receptor |
| **PINK1** | PTEN-induced putative kinase protein 1 |
| **PLA** | Proximity ligation assay |
| **PladB** | Pladienolide B |
| **pLDDT** | Predicted local distance difference test |
| **PPi** | Pyrophosphate |

| | |
|---|---|
| **PSMD (followed by subtype)** | 26S proteasome non-ATPase regulatory subunit (followed by subtype) |
| **PTEN** | Phosphatidylinositol 3,4,5-trisphosphate 3-phosphatase and dual-specificity protein phosphatase |
| **PTM** | Post-translational modification |
| **PVDF** | Polyvinylidene fluoride |
| **Q/Gln** | Glutamine |
| **R/Arg** | Arginine |
| **RAD21** | Double-strand-break repair protein rad21 homolog |
| **RAD51** | DNA repair protein RAD51 homolog 1 |
| **Rb** | Retinoblastoma-associated protein |
| **RBR** | RING-between-RING |
| **RBX (followed by subtype)** | RING-box protein (followed by subtype) |
| **RCC1** | Regulator of chromosome condensation |
| **RCR** | RING-Cys-relay E3 ubiquitin ligase |
| **RFC3** | Replication factor C subunit 3 |
| **RING** | Really interesting new gene |
| **RORγt** | Retinoid orphan receptor γ t |
| **RPA1** | Replication protein A 70 kDa DNA-binding subunit |
| **RPE-1** | Retinal pigment epithelial cells |
| **RPN8** | 26S proteasome non-ATPase regulatory subunit 7 |
| **Rpn11** | Ubiquitin carboxyl-terminal hydrolase RPN11 |
| **Rpn13** | Proteasome regulatory particle non-ATPase 13 |
| **RNA** | Ribonucleic acid |
| **RNF (followed by subtype)** | RING finger (followed by subtype) |
| **RZ** | RNF213-ZNFX1 E3 ubiquitin ligases |
| **(p)S/Ser** | (phospho-)Serine |
| **SAGA** | SPT-ADA-GCN5 acetyltransferase |
| **SCA3** | Spinocerebellar ataxia type 3 |
| **SCF** | SKP1-Cullin-F-box E3 ubiquitin ligase complex |
| **SDS-PAGE** | Sodium dodecyl sulfate-polyacrilamide gel electrophoresis |

| | |
|---|---|
| **SILAC** | Stable isotope labeling by amino acids in cell culture |
| **siRNA** | Small interfering RNA |
| **SKP1** | S-phase kinase-associated protein 1 |
| **Skp2** | S-phase kinase-associated protein 2 |
| **SMC (followed by subtype)** | Structural maintenance of chromosomes protein (followed by subtype) |
| **SMURF (followed by subtype)** | SMAD ubiquitination regulatory factor (followed by subtype) |
| **SPT (followed by subtype)** | DRB sensitivity-inducing factor (followed by subtype) |
| **SSC** | Side scatter |
| **ssDNA** | Single-stranded DNA |
| **STAG2** | Cohesin subunit SA-2 |
| **STING** | Stimulator of interferon genes protein |
| **SUMO (followed by subtype)** | Small ubiquitin-related modifier (followed by subtype) |
| **SUPTH (followed by subtype)** | DRB sensitivity-inducing factor (followed by subtype) |
| **T/Thr** | Threonine |
| **TCEP** | Tris(2-carboxyethyl)phosphine |
| **TFA** | Trifluoroacetic acid |
| **TMT** | Tandem mass tag |
| **TPX2** | Targeting protein for Xklp2 |
| **TRAF3** | TNF receptor-associated factor 3 |
| **TRIAD3A** | Triad domain-containing protein 3 |
| **TRIM25** | Tripartite motif-containing protein 25 |
| **TRIP12** | Thyroid receptor-interacting protein 12 |
| **Tris** | Tris(hydroxymethyl)aminomethane |
| **TXNIP** | Thioredoxin-interacting protein |
| **UAE** | Ubiquitin activating enzyme |
| **Ub** | Ubiquitin |
| **UBA** | Ubiquitin-associated domain |
| **UBA6** | Ubiquitin-like modifier-activating enzyme 6 |
| **UBAN** | Ub-binding domain in ABIN proteins and NEMO |

| | |
|---|---|
| **UBD** | Ubiquitin binding domain |
| **UBE2S** | Ubiquitin-conjugating enzyme E2 S |
| **UBE3A** | Ubiquitin-protein ligase E3A |
| **UBE4B** | Ubiquitin conjugation factor E4 B |
| **UbiCRest** | Ubiquitin chain restriction |
| **UBIP** | Ubiquitous immunopoietic polypeptide |
| **UBL** | Ubiquitin-like protein |
| **UBR (followed by subtype)** | E3 ubiquitin-protein ligase UBR (followed by subtype) |
| **UBXL** | Ubiquitin regulatory X-like domain |
| **UCH (followed by subtype)** | Ubiquitin carboxyl-terminal hydrolase isozyme (followed by subtype) |
| **Ufd1** | Ubiquitin fusion degradation protein 1 |
| **UFD1L** | Ubiquitin recognition factor in ER-associated degradation protein 1 |
| **UFM1** | Ubiquitin-fold modifier 1 |
| **UIM** | Ubiquitin interacting motif |
| **ULP** | Ubiquitin like proteases |
| **UN** | Ufd1/Npl4 dimer or UFD1L/NPLOC4 dimer |
| **UPS** | Ubiquitin proteasome system |
| **URM1** | Ubiquitin-related modifier 1 |
| **USP (followed by subtype)** | Ubiquitin specific protease (followed by subtype) |
| **USPL1** | SUMO-specific isopeptidase USPL1 |
| **UV-C** | Ultraviolet C |
| **V/Val** | Valine |
| **VCP** | Valosin-containing protein |
| **VCPIP1** | Valosin-containing protein p97/p47 complex-interacting protein 1 |
| **W/Trp** | Tryptophan |
| **WB** | Western blot |
| **XRCC5/Ku80** | X-ray repair cross-complementing protein 5 |
| **Y/Tyr** | Tyrosine |
| **Ycg1** | Condensin complex subunit 3 |

| | |
|---|---|
| **ZNF** | Zinc finger |
| **ZUFSP** | Zinc finger with UFM1-specific peptidase domain protein |

# 7. Appendix

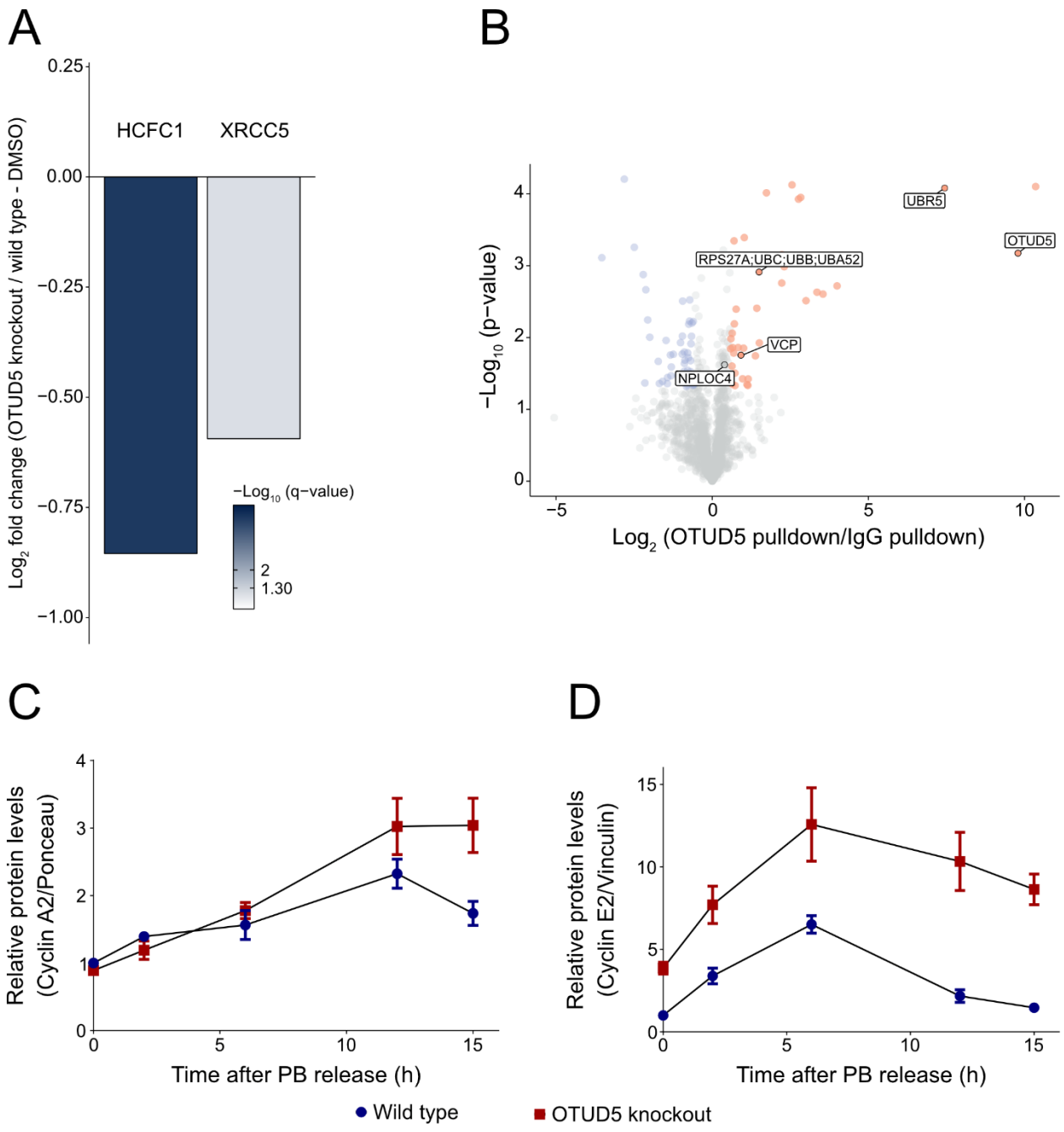


Figure 18: Appendix figures.
A) Bar plot of the chromatin proteome quantification, as described in 3.4. The $\log_2$-transformed fold change between OTUD5 knockout and wild type, in the DMSO control treatment, is indicated for proteins HCFC1 (or HCF1) and XRCC5/Ku80. Filling color of the bars indicates the $-\log_{10}$-transformed *q*-value, or FDR. B) Extended volcano plot from Figure 12B. Apart from previously mentioned proteins, NPLOC4 is also indicated. C-D) Quantification of total levels of cyclins A2

and E2, respectively – complementary to the data from Figure 16F –, normalized to wild type cells after 0 hours of release from PB arrest (arbitrarily considered as 1). Dots indicate the average value between the three replicates.

# 8. References


1. Goldstein, G. *et al.* Isolation of a polypeptide that has lymphocyte-differentiating properties and is probably represented universally in living cells. *Proc. Natl. Acad. Sci. U.S.A.* **72**, 11–15 (1975).

2. Schlesinger, D. H., Goldstein, G. & Niall, H. D. Complete amino acid sequence of ubiquitin, an adenylate cyclase stimulating polypeptide probably universal in living cells. *Biochemistry* **14**, 2214–2218 (1975).

3. Goldknopf, I. L. & Busch, H. Isopeptide linkage between nonhistone and histone 2A polypeptides of chromosomal conjugate-protein A24. *Proc. Natl. Acad. Sci. U.S.A.* **74**, 864–868 (1977).

4. Etlinger, J. D. & Goldberg, A. L. A soluble ATP-dependent proteolytic system responsible for the degradation of abnormal proteins in reticulocytes. *Proc. Natl. Acad. Sci. U.S.A.* **74**, 54–58 (1977).

5. Ciehanover, A., Hod, Y. & Rershkol, A. A heat-stable polypeptide component of an ATP-dependent proteolytic system from reticulocytes. *BIOCHEMICAL AND BIOPHYSICAL RESEARCH COMMUNICATIONS* **81**, 1100–1105 (1978).

6. Hershko, A., Ciechanover, A. & Rose, I. A. Resolution of the ATP-dependent proteolytic system from reticulocytes: a component that interacts with ATP. *Proc. Natl. Acad. Sci. U.S.A.* **76**, 3107–3110 (1979).

7. Hershko, A., Ciechanover, A., Heller, H., Haas, A. L. & Rose, I. A. Proposed role of ATP in protein breakdown: conjugation of protein with multiple chains of the polypeptide of ATP-dependent proteolysis. *Proc. Natl. Acad. Sci. U.S.A.* **77**, 1783–1786 (1980).

8. Wilkinson, K. D., Urban, M. K. & Haas, A. L. Ubiquitin is the ATP-dependent proteolysis factor I of rabbit reticulocytes. *Journal of Biological Chemistry* **255**, 7529–7532 (1980).

9. Hershko, A., Heller, H., Elias, S. & Ciechanover, A. Components of ubiquitin-protein ligase system. Resolution, affinity purification, and role in protein breakdown. *Journal of Biological Chemistry* **258**, 8206–8214 (1983).

10. Hershko, A., Leshinsky, E., Ganoth, D. & Heller, H. ATP-dependent degradation of ubiquitin-protein conjugates. *Proc. Natl. Acad. Sci. U.S.A.* **81**, 1619–1623 (1984).

11. Kimura, Y. & Tanaka, K. Regulatory mechanisms involved in the control of ubiquitin homeostasis. *Journal of Biochemistry* **147**, 793–798 (2010).

12. Upadhyay, A. & Joshi, V. The Ubiquitin Tale: Current Strategies and Future Challenges. *ACS Pharmacol. Transl. Sci.* **7**, 2573–2587 (2024).

13. Ramazi, S. & Zahiri, J. Post-translational modifications in proteins: resources, tools and prediction methods. *Database* **2021**, baab012 (2021).

14. Damgaard, R. B. The ubiquitin system: from cell signalling to disease biology and new therapeutic opportunities. *Cell Death Differ* **28**, 423–426 (2021).

15. Sap, K. A., Geijtenbeek, K. W., Schipper-Krom, S., Guler, A. T. & Reits, E. A. Ubiquitin-modifying enzymes in Huntington's disease. *Front. Mol. Biosci.* **10**, 1107323 (2023).

16. Barghout, S. H. & Schimmer, A. D. E1 Enzymes as Therapeutic Targets in Cancer. *Pharmacological Reviews* **73**, 1–58 (2021).

17. Clague, M. J., Heride, C. & Urbé, S. The demographics of the ubiquitin system. *Trends in Cell Biology* **25**, 417–426 (2015).

18. Stewart, M. D., Ritterhoff, T., Klevit, R. E. & Brzovic, P. S. E2 enzymes: more than just middle men. *Cell Res* **26**, 423–440 (2016).

19. Clague, M. J., Urbé, S. & Komander, D. Breaking the chains: deubiquitylating enzyme specificity begets function. *Nat Rev Mol Cell Biol* **20**, 338–352 (2019).

20. Qiu, J. *et al.* Ubiquitination independent of E1 and E2 enzymes by bacterial effectors. *Nature* **533**, 120–124 (2016).

21. Kaiser, S. E. *et al.* Protein standard absolute quantification (PSAQ) method for the measurement of cellular ubiquitin pools. *Nat Methods* **8**, 691–696 (2011).

22. Mattiroli, F. & Penengo, L. Histone Ubiquitination: An Integrative Signaling Platform in Genome Stability. *Trends in Genetics* **37**, 566–581 (2021).

23. Chen, S., Pan, C., Huang, J. & Liu, T. ATR limits Rad18-mediated PCNA monoubiquitination to preserve replication fork and telomerase-independent telomere stability. *EMBO J* **43**, 1301–1324 (2024).

24. Walden, H. & Deans, A. J. The Fanconi Anemia DNA Repair Pathway: Structural and Functional Insights into a Complex Disorder. *Annu. Rev. Biophys.* **43**, 257–278 (2014).

25. McCormick, L. E. *et al.* Multi-monoubiquitylation controls VASP-mediated actin dynamics. *Journal of Cell Science* **137**, jcs261527 (2024).

26. Komander, D. & Rape, M. The Ubiquitin Code. *Annu. Rev. Biochem.* **81**, 203–229 (2012).

27. Chau, V. *et al.* A Multiubiquitin Chain Is Confined to Specific Lysine in a Targeted Short-Lived Protein. *Science* **243**, 1576–1583 (1989).

28. Alfano, C., Faggiano, S. & Pastore, A. The Ball and Chain of Polyubiquitin Structures. *Trends in Biochemical Sciences* **41**, 371–385 (2016).

29. Yau, R. & Rape, M. The increasing complexity of the ubiquitin code. *Nat Cell Biol* **18**, 579–586 (2016).

30. Singh, G., Kumar, S. & Das, R. Decoding the Assembly of Mixed and Branched Heterotypic Ubiquitin Chains. *Anal. Chem.* **95**, 10061–10067 (2023).

31. Emmerich, C. H. *et al.* Activation of the canonical IKK complex by K63/M1-linked hybrid ubiquitin chains. *Proc. Natl. Acad. Sci. U.S.A.* **110**, 15247–15252 (2013).

32. Zhou, J. *et al.* The autophagy adaptor TRIAD3A promotes tau fibrillation by nested phase separation. *Nat Cell Biol* **26**, 1274–1286 (2024).

33. Haakonsen, D. L. & Rape, M. Branching Out: Improved Signaling by Heterotypic Ubiquitin Chains. *Trends in Cell Biology* **29**, 704–716 (2019).

34. Michel, M. A., Swatek, K. N., Hospenthal, M. K. & Komander, D. Ubiquitin Linkage-Specific Affimers Reveal Insights into K6-Linked Ubiquitin Signaling. *Molecular Cell* **68**, 233-246.e5 (2017).

35. Peng, J. *et al.* A proteomics approach to understanding protein ubiquitination. *Nat Biotechnol* **21**, 921–926 (2003).

36. Tsuchiya, H. *et al.* Ub-ProT reveals global length and composition of protein ubiquitylation in cells. *Nat Commun* **9**, 524 (2018).

37. Ohtake, F., Tsuchiya, H., Saeki, Y. & Tanaka, K. K63 ubiquitylation triggers proteasomal degradation by seeding branched ubiquitin chains. *Proc. Natl. Acad. Sci. U.S.A.* **115**, (2018).

38. Yau, R. G. *et al.* Assembly and Function of Heterotypic Ubiquitin Chains in Cell-Cycle and Protein Quality Control. *Cell* **171**, 918-933.e20 (2017).

39. Meyer, H.-J. & Rape, M. Enhanced Protein Degradation by Branched Ubiquitin Chains. *Cell* **157**, 910–921 (2014).

40. Morita, M. *et al.* Combinatorial ubiquitin code degrades deubiquitylation-protected substrates. *Nat Commun* **16**, 2496 (2025).

41. Pohl, C. & Dikic, I. Cellular quality control by the ubiquitin-proteasome system and autophagy. *Science* **366**, 818–822 (2019).

42. Tracz, M. & Bialek, W. Beyond K48 and K63: non-canonical protein ubiquitination. *Cell Mol Biol Lett* **26**, 1 (2021).

43. Dittmar, G. & Winklhofer, K. F. Linear Ubiquitin Chains: Cellular Functions and Strategies for Detection and Quantification. *Front. Chem.* **7**, 915 (2020).

44. Swatek, K. N. & Komander, D. Ubiquitin modifications. *Cell Res* **26**, 399–422 (2016).

45. Kane, L. A. *et al.* PINK1 phosphorylates ubiquitin to activate Parkin E3 ubiquitin ligase activity. *Journal of Cell Biology* **205**, 143–153 (2014).

46. Kazlauskaite, A. *et al.* Parkin is activated by PINK1-dependent phosphorylation of ubiquitin at Ser65. *Biochemical Journal* **460**, 127–141 (2014).

47. Koyano, F. *et al.* Ubiquitin is phosphorylated by PINK1 to activate parkin. *Nature* **510**, 162–166 (2014).

48. Wauer, T. *et al.* Ubiquitin Ser65 phosphorylation affects ubiquitin structure, chain assembly and hydrolysis. *The EMBO Journal* **34**, 307–325 (2015).

49. Li, M., Luo, J., Brooks, C. L. & Gu, W. Acetylation of p53 Inhibits Its Ubiquitination by Mdm2. *Journal of Biological Chemistry* **277**, 50607–50611 (2002).

50. Lacoursiere, R. E., Hadi, D. & Shaw, G. S. Acetylation, Phosphorylation, Ubiquitination (Oh My!): Following Post-Translational Modifications on the Ubiquitin Road. *Biomolecules* **12**, 467 (2022).

51. Ohtake, F. *et al.* Ubiquitin acetylation inhibits polyubiquitin chain elongation. *EMBO Reports* **16**, 192–201 (2015).

52. Lacoursiere, R. E. & Shaw, G. S. Acetylated Ubiquitin Modulates the Catalytic Activity of the E1 Enzyme Uba1. *Biochemistry* **60**, 1276–1285 (2021).

53. Lacoursiere, R. E., O'Donoghue, P. & Shaw, G. S. Programmed ubiquitin acetylation using genetic code expansion reveals altered ubiquitination patterns. *FEBS Letters* **594**, 1226–1234 (2020).

54. Kienle, S. M. *et al.* Electrostatic and steric effects underlie acetylation-induced changes in ubiquitin structure and function. *Nat Commun* **13**, 5435 (2022).

55. Cadwell, K. & Coscoy, L. Ubiquitination on Nonlysine Residues by a Viral E3 Ubiquitin Ligase. *Science* **309**, 127–130 (2005).

56. Wang, X. *et al.* Ubiquitination of serine, threonine, or lysine residues on the cytoplasmic tail can induce ERAD of MHC-I by viral E3 ligase mK3. *The Journal of Cell Biology* **177**, 613–624 (2007).

57. Kelsall, I. R. Non-lysine ubiquitylation: Doing things differently. *Front. Mol. Biosci.* **9**, 1008175 (2022).

58. De Cesare, V. *et al.* Deubiquitinating enzyme amino acid profiling reveals a class of ubiquitin esterases. *Proc. Natl. Acad. Sci. U.S.A.* **118**, e2006947118 (2021).

59. Dearlove, E. L. & Huang, D. T. Insights into non-proteinaceous ubiquitination. *Biochemical Society Transactions* **53**, 399–407 (2025).

60. Sakamaki, J. *et al.* Ubiquitination of phosphatidylethanolamine in organellar membranes. *Molecular Cell* **82**, 3677-3692.e11 (2022).

61. Kelsall, I. R. *et al.* HOIL-1 ubiquitin ligase activity targets unbranched glucosaccharides and is required to prevent polyglucosan accumulation. *The EMBO Journal* **41**, e109700 (2022).

62. Zhu, K. *et al.* Ubiquitylation of nucleic acids by DELTEX ubiquitin E3 ligase DTX3L. *EMBO Rep* **25**, 4172–4189 (2024).

63. Dearlove, E. L. *et al.* DTX3L ubiquitin ligase ubiquitinates single-stranded nucleic acids. *eLife* **13**, RP98070 (2024).

64. Dikic, I. & Schulman, B. A. An expanded lexicon for the ubiquitin code. *Nat Rev Mol Cell Biol* **24**, 273–287 (2023).

65. Cappadocia, L. & Lima, C. D. Ubiquitin-like Protein Conjugation: Structures, Chemistry, and Mechanism. *Chem. Rev.* **118**, 889–918 (2018).

66. Hepowit, N. L., Kolbe, C., Zelle, S. R., Latz, E. & MacGurn, J. A. Regulation of ubiquitin and ubiquitin-like modifiers by phosphorylation. *The FEBS Journal* **289**, 4797–4810 (2022).

67. Foster, B. M., Wang, Z. & Schmidt, C. K. DoUBLing up: ubiquitin and ubiquitin-like proteases in genome stability. *Biochemical Journal* **481**, 515–545 (2024).

68. Liu, L. *et al.* UbiHub: a data hub for the explorers of ubiquitination pathways. *Bioinformatics* **35**, 2882–2884 (2019).

69. Ebadi, P., Stratton, C. M. & Olsen, S. K. E3 ubiquitin ligases in signaling, disease, and therapeutics. *Trends in Biochemical Sciences* S0968000425001860 (2025) doi:10.1016/j.tibs.2025.07.009.

70. Yang, Q., Zhao, J., Chen, D. & Wang, Y. E3 ubiquitin ligases: styles, structures and functions. *Mol Biomed* **2**, 23 (2021).

71. Baek, K., Scott, D. C. & Schulman, B. A. NEDD8 and ubiquitin ligation by cullin-RING E3 ligases. *Current Opinion in Structural Biology* **67**, 101–109 (2021).

72. David, Y. *et al.* E3 Ligases Determine Ubiquitination Site and Conjugate Type by Enforcing Specificity on E2 Enzymes. *Journal of Biological Chemistry* **286**, 44104–44115 (2011).

73. Cruz Walma, D. A., Chen, Z., Bullock, A. N. & Yamada, K. M. Ubiquitin ligases: guardians of mammalian development. *Nat Rev Mol Cell Biol* **23**, 350–367 (2022).

74. Rusnac, D.-V. & Zheng, N. Structural Biology of CRL Ubiquitin Ligases. in *Cullin-RING Ligases and Protein Neddylation* (eds Sun, Y., Wei, W. & Jin, J.) vol. 1217 9–31 (Springer Singapore, Singapore, 2020).

75. Zheng, N. *et al.* Structure of the Cul1–Rbx1–Skp1–F boxSkp2 SCF ubiquitin ligase complex. *Nature* **416**, 703–709 (2002).

76. Baek, K. *et al.* NEDD8 nucleates a multivalent cullin–RING–UBE2D ubiquitin ligation assembly. *Nature* **578**, 461–466 (2020).

77. Huibregtse, J. M., Scheffner, M., Beaudenon, S. & Howley, P. M. A family of proteins structurally and functionally related to the E6-AP ubiquitin-protein ligase. *Proc. Natl. Acad. Sci. U.S.A.* **92**, 2563–2567 (1995).

78. Wang, Y., Argiles-Castillo, D., Kane, E. I., Zhou, A. & Spratt, D. E. HECT E3 ubiquitin ligases – emerging insights into their biological roles and disease relevance. *Journal of Cell Science* **133**, jcs228072 (2020).

79. Scheffner, M. & Kumar, S. Mammalian HECT ubiquitin-protein ligases: Biological and pathophysiological aspects. *Biochimica et Biophysica Acta (BBA) - Molecular Cell Research* **1843**, 61–74 (2014).

80. Metzger, M. B., Pruneda, J. N., Klevit, R. E. & Weissman, A. M. RING-type E3 ligases: Master manipulators of E2 ubiquitin-conjugating enzymes and ubiquitination. *Biochimica et Biophysica Acta (BBA) - Molecular Cell Research* **1843**, 47–60 (2014).

81. Zheng, N. & Shabek, N. Ubiquitin Ligases: Structure, Function, and Regulation. *Annu. Rev. Biochem.* **86**, 129–157 (2017).

82. Kim, H. C. & Huibregtse, J. M. Polyubiquitination by HECT E3s and the Determinants of Chain Type Specificity. *Molecular and Cellular Biology* **29**, 3307–3318 (2009).

83. Lan, W. & Miao, Y. New Aspects of HECT-E3 Ligases in Cell Senescence and Cell Death of Plants. *Plants* **8**, 483 (2019).

84. Sluimer, J. & Distel, B. Regulating the human HECT E3 ligases. *Cell. Mol. Life Sci.* **75**, 3121–3141 (2018).

85. Wan, L. *et al.* Cdh1 Regulates Osteoblast Function through an APC/C-Independent Modulation of Smurf1. *Molecular Cell* **44**, 721–733 (2011).

86. Wang, J. *et al.* Calcium Activates Nedd4 E3 Ubiquitin Ligases by Releasing the C2 Domain-mediated Auto-inhibition. *Journal of Biological Chemistry* **285**, 12279–12288 (2010).

87. Smit, J. J. & Sixma, T. K. RBR E3-ligases at work. *EMBO Reports* **15**, 142–154 (2014).

88. Walden, H. & Rittinger, K. RBR ligase–mediated ubiquitin transfer: a tale with many twists and turns. *Nat Struct Mol Biol* **25**, 440–445 (2018).

89. Jevtić, P., Haakonsen, D. L. & Rapé, M. An E3 ligase guide to the galaxy of small-molecule-induced protein degradation. *Cell Chemical Biology* **28**, 1000–1013 (2021).

90. AlAbdi, L. *et al.* Loss-of-function variants in *MYCBP2* cause neurobehavioural phenotypes and corpus callosum defects. *Brain* **146**, 1373–1387 (2023).

91. Mabbitt, P. D. *et al.* Structural basis for RING-Cys-Relay E3 ligase activity and its role in axon integrity. *Nat Chem Biol* **16**, 1227–1236 (2020).

92. Otten, E. G. *et al.* Ubiquitylation of lipopolysaccharide by RNF213 during bacterial infection. *Nature* **594**, 111–116 (2021).

93. Ahel, J. *et al.* ATP functions as a pathogen-associated molecular pattern to activate the E3 ubiquitin ligase RNF213. *Nat Commun* **16**, 4414 (2025).

94. Radley, E., Long, J., Gough, K. & Layfield, R. The 'dark matter' of ubiquitin-mediated processes: opportunities and challenges in the identification of ubiquitin-binding domains. *Biochemical Society Transactions* **47**, 1949–1962 (2019).

95. Michel, M. A., Scutts, S. & Komander, D. Secondary interactions in ubiquitin-binding domains achieve linkage or substrate specificity. *Cell Reports* **43**, 114545 (2024).

96. Husnjak, K. & Dikic, I. Ubiquitin-Binding Proteins: Decoders of Ubiquitin-Mediated Cellular Functions. *Annu. Rev. Biochem.* **81**, 291–322 (2012).

97. Kamadurai, H. B. *et al.* Insights into Ubiquitin Transfer Cascades from a Structure of a UbcH5B~Ubiquitin-HECT(NEDD4L) Complex. *Molecular Cell* **36**, 1095–1102 (2009).

98. Kazansky, Y., Lai, M.-Y., Singh, R. K. & Fushman, D. Impact of different ionization states of phosphorylated Serine-65 on ubiquitin structure and interactions. *Sci Rep* **8**, 2651 (2018).

99. Fennell, L. M., Rahighi, S. & Ikeda, F. Linear ubiquitin chain-binding domains. *The FEBS Journal* **285**, 2746–2761 (2018).

100. Sato, Y. Structural basis for the linkage specificity of ubiquitin-binding domain and deubiquitinase. *The Journal of Biochemistry* **172**, 1–7 (2022).

101. Randles, L. Ubiquitin and its binding domains. *Front Biosci (Landmark Ed.)* **17**, 2140–2157 (2012).

102. Meyer, H. H., Shorter, J. G., Seemann, J., Pappin, D. & Warren, G. A complex of mammalian Ufd1 and Npl4 links the AAA-ATPase, p97, to ubiquitin and nuclear transport pathways. *EMBO J* **19**, 2181–2192 (2000).

103. Meyer, H. H., Wang, Y. & Warren, G. Direct binding of ubiquitin conjugates by the mammalian p97 adaptor complexes, p47 and Ufd1-Npl4. *The EMBO Journal* **21**, 5645–5652 (2002).

104. Tsuchiya, H. *et al.* In Vivo Ubiquitin Linkage-type Analysis Reveals that the Cdc48-Rad23/Dsk2 Axis Contributes to K48-Linked Chain Specificity of the Proteasome. *Molecular Cell* **66**, 488-502.e7 (2017).

105. Barthelme, D. & Sauer, R. T. Origin and Functional Evolution of the Cdc48/p97/VCP AAA+ Protein Unfolding and Remodeling Machine. *Journal of Molecular Biology* **428**, 1861–1869 (2016).

106. Stach, L. & Freemont, P. S. The AAA+ ATPase p97, a cellular multitool. *Biochemical Journal* **474**, 2953–2976 (2017).

107. Niwa, H. *et al.* The Role of the N-Domain in the ATPase Activity of the Mammalian AAA ATPase p97/VCP. *Journal of Biological Chemistry* **287**, 8561–8570 (2012).

108. Van Den Boom, J. & Meyer, H. VCP/p97-Mediated Unfolding as a Principle in Protein Homeostasis and Signaling. *Molecular Cell* **69**, 182–194 (2018).

109. Suryo Rahmanto, A. *et al.* K6-linked ubiquitylation marks formaldehyde-induced RNA-protein crosslinks for resolution. *Molecular Cell* **83**, 4272-4289.e10 (2023).

110. Dantuma, N. P. & Hoppe, T. Growing sphere of influence: Cdc48/p97 orchestrates ubiquitin-dependent extraction from chromatin. *Trends in Cell Biology* **22**, 483–491 (2012).

111. Vaz, B., Halder, S. & Ramadan, K. Role of p97/VCP (Cdc48) in genome stability. *Front. Genet.* **4**, (2013).

112. Dantuma, N. P., Acs, K. & Luijsterburg, M. S. Should I stay or should I go: VCP/p97-mediated chromatin extraction in the DNA damage response. *Experimental Cell Research* **329**, 9–17 (2014).

113. Braxton, J. R. & Southworth, D. R. Structural insights of the p97/VCP AAA+ ATPase: How adapter interactions coordinate diverse cellular functionality. *Journal of Biological Chemistry* **299**, 105182 (2023).

114. Lee, J.-J. *et al.* Complex of Fas-associated Factor 1 (FAF1) with Valosin-containing Protein (VCP)-Npl4-Ufd1 and Polyubiquitinated Proteins Promotes Endoplasmic Reticulum-associated Degradation (ERAD). *Journal of Biological Chemistry* **288**, 6998–7011 (2013).

115. Komander, D., Clague, M. J. & Urbé, S. Breaking the chains: structure and function of the deubiquitinases. *Nat Rev Mol Cell Biol* **10**, 550–563 (2009).

116. Mevissen, T. E. T. & Komander, D. Mechanisms of Deubiquitinase Specificity and Regulation. *Annu. Rev. Biochem.* **86**, 159–192 (2017).

117. Snyder, N. A. & Silva, G. M. Deubiquitinating enzymes (DUBs): Regulation, homeostasis, and oxidative stress response. *Journal of Biological Chemistry* **297**, 101077 (2021).

118. Hermanns, T. *et al.* A family of bacterial Josephin-like deubiquitinases with an irreversible cleavage mode. *Molecular Cell* **85**, 1202-1215.e5 (2025).

119. Sowa, M. E., Bennett, E. J., Gygi, S. P. & Harper, J. W. Defining the Human Deubiquitinating Enzyme Interaction Landscape. *Cell* **138**, 389–403 (2009).

120. Bolhuis, D. L., Emanuele, M. J. & Brown, N. G. Friend or foe? Reciprocal regulation between E3 ubiquitin ligases and deubiquitinases. *Biochemical Society Transactions* **52**, 241–267 (2024).

121. Clague, M. J. *et al.* Deubiquitylases From Genes to Organism. *Physiological Reviews* **93**, 1289–1315 (2013).

122. Walden, M., Masandi, S. K., Pawłowski, K. & Zeqiraj, E. Pseudo-DUBs as allosteric activators and molecular scaffolds of protein complexes. *Biochemical Society Transactions* **46**, 453–466 (2018).

123. Pathare, G. R. *et al.* Crystal structure of the proteasomal deubiquitylation module Rpn8-Rpn11. *Proc. Natl. Acad. Sci. U.S.A.* **111**, 2984–2989 (2014).

124. Rinaldi, T. *et al.* Participation of the proteasomal lid subunit Rpn11 in mitochondrial morphology and function is mapped to a distinct C-terminal domain. *Biochemical Journal* **381**, 275–285 (2004).

125. Li, Y. & Reverter, D. Molecular Mechanisms of DUBs Regulation in Signaling and Disease. *IJMS* **22**, 986 (2021).

126. Komander, D. & Barford, D. Structure of the A20 OTU domain and mechanistic insights into deubiquitination. *Biochemical Journal* **409**, 77–85 (2008).

127. Kwasna, D. *et al.* Discovery and Characterization of ZUFSP/ZUP1, a Distinct Deubiquitinase Class Important for Genome Stability. *Molecular Cell* **70**, 150-164.e6 (2018).

128. Haahr, P. *et al.* ZUFSP Deubiquitylates K63-Linked Polyubiquitin Chains to Promote Genome Stability. *Molecular Cell* **70**, 165-174.e6 (2018).

129. Larsen, C. N., Krantz, B. A. & Wilkinson, K. D. Substrate Specificity of Deubiquitinating Enzymes: Ubiquitin C-Terminal Hydrolases. *Biochemistry* **37**, 3358–3368 (1998).

130. Wang, Y. & Wang, F. Post-Translational Modifications of Deubiquitinating Enzymes: Expanding the Ubiquitin Code. *Front. Pharmacol.* **12**, 685011 (2021).

131. Pinto-Fernandez, A. & Kessler, B. M. DUBbing Cancer: Deubiquitylating Enzymes Involved in Epigenetics, DNA Damage and the Cell Cycle As Therapeutic Targets. *Front. Genet.* **7**, (2016).

132. De Poot, S. A. H., Tian, G. & Finley, D. Meddling with Fate: The Proteasomal Deubiquitinating Enzymes. *Journal of Molecular Biology* **429**, 3525–3545 (2017).

133. Deol, K. K. *et al.* Proteasome-Bound UCH37/UCHL5 Debranches Ubiquitin Chains to Promote Degradation. *Molecular Cell* **80**, 796-809.e9 (2020).

134. Albrecht, M., Golatta, M., Wüllner, U. & Lengauer, T. Structural and functional analysis of ataxin-2 and ataxin-3. *European Journal of Biochemistry* **271**, 3155–3170 (2004).

135. Zeng, C. *et al.* Machado-Joseph Deubiquitinases: From Cellular Functions to Potential Therapy Targets. *Front. Pharmacol.* **11**, 1311 (2020).

136. Sousa E Silva, R., Sousa, A. D., Vieira, J. & Vieira, C. P. The Josephin domain (JD) containing proteins are predicted to bind to the same interactors: Implications for spinocerebellar ataxia type 3 (SCA3) studies using Drosophila melanogaster mutants. *Front. Mol. Neurosci.* **16**, 1140719 (2023).

137. Felício, D., Du Mérac, T. R., Amorim, A. & Martins, S. Functional implications of paralog genes in polyglutamine spinocerebellar ataxias. *Hum. Genet.* **142**, 1651–1676 (2023).

138. Lange, S. M. *et al.* VCP/p97-associated proteins are binders and debranching enzymes of K48–K63-branched ubiquitin chains. *Nat Struct Mol Biol* **31**, 1872–1887 (2024).

139. Abdul Rehman, S. A. *et al.* MINDY-1 Is a Member of an Evolutionarily Conserved and Structurally Distinct New Family of Deubiquitinating Enzymes. *Molecular Cell* **63**, 146–155 (2016).

140. Abdul Rehman, S. A. *et al.* Mechanism of activation and regulation of deubiquitinase activity in MINDY1 and MINDY2. *Molecular Cell* **81**, 4176-4190.e6 (2021).

141. Kristariyanto, Y. A., Abdul Rehman, S. A., Weidlich, S., Knebel, A. & Kulathu, Y. A single MIU motif of MINDY-1 recognizes K48-linked polyubiquitin chains. *EMBO Reports* **18**, 392–402 (2017).

142. Hu, M. *et al.* Crystal Structure of a UBP-Family Deubiquitinating Enzyme in Isolation and in Complex with Ubiquitin Aldehyde. *Cell* **111**, 1041–1054 (2002).

143. Lange, S. M., Armstrong, L. A. & Kulathu, Y. Deubiquitinases: From mechanisms to their inhibition by small molecules. *Molecular Cell* **82**, 15–29 (2022).

144. Keijzer, N. *et al.* Variety in the USP deubiquitinase catalytic mechanism. *Life Sci. Alliance* **7**, e202302533 (2024).

145. Ritorto, M. S. *et al.* Screening of DUB activity and specificity by MALDI-TOF mass spectrometry. *Nat Commun* **5**, 4763 (2014).

146. Faesen, A. C. *et al.* The Differential Modulation of USP Activity by Internal Regulatory Domains, Interactors and Eight Ubiquitin Chain Types. *Chemistry & Biology* **18**, 1550–1561 (2011).

147. Gersch, M. *et al.* Mechanism and regulation of the Lys6-selective deubiquitinase USP30. *Nat Struct Mol Biol* **24**, 920–930 (2017).

148. Sato, Y. *et al.* Structural basis for specific cleavage of Lys6-linked polyubiquitin chains by USP30. *Nat Struct Mol Biol* **24**, 911–919 (2017).

149. Fuchs, G. & Oren, M. Writing and reading H2B monoubiquitylation. *Biochimica et Biophysica Acta (BBA) - Gene Regulatory Mechanisms* **1839**, 694–701 (2014).

150. Nijman, S. M. B. *et al.* The Deubiquitinating Enzyme USP1 Regulates the Fanconi Anemia Pathway. *Molecular Cell* **17**, 331–339 (2005).

151. Huang, T. T. *et al.* Regulation of monoubiquitinated PCNA by DUB autocleavage. *Nat Cell Biol* **8**, 341–347 (2006).

152. Reyes-Turcu, F. E. *et al.* The Ubiquitin Binding Domain ZnF UBP Recognizes the C-Terminal Diglycine Motif of Unanchored Ubiquitin. *Cell* **124**, 1197–1208 (2006).

153. Lee, B.-H. *et al.* USP14 deubiquitinates proteasome-bound substrates that are ubiquitinated at multiple sites. *Nature* **532**, 398–401 (2016).

154. Messick, T. E. *et al.* Structural Basis for Ubiquitin Recognition by the Otu1 Ovarian Tumor Domain Protein. *Journal of Biological Chemistry* **283**, 11038–11049 (2008).

155. Mevissen, T. E. T. *et al.* OTU Deubiquitinases Reveal Mechanisms of Linkage Specificity and Enable Ubiquitin Chain Restriction Analysis. *Cell* **154**, 169–184 (2013).

156. Hospenthal, M. K., Mevissen, T. E. T. & Komander, D. Deubiquitinase-based analysis of ubiquitin chain architecture using Ubiquitin Chain Restriction (UbiCRest). *Nat Protoc* **10**, 349–361 (2015).

157. Bremm, A., Freund, S. M. V. & Komander, D. Lys11-linked ubiquitin chains adopt compact conformations and are preferentially hydrolyzed by the deubiquitinase Cezanne. *Nat Struct Mol Biol* **17**, 939–947 (2010).

158. Keusekotten, K. *et al.* OTULIN Antagonizes LUBAC Signaling by Specifically Hydrolyzing Met1-Linked Polyubiquitin. *Cell* **153**, 1312–1326 (2013).

159. Mevissen, T. E. T. *et al.* Molecular basis of Lys11-polyubiquitin specificity in the deubiquitinase Cezanne. *Nature* **538**, 402–405 (2016).

160. Bonacci, T. *et al.* Cezanne/OTUD7B is a cell cycle-regulated deubiquitinase that antagonizes the degradation of APC/C substrates. *The EMBO Journal* **37**, e98701 (2018).

161. Kayagaki, N. *et al.* DUBA: A Deubiquitinase That Regulates Type I Interferon Production. *Science* **318**, 1628–1632 (2007).

162. Erdős, G., Pajkos, M. & Dosztányi, Z. IUPred3: prediction of protein disorder enhanced with unambiguous experimental annotation and visualization of evolutionary conservation. *Nucleic Acids Research* **49**, W297–W303 (2021).

163. Mayya, V. *et al.* Quantitative Phosphoproteomic Analysis of T Cell Receptor Signaling Reveals System-Wide Modulation of Protein-Protein Interactions. *Sci. Signal.* **2**, (2009).

164. Dephoure, N. *et al.* A quantitative atlas of mitotic phosphorylation. *Proc. Natl. Acad. Sci. U.S.A.* **105**, 10762–10767 (2008).

165. Huang, O. W. *et al.* Phosphorylation-dependent activity of the deubiquitinase DUBA. *Nat Struct Mol Biol* **19**, 171–175 (2012).

166. Kulathu, Y. *et al.* Regulation of A20 and other OTU deubiquitinases by reversible oxidation. *Nat Commun* **4**, 1569 (2013).

167. Li, F. *et al.* OTUD5 cooperates with TRIM25 in transcriptional regulation and tumor progression via deubiquitination activity. *Nat Commun* **11**, 4184 (2020).

168. Beck, D. B. *et al.* Linkage-specific deubiquitylation by OTUD5 defines an embryonic pathway intolerant to genomic variation. *Sci. Adv.* **7**, eabe2116 (2021).

169. Rutz, S. *et al.* Deubiquitinase DUBA is a post-translational brake on interleukin-17 production in T cells. *Nature* **518**, 417–421 (2015).

170. Guo, Y. *et al.* OTUD5 promotes innate antiviral and antitumor immunity through deubiquitinating and stabilizing STING. *Cell Mol Immunol* **18**, 1945–1955 (2021).

171. Luo, J. *et al.* OTUD5 Regulates p53 Stability by Deubiquitinating p53. *PLoS ONE* **8**, e77682 (2013).

172. Park, S.-Y. *et al.* Deubiquitinase OTUD5 mediates the sequential activation of PDCD5 and p53 in response to genotoxic stress. *Cancer Letters* **357**, 419–427 (2015).

173. Bai, M., Che, Y., Lu, K. & Fu, L. Analysis of deubiquitinase OTUD5 as a biomarker and therapeutic target for cervical cancer by bioinformatic analysis. *PeerJ* **8**, e9146 (2020).

174. Hou, T. *et al.* Deubiquitinase OTUD5 modulates mTORC1 signaling to promote bladder cancer progression. *Cell Death Dis* **13**, 778 (2022).

175. Cho, J. H. *et al.* Deubiquitinase OTUD5 is a positive regulator of mTORC1 and mTORC2 signaling pathways. *Cell Death Differ* **28**, 900–914 (2021).

176. Li, F. *et al.* The deubiquitinase OTUD5 regulates Ku80 stability and non-homologous end joining. *Cell. Mol. Life Sci.* **76**, 3861–3873 (2019).

177. de Vivo, A. *et al.* The OTUD5–UBR5 complex regulates FACT-mediated transcription at damaged chromatin. *Nucleic Acids Research* **47**, 729–746 (2019).

178. de Vivo, A. *et al.* OTUD5 limits replication fork instability by organizing chromatin remodelers. *Nucleic Acids Research* **51**, 10467–10483 (2023).

179. Méndez, J. & Stillman, B. Chromatin Association of Human Origin Recognition Complex, Cdc6, and Minichromosome Maintenance Proteins during the Cell Cycle: Assembly of Prereplication Complexes in Late Mitosis. *Molecular and Cellular Biology* **20**, 8602–8612 (2000).

180. Zhang, M., Berk, J. M., Mehrtash, A. B., Kanyo, J. & Hochstrasser, M. A versatile new tool derived from a bacterial deubiquitylase to detect and purify ubiquitylated substrates and their interacting proteins. *PLoS Biol* **20**, e3001501 (2022).

181. Oliveira, C. A. B., Isaakova, E., Beli, P. & Xirodimas, D. P. A Mass Spectrometry-Based Strategy for Mapping Modification Sites for the Ubiquitin-Like Modifier NEDD8. in *The Ubiquitin Code* (eds Rodriguez, M. S. & Barrio, R.) vol. 2602 137–149 (Springer US, New York, NY, 2023).

182. Li, J. *et al.* TMTpro reagents: a set of isobaric labeling mass tags enables simultaneous proteome-wide measurements across 16 samples. *Nat Methods* **17**, 399–404 (2020).

183. Zhang, L. & Elias, J. E. Relative Protein Quantification Using Tandem Mass Tag Mass Spectrometry. in *Proteomics* (eds Comai, L., Katz, J. E. & Mallick, P.) vol. 1550 185–198 (Springer New York, New York, NY, 2017).

184. Wiśniewski, J. R., Zougman, A. & Mann, M. Combination of FASP and StageTip-Based Fractionation Allows In-Depth Analysis of the Hippocampal Membrane Proteome. *J. Proteome Res.* **8**, 5674–5678 (2009).

185. Weinert, B. T. *et al.* Lysine Succinylation Is a Frequently Occurring Modification in Prokaryotes and Eukaryotes and Extensively Overlaps with Acetylation. *Cell Reports* **4**, 842–851 (2013).

186. Rappsilber, J., Mann, M. & Ishihama, Y. Protocol for micro-purification, enrichment, pre-fractionation and storage of peptides for proteomics using StageTips. *Nat Protoc* **2**, 1896–1906 (2007).

187. Cox, J. & Mann, M. MaxQuant enables high peptide identification rates, individualized p.p.b.-range mass accuracies and proteome-wide protein quantification. *Nat Biotechnol* **26**, 1367–1372 (2008).

188. Cox, J. *et al.* Andromeda: A Peptide Search Engine Integrated into the MaxQuant Environment. *J. Proteome Res.* **10**, 1794–1805 (2011).

189. Elias, J. E. & Gygi, S. P. Target-decoy search strategy for increased confidence in large-scale protein identifications by mass spectrometry. *Nat Methods* **4**, 207–214 (2007).

190. Schindelin, J. *et al.* Fiji: an open-source platform for biological-image analysis. *Nat Methods* **9**, 676–682 (2012).

191. Rega, C. *et al.* High resolution profiling of cell cycle-dependent protein and phosphorylation abundance changes in non-transformed cells. *Nat Commun* **16**, 2579 (2025).

192. Watson, J. V., Chambers, S. H. & Smith, P. J. A pragmatic approach to the analysis of DNA histograms with a definable G1 peak. *Cytometry* **8**, 1–8 (1987).

193. Jumper, J. *et al.* Highly accurate protein structure prediction with AlphaFold. *Nature* **596**, 583–589 (2021).

194. Takei, Y. & Ishida, T. How to select the best model from AlphaFold2 structures? Preprint at https://doi.org/10.1101/2022.04.05.487218 (2022).

195. Ruff, K. M. & Pappu, R. V. AlphaFold and Implications for Intrinsically Disordered Proteins. *Journal of Molecular Biology* **433**, 167208 (2021).

196. Evans, R. *et al.* Protein complex prediction with AlphaFold-Multimer. Preprint at https://doi.org/10.1101/2021.10.04.463034 (2021).

197. Varadi, M. & Velankar, S. The impact of AlphaFold Protein Structure Database on the fields of life sciences. *Proteomics* **23**, 2200128 (2023).

198. Varadi, M. *et al.* AlphaFold Protein Structure Database in 2024: providing structure coverage for over 214 million protein sequences. *Nucleic Acids Research* **52**, D368–D375 (2024).

199. Terwilliger, T. C. *et al.* AlphaFold predictions are valuable hypotheses and accelerate but do not replace experimental structure determination. *Nat Methods* **21**, 110–116 (2024).

200. Meng, E. C. *et al.* UCSF ChimeraX: Tools for structure building and analysis. *Protein Science* **32**, e4792 (2023).

201. Tyanova, S. *et al.* The Perseus computational platform for comprehensive analysis of (prote)omics data. *Nat Methods* **13**, 731–740 (2016).

202. Ritchie, M. E. *et al.* limma powers differential expression analyses for RNA-sequencing and microarray studies. *Nucleic Acids Research* **43**, e47–e47 (2015).

203. Ulgen, E., Ozisik, O. & Sezerman, O. U. pathfindR: An R Package for Comprehensive Identification of Enriched Pathways in Omics Data Through Active Subnetworks. *Front. Genet.* **10**, 858 (2019).

204. Wagner, S. A. *et al.* A Proteome-wide, Quantitative Survey of In Vivo Ubiquitylation Sites Reveals Widespread Regulatory Roles. *Molecular & Cellular Proteomics* **10**, M111.013284 (2011).

205. Ong, S.-E. *et al.* Stable Isotope Labeling by Amino Acids in Cell Culture, SILAC, as a Simple and Accurate Approach to Expression Proteomics. *Molecular & Cellular Proteomics* **1**, 376–386 (2002).

206. Park, J., Park, S. & Lee, J. Role of the Paf1 complex in the maintenance of stem cell pluripotency and development. *The FEBS Journal* **290**, 951–961 (2023).

207. Kim, J., Guermah, M. & Roeder, R. G. The Human PAF1 Complex Acts in Chromatin Transcription Elongation Both Independently and Cooperatively with SII/TFIIS. *Cell* **140**, 491–503 (2010).

208. Francette, A. M., Tripplehorn, S. A. & Arndt, K. M. The Paf1 Complex: A Keystone of Nuclear Regulation Operating at the Interface of Transcription and Chromatin. *Journal of Molecular Biology* **433**, 166979 (2021).

209. Song, A. & Chen, F. X. The pleiotropic roles of SPT5 in transcription. *Transcription* **13**, 53–69 (2022).

210. Fuchs, G. *et al.* RNF20 and USP44 Regulate Stem Cell Differentiation by Modulating H2B Monoubiquitylation. *Molecular Cell* **46**, 662–673 (2012).

211. Xue, Y. *et al.* NURD, a Novel Complex with Both ATP-Dependent Chromatin-Remodeling and Histone Deacetylase Activities. *Molecular Cell* **2**, 851–861 (1998).

212. Jasim, S. A. *et al.* Histone Deacetylases (HDACs) Roles in Inflammation-mediated Diseases; Current Knowledge. *Cell Biochem Biophys* **83**, 1375–1386 (2024).

213. Milazzo, G. *et al.* Histone Deacetylases (HDACs): Evolution, Specificity, Role in Transcriptional Complexes, and Pharmacological Actionability. *Genes* **11**, 556 (2020).

214. Koit, S. *et al.* A conserved phosphorylation mechanism for regulating the interaction between the CMG replicative helicase and its forked DNA substrate. *Journal of Biological Chemistry* **301**, 108408 (2025).

215. Wold, M. S. REPLICATION PROTEIN A: A Heterotrimeric, Single-Stranded DNA-Binding Protein Required for Eukaryotic DNA Metabolism. *Annu. Rev. Biochem.* **66**, 61–92 (1997).

216. Maréchal, A. & Zou, L. RPA-coated single-stranded DNA as a platform for post-translational modifications in the DNA damage response. *Cell Res* **25**, 9–23 (2015).

217. Yao, N. Y. & O'Donnell, M. The RFC Clamp Loader: Structure and Function. in *The Eukaryotic Replisome: a Guide to Protein Structure and Function* (ed. MacNeill, S.) vol. 62 259–279 (Springer Netherlands, Dordrecht, 2012).

218. Kim, E., Barth, R. & Dekker, C. Looping the Genome with SMC Complexes. *Annu. Rev. Biochem.* **92**, 15–41 (2023).

219. Hoencamp, C. & Rowland, B. D. Genome control by SMC complexes. *Nat Rev Mol Cell Biol* **24**, 633–650 (2023).

220. Hyer, M. L. *et al.* A small-molecule inhibitor of the ubiquitin activating enzyme for cancer treatment. *Nat Med* **24**, 186–193 (2018).

221. Misteli, T. Protein Dynamics: Implications for Nuclear Architecture and Gene Expression. *Science* **291**, 843–847 (2001).

222. Phair, R. D. *et al.* Global Nature of Dynamic Protein-Chromatin Interactions In Vivo: Three-Dimensional Genome Scanning and Dynamic Interaction Networks of Chromatin Proteins. *Molecular and Cellular Biology* **24**, 6393–6402 (2004).

223. Hansen, A. S., Pustova, I., Cattoglio, C., Tjian, R. & Darzacq, X. CTCF and cohesin regulate chromatin loop stability with distinct dynamics. *eLife* **6**, e25776 (2017).

224. Kilgas, S. & Ramadan, K. Inhibitors of the ATPase p97/VCP: From basic research to clinical applications. *Cell Chemical Biology* **30**, 3–21 (2023).

225. Rycenga, H. B., Wolfe, K. B., Yeh, E. S. & Long, D. T. Uncoupling of p97 ATPase activity has a dominant negative effect on protein extraction. *Sci Rep* **9**, 10329 (2019).

226. Jao, C. Y. & Salic, A. Exploring RNA transcription and turnover *in vivo* by using click chemistry. *Proc. Natl. Acad. Sci. U.S.A.* **105**, 15779–15784 (2008).

227. Rostovtsev, V. V., Green, L. G., Fokin, V. V. & Sharpless, K. B. A Stepwise Huisgen Cycloaddition Process: Copper(I)-Catalyzed Regioselective "Ligation" of Azides and Terminal Alkynes. *Angew. Chem. Int. Ed.* **41**, 2596–2599 (2002).

228. Tornøe, C. W., Christensen, C. & Meldal, M. Peptidotriazoles on Solid Phase: [1,2,3]-Triazoles by Regiospecific Copper(I)-Catalyzed 1,3-Dipolar Cycloadditions of Terminal Alkynes to Azides. *J. Org. Chem.* **67**, 3057–3064 (2002).

229. Borisova, M. E. *et al.* p38-MK2 signaling axis regulates RNA metabolism after UV-light-induced DNA damage. *Nat Commun* **9**, 1017 (2018).

230. Williamson, L. *et al.* UV Irradiation Induces a Non-coding RNA that Functionally Opposes the Protein Encoded by the Same Gene. *Cell* **168**, 843-855.e13 (2017).

231. Wickramasinghe, V. O. & Venkitaraman, A. R. RNA Processing and Genome Stability: Cause and Consequence. *Molecular Cell* **61**, 496–505 (2016).

232. Muñoz, M. J. *et al.* DNA Damage Regulates Alternative Splicing through Inhibition of RNA Polymerase II Elongation. *Cell* **137**, 708–720 (2009).

233. Cramer, P. Organization and regulation of gene transcription. *Nature* **573**, 45–54 (2019).

234. Rawat, P. *et al.* Stress-induced nuclear condensation of NELF drives transcriptional downregulation. *Molecular Cell* **81**, 1013-1026.e11 (2021).

235. Shao, X., Joergensen, A. M., Howlett, N. G., Lisby, M. & Oestergaard, V. H. A distinct role for recombination repair factors in an early cellular response to transcription–replication conflicts. *Nucleic Acids Research* **48**, 5467–5484 (2020).

236. Kotake, Y. *et al.* Splicing factor SF3b as a target of the antitumor natural product pladienolide. *Nat Chem Biol* **3**, 570–575 (2007).

237. Crozier, L. *et al.* CDK4/6 inhibitors induce replication stress to cause long-term cell cycle withdrawal. *The EMBO Journal* **41**, e108599 (2022).

238. De Groot, A. F., Kuijpers, C. J. & Kroep, J. R. CDK4/6 inhibition in early and metastatic breast cancer: A review. *Cancer Treatment Reviews* **60**, 130–138 (2017).

239. Martínez-Alonso, D. & Malumbres, M. Mammalian cell cycle cyclins. *Seminars in Cell & Developmental Biology* **107**, 28–35 (2020).

240. Stewart, S. & Fang, G. Anaphase-Promoting Complex/Cyclosome Controls the Stability of TPX2 during Mitotic Exit. *Molecular and Cellular Biology* **25**, 10516–10527 (2005).

241. Akimov, V. *et al.* UbiSite approach for comprehensive mapping of lysine and N-terminal ubiquitination sites. *Nat Struct Mol Biol* **25**, 631–640 (2018).

242. Bingol, B. *et al.* The mitochondrial deubiquitinase USP30 opposes parkin-mediated mitophagy. *Nature* **510**, 370–375 (2014).

243. Sapmaz, A. *et al.* USP32 regulates late endosomal transport and recycling through deubiquitylation of Rab7. *Nat Commun* **10**, 1454 (2019).

244. Steger, M. *et al.* Time-resolved in vivo ubiquitinome profiling by DIA-MS reveals USP7 targets on a proteome-wide scale. *Nat Commun* **12**, 5399 (2021).

245. Trulsson, F. *et al.* Deubiquitinating enzymes and the proteasome regulate preferential sets of ubiquitin substrates. *Nat Commun* **13**, 2736 (2022).

246. Hershko, A. Ubiquitin-mediated protein degradation. *Journal of Biological Chemistry* **263**, 15237–15240 (1988).

247. Harris, L. D. *et al.* The deubiquitinase TRABID stabilizes the K29/K48-specific E3 ubiquitin ligase HECTD1. *Journal of Biological Chemistry* **296**, 100246 (2021).

248. Vaughan, R. M., Kupai, A. & Rothbart, S. B. Chromatin Regulation through Ubiquitin and Ubiquitin-like Histone Modifications. *Trends in Biochemical Sciences* **46**, 258–269 (2021).

249. Clague, M. J., Coulson, J. M. & Urbé, S. Deciphering histone 2A deubiquitination. *Genome Biol* **9**, 202 (2008).

250. Chandrasekharan, M. B., Huang, F. & Sun, Z.-W. Ubiquitination of histone H2B regulates chromatin dynamics by enhancing nucleosome stability. *Proc. Natl. Acad. Sci. U.S.A.* **106**, 16686–16691 (2009).

251. Gatti, M., Imhof, R., Huang, Q., Baudis, M. & Altmeyer, M. The Ubiquitin Ligase TRIP12 Limits PARP1 Trapping and Constrains PARP Inhibitor Efficiency. *Cell Reports* **32**, 107985 (2020).

252. Rodríguez-Acebes, S. *et al.* DNA polymerase α/primase extraction from chromatin by VCP/p97 restricts ATR activation during unperturbed DNA replication. *Nat Commun* **16**, 5706 (2025).

253. Bolhuis, D. L. *et al.* USP37 prevents unscheduled replisome unloading through MCM complex deubiquitination. *Nat Commun* **16**, (2025).

254. Franz, A. *et al.* USP7 and VCPFAF1 define the SUMO/Ubiquitin landscape at the DNA replication fork. *Cell Reports* **37**, 109819 (2021).

255. van den Boom, J. *et al.* VCP/p97 Extracts Sterically Trapped Ku70/80 Rings from DNA in Double-Strand Break Repair. *Molecular Cell* **64**, 189–198 (2016).

256. Thattikota, Y. *et al.* Cdc48/VCP Promotes Chromosome Morphogenesis by Releasing Condensin from Self-Entrapment in Chromatin. *Molecular Cell* **69**, 664-676.e5 (2018).

257. Heidelberger, J. B. *et al.* Proteomic profiling of VCP substrates links VCP to K6-linked ubiquitylation and c-Myc function. *EMBO Reports* **19**, e44754 (2018).

258. Bodnar, N. O. *et al.* Structure of the Cdc48 ATPase with its ubiquitin-binding cofactor Ufd1–Npl4. *Nat Struct Mol Biol* **25**, 616–622 (2018).

259. Twomey, E. C. *et al.* Substrate processing by the Cdc48 ATPase complex is initiated by ubiquitin unfolding. *Science* **365**, eaax1033 (2019).

260. Sato, Y. *et al.* Structural insights into ubiquitin recognition and Ufd1 interaction of Npl4. *Nat Commun* **10**, 5708 (2019).

261. Mark, K. G. *et al.* Orphan quality control shapes network dynamics and gene expression. *Cell* **186**, 3460-3475.e23 (2023).

262. Hou, L. *et al.* Paf1C regulates RNA polymerase II progression by modulating elongation rate. *Proc. Natl. Acad. Sci. U.S.A.* **116**, 14583–14592 (2019).

263. Wang, Z. *et al.* Coordinated regulation of RNA polymerase II pausing and elongation progression by PAF1. *Sci. Adv.* **8**, eabm5504 (2022).

264. Hirota, T., Gerlich, D., Koch, B., Ellenberg, J. & Peters, J.-M. Distinct functions of condensin I and II in mitotic chromosome assembly. *Journal of Cell Science* **117**, 6435–6445 (2004).

265. Doughty, T. W., Arsenault, H. E. & Benanti, J. A. Levels of Ycg1 Limit Condensin Function during the Cell Cycle. *PLoS Genet* **12**, e1006216 (2016).

266. Nguyen, H. Q. *et al.* Drosophila Casein Kinase I Alpha Regulates Homolog Pairing and Genome Organization by Modulating Condensin II Subunit Cap-H2 Levels. *PLoS Genet* **11**, e1005014 (2015).

267. Buster, D. W. *et al.* SCFSlimb ubiquitin ligase suppresses condensin II–mediated nuclear reorganization by degrading Cap-H2. *Journal of Cell Biology* **201**, 49–63 (2013).

268. Kakui, Y. *et al.* Fission yeast condensin contributes to interphase chromatin organization and prevents transcription-coupled DNA damage. *Genome Biol* **21**, 272 (2020).

269. Zhang, S. *et al.* The G1-S transition is promoted by Rb degradation via the E3 ligase UBR5. *Science AdvAnceS* (2024).

270. Bretones, G., Delgado, M. D. & León, J. Myc and cell cycle control. *Biochimica et Biophysica Acta (BBA) - Gene Regulatory Mechanisms* **1849**, 506–516 (2015).

271. Schukur, L. *et al.* Identification of the HECT E3 ligase UBR5 as a regulator of MYC degradation using a CRISPR/Cas9 screen. *Sci Rep* **10**, 20044 (2020).

272. Hodáková, Z. *et al.* Cryo-EM structure of the chain-elongating E3 ubiquitin ligase UBR5. *The EMBO Journal* **42**, e113348 (2023).

# Acknowledgments

Redacted for data protection reasons.

# Curriculum vitae

Redacted for data protection reasons.